

Spring 2001

Optical and radar remote sensing of land use and land cover change in the tropics: An assessment of deforestation and secondary vegetation

William Albert Salas

University of New Hampshire, Durham

Follow this and additional works at: <https://scholars.unh.edu/dissertation>

Recommended Citation

Salas, William Albert, "Optical and radar remote sensing of land use and land cover change in the tropics: An assessment of deforestation and secondary vegetation" (2001). *Doctoral Dissertations*. 27.

<https://scholars.unh.edu/dissertation/27>

This Dissertation is brought to you for free and open access by the Student Scholarship at University of New Hampshire Scholars' Repository. It has been accepted for inclusion in Doctoral Dissertations by an authorized administrator of University of New Hampshire Scholars' Repository. For more information, please contact nicole.hentz@unh.edu.

INFORMATION TO USERS

This manuscript has been reproduced from the microfilm master. UMI films the text directly from the original or copy submitted. Thus, some thesis and dissertation copies are in typewriter face, while others may be from any type of computer printer.

The quality of this reproduction is dependent upon the quality of the copy submitted. Broken or indistinct print, colored or poor quality illustrations and photographs, print bleedthrough, substandard margins, and improper alignment can adversely affect reproduction.

In the unlikely event that the author did not send UMI a complete manuscript and there are missing pages, these will be noted. Also, if unauthorized copyright material had to be removed, a note will indicate the deletion.

Oversize materials (e.g., maps, drawings, charts) are reproduced by sectioning the original, beginning at the upper left-hand corner and continuing from left to right in equal sections with small overlaps.

Photographs included in the original manuscript have been reproduced xerographically in this copy. Higher quality 6" x 9" black and white photographic prints are available for any photographs or illustrations appearing in this copy for an additional charge. Contact UMI directly to order.

Bell & Howell Information and Learning
300 North Zeeb Road, Ann Arbor, MI 48106-1346 USA
800-521-0600

UMI[®]

OPTICAL AND RADAR REMOTE SENSING OF LAND USE AND LAND COVER
CHANGE IN THE TROPICS: AN ASSESSMENT OF DEFORESTATION AND
SECONDARY VEGETATION.

BY

WILLIAM A. SALAS

B.S. University of Vermont, 1984
M.S. University of New Hampshire, 1992

DISSERTATION

Submitted to the University of New Hampshire
In Partial Fulfillment of the
Requirements for the Degree of

Doctor of Philosophy
in
Natural Resources

May, 2001

UMI Number: 3006148

UMI[®]

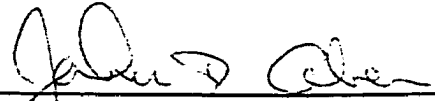
UMI Microform 3006148

Copyright 2001 by Bell & Howell Information and Learning Company.

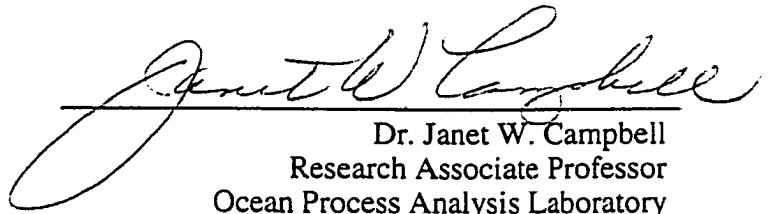
All rights reserved. This microform edition is protected against
unauthorized copying under Title 17, United States Code.

Bell & Howell Information and Learning Company
300 North Zeeb Road
P.O. Box 1346
Ann Arbor, MI 48106-1346

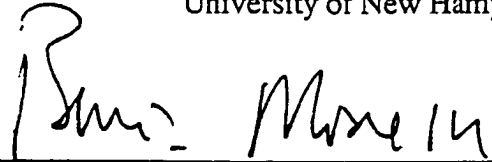
This dissertation has been examined and approved.



Dissertation Director, Dr. John D. Aber
Professor of Natural Resources
Complex Systems Research Center
University of New Hampshire



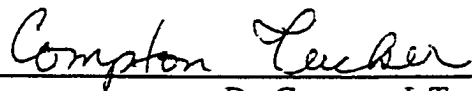
Dr. Janet W. Campbell
Research Associate Professor
Ocean Process Analysis Laboratory
University of New Hampshire



Dr. Berrien Moore
Professor and Director
Institute for the Study of Earth, Oceans, and Space
University of New Hampshire



Dr. David L. Skole
Professor and Director
Basic Science and Remote Sensing Initiative, Department of Geography
Michigan State University



Dr. Compton J. Tucker
Goddard Space Flight Center
National Aeronautics and Space Administration

26 April 2001
Date

DEDICATION

This dissertation is dedicated to Saturnino and Judith Salas.

ACKNOWLEDGEMENTS

This study would not have been possible without support from NASA's LBA and ADRO programs. Chapters 3 & 4 are the culmination of research with Dr. Mark Ducey. Much of the statistical analyses and some writing and figures come directly from Mark Ducey. His statistical expertise is exceptional and greatly appreciated. The last section of Chapter 1 presents a "proposal". A large section of this text comes from a proposal that was a joint effort with my colleagues Dr. Jiaguo Qi, Dr. Dan Zarin, Dr. Mark Ducey, and Dr. Diogenes Alves.

I would like to acknowledge the National Space Development Agency of Japan for their provision of JERS-1 data and the NASA Landsat Pathfinder program for the Landsat data. I feel indebted to Walter Chomentoswki and Chaowalit Silapathong for their assistance in the field. I would also like to thank Steve Boles, Stanley Glidden, and Mike Routhier for their help in image processing, generating figures and overall help.

I wish to extend my sincere thanks to Dr. John Aber, Dr. Janet Campbell, Dr. Berrien Moore, Dr. David Skole, and Dr. Compton Tucker for being on my committee and providing expert guidance and support for this dissertation. I feel very fortunate to have had a committee of such respected scientists. In addition, I wish to give special thanks to Dr. David Skole, mentor and friend, for his research leadership, forthrightness, and love of science.

Lastly, my heartfelt thanks and love to my family whose understanding and love are the foundation of my life!

TABLE OF CONTENTS

ACKNOWLEDGEMENTS.....	iv
PREFACE	ix
LIST OF TABLES.....	xii
LIST OF FIGURES.....	xiii
ABSTRACT	xv

CHAPTER	PAGE
CHAPTER 1: MAPPING AND MONITORING SECONDARY VEGETATION IN THE TROPICS WITH REMOTE SENSING	1
Abstract.....	1
Introduction.....	2
Disturbance in the Legal Amazon	6
Rate of Biomass Accumulation	8
Remote Sensing of Secondary Vegetation.....	10
Spectral Properties of Secondary Vegetation.....	10
Mapping Extent of Secondary Vegetation.....	12
SAR Mapping of Secondary Vegetation.....	19
Estimation of Age of Secondary Vegetation.....	21
Persistence and Rates of Secondary Vegetation Formation.....	25
Mapping Successional Stage.....	26
Estimating Rates of Succession and Successional Pathways.....	27
Estimating Biomass of Secondary Vegetation.....	28
Proposal for Monitoring Secondary Succession in Amazonia.....	31
Component 1: Mapping Extent, Age, and Disturbance Intensity.....	33
Component 2: Development of Scalable BRDF Estimates of Canopy Structure	34
Component 3: Mapping Structural Classes of Secondary Vegetation.....	36
Component 4: Mapping Recovery Rates.....	38

Component 5: Assessment of Disturbance Specific Controls.....	38
Figures and Tables.....	39

CHAPTER 2: INTER-ANNUAL VARIABILITY IN DEFORESTATION AND

REGROWTH IN THE TROPICS..... 43

Abstract.....	43
Introduction.....	44
Global Carbon Cycle.....	44
Estimates of Deforestation and Secondary Vegetation Formation.....	51
Role of Secondary Vegetation in Net Biotic Release of Carbon.....	52
Methods.....	53
Landsat Classification.....	53
Change Detection.....	56
Accuracy Assessment.....	57
Results and Discussion.....	60
Amazonia Sites: Alto Paraiso, Ruropolis, and Uruara.....	60
Southeast Asia Sites: Chiang Mai, Upper and Lower Ca River, and Kachin... ..	63
Conclusion.....	67
Figures and Tables.....	69

**CHAPTER 3: ASSESSMENT OF JERS-1 SAR FOR MONITORING SECONDARY
VEGETATION IN AMAZONIA: I. SPATIAL AND TEMPORAL VARIABILITY IN
BACKSCATTER ACROSS A CHRONO-SEQUENCE OF SECONDARY**

VEGETATION STANDS IN RONDONIA..... 87

Abstract.....	87
Introduction.....	88
Land Use and Inter-Annual Variability of Global Carbon Cycle.....	88
Remote Sensing Land Use and Land Cover Change in the Tropics.....	90
Methods.....	95

Multi-Temporal TM Classifications.....	95
Mapping Age of Individual Secondary Vegetation Stands and Clearings.....	96
Accuracy Assessment of Secondary Vegetation and Clearing Age.....	97
JERS-1 SAR Data Pre-Processing.....	98
Extraction of Sigma Naught Statistics and Confidence Limits.....	100
Biomass Density Model.....	104
Results and Discussion.....	105
Landscape Variability in Sigma Naught.....	105
JERS Sigma Naught Statistics.....	106
Analysis of Variance.....	111
Conclusion.....	114
Figures and Tables.....	117

CHAPTER 4: ASSESSMENT OF JERS-1 SAR FOR MONITORING SECONDARY VEGETATION IN AMAZONIA: II. SPATIAL, TEMPORAL, AND RADIOMETRIC CONSIDERATIONS FOR OPERATIONAL MONITORING

Abstract.....	130
Introduction.....	131
Methods.....	135
TM Analysis of Secondary Vegetation Stand Age and Size.....	136
JERS-1 SAR Data Pre-Processing.....	137
Extraction of Sigma Naught Statistics and Confidence Limits.....	138
Biomass Density Model.....	139
Statistical Methods and Models.....	140
Results and Discussion.....	143
Effects of Factors Other Than Speckle and Texture.....	143
Coefficient of Variation of Biomass Predictions.....	146
Single vs Multi-Temporal JERS Observations for Estimating Biomass.....	147
Impact of Noise on Estimating Biomass.....	148
Conclusion.....	151

Figures and Tables.....	153
APPENDIX.....	163
REFERENCES.....	174

PREFACE

Tropical forests are a critical and diverse ecosystem. They harbor a large proportion of the Earth's biodiversity, provide natural chemical compounds that form the basis of medicine, provide food and shelter for indigenous peoples, account for one-third to one-half of terrestrial primary productivity, and contain as much as 40% of terrestrial biomass. Tropical forests have been called the "Lungs of the World". However, they are disappearing due to widespread deforestation and logging, causing significant changes to the biological, physical and social environment within the tropical forest biome. Large-scale tropical deforestation can alter the local carbon cycle, hydrological cycle, and even the climate. In addition to the direct impacts of deforestation and logging, secondary impacts include an increase in tree mortality rates and susceptibility to fire surrounding the areas of disturbance.

Tropical deforestation is, at times, thought of as a one-way process. However, many areas that are cleared cannot support agricultural use for extended periods and are abandoned and revert to secondary forests. Secondary forests are estimated to occupy over 30% of closed tropical forests and almost 20% of the open tropical forests. Some studies indicate that these percentages will increase substantially over the next 50 to 100 years. Despite the widespread extent of secondary forests in the tropics, the biophysical, ecological, and social processes of succession are not well understood. Clearly, a better understanding is needed.

The rate at which forests grow following disturbance depends on the type of disturbance, post-disturbance land use, and climatic and edaphic conditions. Rate of forest regrowth can provide an indication of the suitability of a particular region to support sustainable agriculture as well as the potential for carbon sequestration to reduce the net carbon flux from forest clearing. Hence, developing an ability to predict forest regrowth potential has considerable implications for our understanding of carbon dynamics in a future characterized by increased conversion of old-growth forests and the subsequent abandonment of many areas originally cleared for agricultural activity.

Deforestation of tropical forests and creation of secondary forests are inexorably linked. The processes that control rates of deforestation also influence the extent and persistence of secondary forests. Understanding the magnitude and spatial patterns of deforestation and, thus, secondary forests requires the synoptic capabilities of remote sensing. Thus, remote sensing is a valuable tool for research on tropical deforestation and secondary vegetation. This tool can provide not only information on the timing, extent and spatial patterns of deforestation and secondary vegetation, but also characteristics of the land use processes and post-disturbance vegetation conditions.

Loss of tropical forests has captured the interest of both the scientific community and the general public. Within both communities, there have been very pointed debates on the protection of tropical forests. While the loss of pristine tropical forests can create a strong emotional response, we need to be rational in our assessment of how to deal with the best utilization of natural resources within the tropical forest biome. Clearly the demand for food and fiber will continue to rise as global population increases. Tropical forests can

help meet some of the increase in demand, either directly by providing natural resources, or indirectly by providing economic returns through ecosystem services.

Since tropical deforestation will continue, research efforts should focus on developing strategies that address the needs for sustainable development of the tropical biome and mitigate long-term degradation or destruction of tropical forests. Developing an improved understanding of forest growth potential in the tropics would be extremely useful for land use planning for sustainable development. However, there is a lack of sufficient field measurements of secondary forest biomass to refine models of forest regrowth potential. Development of remote sensing techniques for estimating biomass of secondary forests and patterns of land use would be beneficial for improving our understanding of the controls on rates of regrowth and, thus, capabilities for modeling regrowth potential. This dissertation addresses the use of remote sensing as a tool for quantifying the spatial and temporal patterns of deforestation and secondary vegetation and an evaluation of how remote sensing can be used to quantify the structure or biomass of secondary vegetation.

LIST OF TABLES

TABLE 1.1. Pre- and post-disturbance area of RADAM vegetation classes.....	41
TABLE 1.2. Spectral properties of secondary vegetation.....	42
TABLE 2.1. Landsat TM data for Southeast Asia analysis	69
TABLE 2.2. Landsat TM data for Amazonia analysis.....	70
TABLE 2.3. Persistence of secondary vegetation at Ruropolis, Alto Paraiso, and Uruara sites.....	71
TABLE 2.4. Disturbance area for Southeast Asia sites.....	72
TABLE 2.5. Persistence of new clearing at Alto Paraiso site.....	73
TABLE 3.1. Landsat TM data for age estimation of secondary vegetation at Alto Paraiso.....	117
TABLE 3.2. Class transitions for estimating age and land use history	118
TABLE 3.3. JERS-1 SAR images used in the analysis.....	119
TABLE 3.4. Results from ANOVA of temporal variability in sigma naught.....	120
TABLE 3.5. Results from ANOVA: magnitude of stand variability, temporal variability and uncorrelated noise	121
TABLE 4.1. JERS-1 SAR images, range ramp corrections, and NESO.....	153

LIST OF FIGURES

FIGURE 1.1:	Conceptual diagram relating biomass recovery and forest structural stages.....	39
FIGURE 1.2:	Location of proposed aircraft calibration and validation sites.....	40
FIGURE 2.1:	Study site locations in Amazonia and Southeast Asia.....	74
FIGURE 2.2:	Results from perimeter-to-area analysis.....	75
FIGURE 2.3:	Area of disturbance in Alto Paraiso, Ruropolis, and Uruara.....	78
FIGURE 2.4:	Influence of timing of Landsat image acquisition on proportion of secondary vegetation.....	79
FIGURE 2.5:	Rates of deforestation	80
FIGURE 2.6:	Rates of secondary vegetation clearing and formation.....	81
FIGURE 2.7:	Persistence of secondary vegetation.....	82
FIGURE 2.8:	Rates of clearing and fallow formation for Southeast Asia sites.....	83
FIGURE 2.9:	Persistence of fallow and new clearings in Chiang Mai.....	84
FIGURE 2.10:	Net clearing rates for Southeast Asia sites.	85
FIGURE 2.11:	Influence of observation frequency on rate estimation.....	86
FIGURE 3.1:	JERS-1 SAR and Landsat TM images of study site.....	122
FIGURE 3.2:	Mean monthly precipitation for Rôndonia	123
FIGURE 3.3:	Landscape statistics of mean sigma naught for cleared, secondary vegetation, and forest classes.....	124
FIGURE 3.4:	Landscape statistics of mean backscatter by age of clearing and secondary vegetation.....	125
FIGURE 3.5:	Mean backscatter by age of clearing.....	126
FIGURE 3.6:	Mean backscatter by age of secondary vegetation.....	127

FIGURE 3.7.	Relative biomass estimates for 8-year old secondary vegetation.....	128
FIGURE 3.8.	Relative biomass estimates for 1-year old secondary vegetation.....	129
FIGURE 4.1.	Map of the South America indicating the location of the study site in Rondonia, JERS-1 & TM imagery, and age map of secondary vegetation	154
FIGURE 4.2.	Influence of speckle and texture and temporal variability on confidence limits in estimating backscatter in linear and db units and biomass	155
FIGURE 4.3.	Size class distribution of secondary vegetation and influence of stand size on 95% confidence limits.....	156
FIGURE 4.4.	Individual stand chi-squared values.....	158
FIGURE 4.5.	Coefficient of variation for biomass estimates, as a function of predicted biomass.	159
FIGURE 4.6.	Coefficient of variation for estimates of changes in biomass.....	160
FIGURE 4.7.	Number of contemporaneous JERS images need at each time period to achieve a 50% coefficient of variation on biomass estimates.	161
FIGURE 4.8.	Differences in relative bias, coefficient of variation, and relative RMSE for "observed" biomass from JERS due to normally distributed noise of 0.5db and 1.0db.	162
FIGURE A.1.	Changes in stand development ration with age of secondary vegetation stand.....	165
FIGURE A.2.	Difference in SDR across a range of stand ages.....	166

ABSTRACT

OPTICAL AND RADAR REMOTE SENSING OF LAND USE AND LAND COVER CHANGE IN THE TROPICS: AN ASSESSMENT OF DEFORESTATION AND SECONDARY VEGETATION.

by

WILLIAM A. SALAS

University of New Hampshire, May, 2001

Quantification of the direct impact of land use in the tropics on net biotic carbon flux requires estimates of rates of deforestation, pre- and post-disturbance biomass, and fate of the cleared land. Synoptic observations of the extent, persistence, rates of secondary succession, and structure or biomass of regrowing forests would also help constrain estimates of net carbon flux due to tropical land use. While remote sensing applications can provide estimates of the rates of deforestation and the fate of the cleared land (pasture, croplands, or secondary vegetation), techniques for estimating persistence, rates of succession, and biomass of secondary vegetation are needed.

We documented the spatial and inter-annual variability in the rates of forest clearing, formation rates and persistence of secondary vegetation for 3 sites in Amazonia and 4 sites in Southeast Asia using Landsat TM data from mid-1980s to late-1990s. Secondary vegetation was a large, rapidly changing pool. Variability in the observed

annual rates of deforestation and secondary vegetation formation was high. The transition probabilities of both the formation and clearing of secondary vegetation decreased with age. Persistence of the secondary vegetation pool was also highly variable, likely indicating two distinct land use trajectories: rotational agriculture/pasture maintenance versus abandonment.

We also evaluated the spatial, temporal, and noise constraints of JERS SAR data for mapping and monitoring biomass of secondary vegetation in Rondonia, Brazil. Results indicate that quantitative estimates of biomass using single date JERS-1 imagery is problematic because of temporal variability in backscatter due to intrinsic texture, system noise, and environmental effects. However, JERS-1 data are still useful for distinguishing of secondary vegetation stands at different stages of development. Multi-temporal analysis significantly improves biomass estimates to the point where it is possible to map changes in biomass. Slight reductions in the variability in estimates of normalized radar cross-section greatly improve biomass estimation. Merging JERS-1 SAR data with Landsat TM derived age estimates improved characterization of clearings and secondary vegetation in Rondonia by providing information on the relative differences in secondary vegetation development and residual slash with age.

CHAPTER 1

MAPPING AND MONITORING SUCCESSIONAL VEGETATION IN THE TROPICS WITH REMOTE SENSING

Abstract

The rate at which forests regrow following major disturbances is a key component of net carbon flux from forest clearing. Consequently, developing an ability to map forest regrowth has considerable implications for our understanding of carbon dynamics in a future characterized by increased conversion of old-growth forests and the subsequent abandonment of many areas originally cleared for agricultural activity (e.g. Houghton et al. 2000). Synoptic observations of the extent, rates of secondary succession, and structure or biomass of regrowing forests using remote sensing would provide critical information for understanding the impact of secondary vegetation on the overall carbon budget of Amazonia. Recent research indicates that the success of remote sensing is likely to be highly dependent on the sensors, scale of the observations, the structure of secondary vegetation, and rates of succession. Remote sensing applications for mapping the extent and persistence of secondary vegetation have been extremely successful, resulting in improved understanding of the extent and spatial patterns of secondary vegetation in Amazonia. Direct estimates of the age and successional stage of secondary vegetation have had mixed results. Remote sensing based estimates of biomass

have been problematic. This chapter presents a brief discussion on the importance of secondary vegetation in the Amazon and controls on rates of regeneration, followed by a detailed review of applications of optical and radar sensors for mapping and monitoring secondary vegetation, and concludes with a “straw-man” proposal for systematic monitoring of secondary vegetation with remote sensing.

Introduction

Secondary forests are estimated to occupy over 30% of closed tropical forests and almost 20% of the open tropical forests (Brown and Lugo 1990). Some studies indicate that these percentages will increase substantially over the next 50 to 100 years (Fearnside 1996). Despite the widespread extent of secondary forests in the tropics, the biophysical, ecological, and social processes of succession are not well understood (Walker et al. 2000).

Land use in Amazonia creates a sequence of land cover conditions and land cover changes: primary or mature secondary forests are cleared for crops and/or pasture; croplands are abandoned or converted to pasture; pastures are invaded by invasive herbaceous or shrubby vegetation and become “degraded” or “dirty” pastures (the rate at which these plants become established depends on the site conditions and maintenance); woody and tree species continue the succession process, with pioneer species establishing the initial tree canopy, followed by late pioneer species, and finally primary tree species (Whitmore 1990, Walker et al 2000, Moran et al. 2000). While secondary succession is

typically described as a sequence of land cover conditions, succession occurs along a continuum without hard separations of land cover conditions.

Secondary vegetation occurs as a result of several types of natural and anthropogenic disturbances, including fire, logging, clear cutting for pasture and cropland. The impact on the post-disturbance vegetation community varies depending on the disturbance intensity. Disturbance regimes in the Amazon range from light disturbance, such as highly selective logging, to severe disturbances from strip mining. The succession process is typically characterized by a transition from grasses, shrubs and herbaceous plants, to pioneer tree species (e.g. *cecropia*, *vismia*, babassu palms with relatively short life spans), followed by late successional tree species, and finally primary tree species. Throughout this process there is a general shift toward trees with higher wood density (Brown and Lugo 1990). However, the development of functional relationships between regrowth rates, age, and environmental conditions suffers from a lack of field data in the tropics. Satellite derived estimates of secondary vegetation condition and growth rates would provide critical data for developing functional relationships between disturbance regime, environmental conditions, and rates of succession. Linking field-based observations with remote sensing observations is often hampered by inconsistent terminology between the field ecologists and remote sensing scientists (Campbell and Browder 1995, Walker et al. 2000).

Optical remote sensing has been used extensively to map the extent and rates of deforestation in Amazonia (e.g. Tucker et al. 1984, Malingreau and Tucker 1988, and Skole and Tucker 1993). More recently there have been several studies to map the extent and temporal dynamics of secondary vegetation at the site level for both upland (e.g.

Alves and Skole 1996, Mausel et al. 1993, Skole et al. 1994, Adams et al. 1995, Steininger 1996, Foody et al. 1996) and floodplain areas (e.g. Moran et al. 1994b, Brondizio et al. 1994, Brondizio et al. 1996). Recent results from NASA's Landsat Pathfinder project have revealed that 30% of the cleared areas in the Brazilian Amazon are in secondary vegetation (Houghton et al. 2000). In addition to clearing, logging and fire disturbances convert the landscape to secondary forests.

Based on Markov transition probabilities derived from remote sensing change detection studies in Rondonia (Skole et al. 1994) and Para (Moran et al. 1994a), Fearnside (1996) estimated that the equilibrium landscape of Brazilian Amazon in 2090 in regions where farmers control 30% and ranchers control 70% would contain over 47% secondary forests. With the relatively high cost of proper pasture maintenance and the decline in government subsidies and inexpensive credit, area of secondary vegetation is likely to increase (Moran et al. 1994b).

The impact of this large and growing secondary vegetation pool on the net biotic flux of carbon has yet to be quantified. Consequently, techniques for measuring pre- and post-disturbance biomass, rates of secondary vegetation formation and turnover, and rates of biomass accumulation for secondary vegetation are needed to more accurately estimate carbon fluxes at the basin scale (Skole 1994). Quantitative estimates of the net biotic flux on a decadal average suffer from lack of quantitative data on pre- and post-disturbance biomass and the fate of the disturbed lands (e.g. logged, perennial and annual crops, pasture, or fallow). Estimates of carbon flux due to deforestation, abandonment to secondary vegetation, logging, and fire indicate a net source that varied between 0.1 and 0.4PgCyr^{-1} from 1989 to 1998 (Houghton et al. 2000). This range is based on estimates of

annual deforestation rates from INPE (Instituto Nacional De Pesquisas Espaciais), coupled with ranges in estimates of above-ground biomass, combustion efficiency, decay rates, and carbon accumulation rates by age of the secondary vegetation. The area in secondary vegetation was assumed to be a fixed percentage (30%) of the total area deforested. Given their assumption on abandonment rates, the sources of uncertainty in the carbon fluxes were due to biomass of pre-disturbed forest, deforestation rates, and decay rates, estimated to account for approximately 60%, 25%, and 15% of the range in fluxes, respectively. These “bookkeeping” approaches for modeling carbon fluxes would benefit from spatially explicit estimates of annual rates of secondary growth formation, rates of carbon accumulation, and persistence of secondary vegetation; fluxes associated with secondary vegetation dynamics in Amazonia is such a poorly constrained component of the regional carbon budget (Zarin et al. 2000) that their dynamics are not modeled (Houghton et al. 2000).

The objective of this chapter is to provide a cursory overview of the rates of biomass accumulation and a detailed review of how remote sensing data have been used to map and monitor the extent, persistence, and structure of secondary vegetation in the tropics. While this review focuses primarily on the Amazonia region, a few studies outside of Amazonia are included to highlight remote sensing techniques that are particularly useful in the application of mapping or monitoring secondary vegetation. The final two sections of this chapter present a discussion of new remote sensing based approaches for mapping and monitoring regrowth in Amazonia and a brief presentation of a potential framework for systematic monitoring. Three broad sets of questions form

the underlying basis for much of the research described in this review. The questions can be summarized as follows:

1. Can secondary vegetation be detected using remote sensing? If so, what classes of secondary vegetation can be discriminated?
2. Can remote sensing be used to stratify or characterize classes of secondary vegetation based on structure?
3. Can remote sensing be used to stratify rates of change in secondary vegetation structure, and possibly biomass?

Disturbance in the Legal Amazonia

Prior to disturbance, the Brazilian Amazon, or Legal Amazon, contained approximately 4 million square kilometers of tropical forest, with several major categories of forest formations (see table 1.1). However, by 1988, approximately 230,000 km² of forest had been cleared, and including edge effects had almost 600,000 km² impacted (assuming 1 km buffer of influence) (Skole and Tucker 1993). By 1998, the extent of deforestation in the Legal Amazon had reached 550,000 km² (INPE 2000). Large-scale deforestation can have a large affect on carbon and hydrological cycles and climate to the extent that forest will not regenerate in areas once forested (Shukla et al. 1990). In addition to clear-cut deforestation, selective logging can lead to a significant impact on the forest through increased mortality rates (Uhl and Vieira 1989) and susceptibility to fire (Uhl and Kauffman 1990). Recent estimates of the rate of selective logging in the Legal Amazon range from 5,300 km² yr⁻¹ (Janeczek 1999) to 10,000-

15,000 km² yr⁻¹ (Nepstad et al. 1999). Assessment of the additional impact of logging beyond deforestation requires care because these logging estimates may include areas that are subsequently deforested. Fires have been observed in the Legal Amazon in areas where fire typically did not occur in the past. While there has not been a systematic mapping of fires, estimates suggest that three times as much forest area was affected by fire in 1995 than was deforested (Alaencar et al. 1997, cited in Cochrane and Souza 1998). Despite the wide range in estimates, it is clear that anthropogenic and natural disturbances are altering vast areas of the Legal Amazon, resulting in a mosaic of undisturbed primary forest, disturbed mature forest, secondary vegetation, and non-forested areas.

Disturbance, and the subsequent potential for secondary vegetation, has occurred across a range of forest types in the Amazon. An assessment of the pre-disturbance and post 1986 deforestation extent of broad vegetation classes is provided as a description of the landscape within which secondary succession is occurring. This assessment is based on two datasets: RADAM (RADAMBRASIL) vegetation map of the Legal Amazon and the 1986 Landsat Pathfinder deforestation analysis (Houghton et al. 2000). Table 1.1 contains pre- and post-disturbance area estimates for 11 broad vegetation classes that have been aggregated from the original 161 vegetation classes found in RADAM. The “pre-disturbance” vegetation distribution is based on the RADAM 1:1M scale vegetation maps. The RADAM maps were derived from field observations and aircraft radar imagery acquired in the early 1970s. The RADAM dataset contained an agricultural class where deforestation had occurred. We replaced the agricultural areas with the surrounding vegetation class to derive our best estimate of pre-disturbance vegetation.

The impact of deforestation on the various forest formations in the Amazon was variable, with losses ranging from a <1% to over 45% (see table 1.1).

During the mid-1990s, 50% of the new deforestation occurred in only 10% of all 1/4° grid cells covering the Amazon, while 95% of the deforestation occurred in a region less than 40% of the grid cells, indicating that the deforestation process is spatially concentrated and persistent (Alves 2000). For example, by 1996, 86% of all deforestation was concentrated and occurred within 25 km of areas deforested as of 1978 (Alves 2000). If these trends continue, it is clear that secondary succession will occur in areas that previously supported a broad range of forest formations. Based on a recent estimate that 30% of deforested areas in the Amazon contain secondary vegetation (Houghton et al. 2000) and the INPE estimate of deforestation extent in 1998, secondary vegetation may cover over 165,000 km² of the Amazon basin.

Rate of Biomass Accumulation

Following disturbance, the rate of forest succession and biomass accumulation can vary widely from stand to stand, both within and among regions of the Amazon. Based on field derived biomass measurements, regeneration rates in the Amazon have been shown to range from less than 1 ton ha⁻¹ yr⁻¹ (Nepstad et al. 1991) to over 13 tons ha⁻¹ yr⁻¹ (Uhl 1987) with a range of estimates in between (see for example Uhl et al. 1988, Alves et al. 1997, Steininger 2000, Salimon & Brown 2000, Tucker et al. *in review*). However, some of the observed variability in rates of regeneration may be due in part to variability in the allometric equations used to estimate biomass (Alves et al. 1997,

Tucker et al. *in review*). Theories on the controls on rates of biomass accumulation in tropical secondary forests vary. Some theories indicate that accumulation rates depend on the type and spatial characteristics of deforestation (Uhl 1987), frequency of clearing and abandonment cycles, and type of land use prior to abandonment (e.g. Uhl et al. 1988, Moran et al. 2000), which can impact seed source, viability, and predation of seed stocks (Uhl and Vieira 1988). Alternatively, some theories suggest that, at the regional level, differences in soil fertility and pre-disturbance vegetation cover control rates of succession (Moran et al. (2000). At the intra-regional scale, land use intensity and landscape diversity (e.g. topography and local variations in soil conditions) account for differences in rates of succession (Moran et al. 2000). In a recent study to characterize the impact of climatic, edaphic (principally soil texture), and forest type (broadleaf vs. needle-leaf) on regrowth rates, Johnson et al. (2000) analyzed data from nearly 300 plots for which data on age and aboveground biomass accumulation were available; the secondary forest plots covered a range of ages and were located throughout the world. They report that above-ground biomass accumulation rates in broadleaf secondary forests can be predicted by climatic controls, expressed by growing season length and average growing season temperature, and adjusted by stand age across a sandy versus non-sandy stratification of soil texture (Johnson et al. 2000). Using the Johnson et al. (2000) empirical relationships derived from the global analysis, Zarin et al. (2001) developed predictions of potential regrowth forest above-ground biomass accumulation rates (ABA) for the Brazilian Amazon region based on soil texture and climate data (precipitation and temperature) and tested the predictions using data collected at sites throughout the Amazon (data from Salimon & Brown 2000, Alves et al. 1997, Lucas et al. 1998,

Steininger 2000, Sorrenson 2000, Guimaraes 1993, Denich 1992, Tucker et al. *in review*).

The empirical relationships turned out to be an unbiased linear predictor of biomass accumulation rates on non-sandy soils, with no significant differences between stands following pasture or rotational agriculture (Zarin et al. 2001). There were fewer data for testing the model for stands on sandy soils; based on these limited statistics, the empirical relationships were heavily biased and, thus, require more data for testing the sandy soil model (Zarin et al. 2001).

Remote Sensing of Secondary Vegetation

This section of the chapter provides a detailed overview of advances in mapping and monitoring secondary vegetation in Amazonia using remote sensing. The review is provided in subsections, starting with a general discussion of the spectral properties of secondary vegetation to provide the biophysical background as to how secondary vegetation can be mapped using remote sensing. The following two subsections provide an overview of how optical and radar remote sensing have been used to map/classify secondary vegetation, respectively. The remaining subsections provide an overview of research in mapping characteristics of secondary vegetation, ranging from mapping age to mapping successional stage and biomass.

Spectral Properties of Secondary Vegetation

Forest succession results in changes in leaf biomass, woody biomass, and canopy roughness - forest attributes that can be estimated from remote sensing and used as indicators of how far succession has progressed (Foody and Curran 1994). In general,

values of these attributes increase during succession, each reaching a peak at different stages of their development (Brown and Lugo 1990). Leaf and woody biomass tend to accumulate more rapidly during early stages of succession, followed by an equilibrium in leaf biomass and a slow rate of woody biomass accumulation until stand maturity (Brown and Lugo 1990). During succession the floristic composition of stands change from initial pioneer species to slower developing pioneer species, which are then eventually replaced by climax species (Whitmore 1990). Changes in floristic composition results in changes in canopy roughness, with a peak in canopy roughness occurring late in the succession process when a tertiary canopy has formed (Whitmore 1990). Figure 1.1 contains a conceptual diagram of changes in biomass and canopy roughness during stand development.

Conceptual models of secondary forest recovery (see figure 1.1) have focused on either biomass (e.g. Bormann and Likens 1979) or structure (e.g. Oliver 1981). For optical remote sensing applications, post-disturbance forest recovery should be assessed in terms of vegetation structure rather than biomass because reflectance is a function of the optical properties and structure of the vegetation and not biomass. Background vegetation properties, sun-sensor-target geometry, and topography are additional factors (Kimes 1991). Theoretical understanding of the spectral properties of the landscape at various stages of secondary succession can be made based on chlorophyll absorption, mesophyll reflectance, moisture absorption, and plant structure or geometry relative to the sensing geometry (Brondizio et al. 1996). As abandoned pastures are invaded by herbaceous and shrubby vegetation, reflectance in the visible spectrum decreases due to increased chlorophyll absorption; mid-infrared reflectance decreases

moderately due to increased canopy density and water content and a masking of soils which tend to be highly reflective in the MIR; near-infrared reflectance initially increases due to increased mesophyll reflectance of the new green biomass (Mausel et al. 1993, Moran et al. 1994a, Steininger 1996, Foody et al. 1996). As secondary vegetation stands mature, visible reflectance continues to decrease while the ratio of green to red reflectance increases due to higher chlorophyll content and some shadowing; the near-infrared and mid-infrared reflectance decrease due to infrared “spectral traps” caused by inter-canopy shading, and eventually the reflectance characteristics become indistinguishable from those of mature, undisturbed forest (Mausel et al. 1993, Boyd et al. 1996). In temperate forests, near-infrared and middle-infrared reflectance data are directly related to canopy geometry and degree of inter-canopy shading (Spanner et al. 1990, Fiorella and Ripple 1993). The radiant temperature of forests has been used to estimate biophysical properties (canopy closure, age class, species composition and canopy structure) of temperate forests (Sader 1987) and tropical forests (Luvall et al. 1990). Mapping of secondary vegetation in montane regions of the tropics is more difficult because variations in illumination geometry and changes in ecological zones can mask or hinder differences in spectral responses between undisturbed forest and various stages of secondary vegetation (Helmer et al. 2000). Nevertheless, topography of the Brazilian Amazon is fairly flat, and, hence, topographic influences should be minor.

Mapping Extent of Secondary Vegetation with Optical Remote Sensing

Data from high-resolution optical sensors have been used successfully for mapping the extent of secondary vegetation across a broad range of sites in Amazonia.

Results using Landsat TM, MSS and Spot HRV data for sites in Amazonas (Lucas et al. 1993, Palubinskas et al. 1995, Adams et al. 1995, Steininger 1996, Foody et al. 1996, Boyd et al. 1996, Lucas et al. 1996), Para (Mausel et al. 1993, Brondizio et al. 1994, Moran et al. 1994, Li et al. 1994, Sant'Anna et al. 1995, Brondizio et al. 1996), Rondonia (Skole et al. 1994, Alves and Skole 1996, Kimes et al. 1999, Nelson et al. 2000), and Acre (Salimon and Brown 2000) with relatively high accuracies (85-97% overall accuracies) have been published.

The optical reflectance properties of areas of secondary vegetation change during succession due to changes in vegetation composition, phenology and structure. On the basis of several studies, it appears that the age at which the spectral properties of secondary vegetation become inseparable from mature forest is highly variable. Some studies have indicated that after 14-15 years secondary forest become spectrally indistinguishable from mature forest (Steininger 1996, Moran et al. 1994a, Foody et al. 1996), where as others have indicated that the spectral properties do not merge until 20-30 years (Lucas et al. 1996, Lucas et al. 2000b). Thermal infrared data coupled with middle-infrared (Boyd et al. 1996) or textural data combined with spectral data (Palubinskas et al. 1995) enabled discrimination of secondary vegetation stands older than 14 years from mature forests. In a region with high quality soils (Alfisols) near Altamira, some 6 year old secondary vegetation stands were similar to mature forest, while others were separable to 15 years (Mausel et al. 1993). SPOT HRV visible and near-infrared data, without the benefit of mid- or thermal-infrared data that have been shown to be best for discriminating secondary vegetation (Boyd et al. 1996), have been used to separate 9 year-old stands of secondary vegetation from mature forest (Kimes et

al. 1999). The wide range of ages when secondary forests become spectrally indistinguishable from mature forest is likely due to several controlling factors, including species composition (Lucas et al. 1996), soil conditions (Mausel et al. 1993), and previous land use (Foody et al. 1996). However, while the accuracy of separating secondary forest from mature forest varies with age of secondary forest stands, overall accuracy does not necessarily decrease monotonically with age as might be expected due to stand development, suggesting that stands were developing along different successional pathways (Nelson et al. 2000). Secondary vegetation that develop on sites that have been cleared multiple times are not always more separable from mature forest as those stands that have only been cleared once (Nelson et al. 2000).

Notwithstanding spectral differences, textural information can also be used to improve identification of secondary forests (Palubinskas et al. 1995, Kimes et al. 1999), particularly for older stages of succession (Li et al. 1994). During succession the biophysical properties (e.g. LAI, height, basal area, and density) change with age of the secondary vegetation stands and reach an asymptote (Brown and Lugo 1990). Average stand height and, to a lesser degree, basal area are good indicators of successional stage, with increasing variability in height at later stages of succession (Moran et al. 2000). At the later stages of succession, dominant trees emerge from the upper canopy and the pioneer species begin to die back, creating gaps and increasing canopy roughness (Whitmore 1990, Brown and Lugo 1990). Indicators of these changes or differences in upper canopy structure are manifested as increased texture in optical and SAR data. In addition to spectral separation of successional classes, texture can enhance separability of successional vegetation in TM (Palubinskas et al. 1995, Nelson et al. 2000, Helmer et al.

2000), SPOT (Kimes et al. 1999) and SAR data (Luckman et al. 1997). For example, a classification of four age classes and two types (see Foody et al. 1996) of secondary vegetation with TM textural-spectral data achieved an overall accuracy of over 85%, an increase of 10% and 20% over traditional maximum likelihood and minimum distance pixel by pixel classifiers, respectively, for a region north of Manaus (Palubinskas et al 1995). In Rondonia, the addition of texture measures with TM spectral data into a neural net classifier resulted in an improvement of overall accuracy in mapping mature forest, non-forest, and secondary forest classes from 92.7% to 98.7% with marked improvement in the accuracy of the secondary and mature forest classes (Nelson et al. 2000).

Linear mixture modeling (LMM) for mapping secondary growth is a new alternative and fundamentally different than the more traditional minimum distance and maximum likelihood classifiers in that the radiance data are interpreted in a physical context, rather than in terms of spectral clusters (Adams et al. 1995). The basic premise of linear mixture modeling is that the radiance measured by a sensor is a linear combination, or mixture, of a set of well defined end-members that have fixed spectral properties. Un-mixing the radiance of each pixel into proportions of the end-members can enhance interpretation of the imagery into classes that can easily be related to ground features (Adams et al. 1990). Changes in these proportions over time can be associated with temporal changes in the land cover (Adams et al. 1990). LMM has been tested for mapping several types of land cover near Manaus, including secondary vegetation with different canopy densities (Adams et al. 1995). Four end-members (derived from green vegetation, non-photosynthetic vegetation, soil and shade) were used to classify and map transformations within the landscape based on changes in proportions of end-members. A

field spectrometer was used to generate end-member spectra. Since precise estimation of end-members fractions can be difficult due differences in the spectral properties of soils and vegetation across space and time, a classification scheme was defined based on ranges of fractions that were empirically defined. Temporal changes in the fractions defined land cover change processes (e.g. pasture creation, or pasture abandonment). The LMM approach is relatively insensitive to the particular successional species or vegetation communities (Adams et al. 1995).

There are very few estimates of the extent of secondary vegetation for the entire Amazon basin due to the effort required to analyze hundreds of high resolution images (e.g. Landsat MSS or TM) or limitations of coarser resolution (e.g. AVHRR) data for precise area mapping. The first wall-to-wall analysis of the extent of deforestation and secondary vegetation for the Brazilian Amazon was completed as part of the NASA Landsat Pathfinder Program (Chomentowski et al. 1994). In the mid-1980s and early-1990s, secondary vegetation covered over 30% of the deforested areas (Houghton et al. 2000). While the scale of fine resolution sensors is commensurate with the scale of the land use and, hence, more appropriate for monitoring land cover change (Townshend and Justice 1988), persistent cloud cover in some regions of the tropics and the large expense and effort in analyzing hundreds of images hampers regional monitoring with high resolution optical data. An alternative to performing wall-to-wall inventories for mapping deforestation (Alves 2000) and secondary vegetation is sub-sampling with high-resolution data (Sanchez et al. 1997, Tucker and Townshend 2000). While pure random sampling does not provide precise estimates unless the sample size is very high (for example, over 85%), there are sub-sampling approaches that can produce reliable results.

The higher the spatial concentration of deforestation and secondary vegetation, the smaller a stratified sample is needed to meet *a priori* defined accuracies (Sanchez et al. 1997, Tucker and Townshend 2000). Deforestation in the Legal Amazon has been concentrated around regions of early pioneer settlement or near the network of major roads through the basin (Alves et al. 1999, Alves 2000). However, even with stratified random sampling, large numbers of high-resolution images are required. Coarse-resolution optical and moderate-resolution SAR data are additional alternatives for systematic mapping of secondary vegetation.

Data from the NOAA Advanced Very High Resolution Radiometer (AVHRR) onboard the NOAA series of polar orbiters are acquired several times a day over the tropics. AVHRR is a 5-channel, visible, infrared, and thermal infrared radiometer with a nominal resolution at nadir of 1.1km (Kidwell 1991). Given the high frequency of overpasses and thus a higher probability of obtaining a cloud free observation when compared with Landsat (16day repeat cycle), AVHRR data have been used for mapping land cover and deforestation (e.g. Malingreau et al. 1989, Stone et al. 1994, D'Souza and Malingreau 1994) and fire (e.g. Malingreau 1990, Setzer and Periera 1991) in the tropics. Lucas et al. (2000a) analyzed AVRRR data from the early 1990s using an unsupervised clustering approach, with cluster labeling based on existing maps of secondary vegetation (from Landsat Pathfinder 1992 analysis) to estimate the extent and successional stage of secondary vegetation for the Brazilian Amazon. Clustering of the AVHRR channels 1,2, and 3 alone resulted in an overestimate of regrowth areas due to confusion with some agricultural areas. However, by adding a synthetic layer of the Global Environmental Monitoring Index or GEMI (Pinty and Verstraete 1992), confusion

with agricultural areas was reduced substantially. They estimated that almost 36% (approx 158,000 km²) of the deforested area contained secondary vegetation, a slightly larger area than estimated by the Landsat Pathfinder analysis used to constrain the unsupervised classification class. In addition, they indicated that 48% of the secondary vegetation was in the early colonization phase of succession and less than 5 years old. At the same time, however, AVHRR has been shown to be unable to separate old stages of secondary vegetation from mature forest, indicating that AVHRR based estimates of secondary vegetation extent may be underestimated (Lucas et al. 2000c). The coarse spatial and spectral resolution of AVHRR hinders its utility for mapping secondary vegetation.

Since the spatial resolution of AVHRR pixels range from 1.1km at nadir to over 2.4km by 6.5km at the edges of the scan lines (Goward et al. 1991), images will contain a large proportion of mixed pixels containing sub-pixel fractions of forest, cleared areas and secondary vegetation. Therefore, precise estimates of forest area, or deforestation, are difficult because, pixels typically classified as forest may contain as little as 66% forest (Cross et al. 1991), making area estimates problematic (Skole and Tucker 1993). While non-linear mixture modeling using artificial neural networks can provide estimates of sub-pixel fractions of forest and pasture (Foody et al. 1997a,b), unmixing secondary vegetation fractions is difficult because the range in spectral properties is high and can become indistinguishable from mature forests.

At the basin scale, estimates of the extent of secondary vegetation in the early 1990s range from 107,000 km² (Landsat Pathfinder) to 158,000 km² (Lucas et al. 2000). Based on the Landsat Pathfinder results, 31% of the total area deforested contained

secondary vegetation during this time period. Between states there was significant variability in percentage of deforested lands that contained secondary vegetation, ranging from 5% in Gois to over 65% in Maranhao (Landsat Pathfinder, Houghton et al. 2000). At the landscape scale the percentage of secondary vegetation is also highly variable across landscapes in upland (Moran et al. 1994b, Mausel et al. 1993) and floodplain (Moran et al. 1994b, Brondizio et al 1994) and in time (e.g. Mausel et al. 1993, Alves and Skole 1996, Kimes et al. 1999, Nelson et al. 2000). Variability in the proportion of secondary vegetation at the regional, state and local level, is due in part to types of disturbances. Disturbance regimes vary across the Amazon from, for example, regions of colonization along the trans-Amazon highway, to cattle ranching in Southeast Amazon, to cobocolos and indigenous areas, and to areas of intense logging and mining in Eastern Para (Brondizio et al. 1994, Moran et al. 1994).

SAR Mapping of Secondary Vegetation

While over 25 years of Landsat data have been acquired over the Amazon, high cloud cover limits the usefulness of these data in the Amazon. Synthetic aperture radar (SAR) is an additional tool for monitoring deforestation and forest regrowth in the tropics due to the all weather imaging capability and sensitivity to vegetation structure and biomass. (Sader 1987, Dobson *et al.* 1992, Rignot *et al.* 1995). Over the past few years there have been several studies using synthetic aperture radar (SAR) to map deforestation and secondary vegetation in Amazonia. These studies have been limited by the lack of a space-borne multi-frequency or polarimetric SAR system. Consequently, studies have focused on using single frequency and single polarization space-borne systems (e.g.

JERS-1 and ERS-1) or Space Shuttle based missions of opportunity (e.g. SIR-C). These studies have focused on using SAR intensity, texture, and phase coherence data to map regrowth and estimate regeneration stage (e.g. Rignot et al. 1997, Luckman et al. 1997, Saatchi et al. 1997, and Yanasse et al. 1997).

At C-band, microwave radiation from SAR does not penetrate much into tropical forests and the backscattering coefficient from moist soils can be comparable to the signal from mature undisturbed forest (Rignot et al. 1997, Saatchi et al. 1997, Luckman et al. 1997a). However, even when the micro-scale (sub-pixel) roughness is high (e.g. strong backscatter from soils that is comparable to the response from forests) textural information due to meso-scale (larger than single pixels) roughness can be used to discriminate broad land cover types. Therefore, the utility of textural information for enhancing remote sensing based characterization of secondary vegetation depends on both the canopy structure, spatial resolution of the sensor, and the imaging geometry. Using textural information from an aircraft C-band SAR system with a resolution of 6 meters, Luckman et al. (1997b) were able to separate only mature forest from secondary vegetation at least 6 years old and cleared areas using, while the image amplitude data were indistinguishable across these land covers. However, textural information was not useful for differentiating between young (<6 years) stands and deforested areas without secondary vegetation (Luckman et al. 1997b). L-band data are better than C-band for discriminating secondary vegetation (Luckman et al. 1997a). Furthermore, multi-temporal L-band data significantly increases overall accuracy (Curran and Kuplich 1999). However, accuracy decreases significantly for smaller stands due to the inherent limitations of SAR imagery due to speckle (Yanasee et al. 1997).

Estimation of Age of Secondary Vegetation

Carbon sequestration is typically faster in younger secondary vegetation during the first 30 years, after which the rate of sequestration declines and becomes negligible or zero at 80 years or so (Brown and Lugo 1990). Therefore, research has focused on estimating age of secondary vegetation as a surrogate for carbon content by utilizing general age-biomass relationships (Lucas et al. 1993). Age and age classes of secondary vegetation can be mapped directly using multi-temporal Spot HRV (Skole et al. 1994, Alves and Skole 1996, Kimes et al. 1999) or Landsat MSS/TM (Lucas et al. 1993, Brondizio et al. 1994, Sant'Anna 1995, Nelson et al. 2000) through post classification change detection or Boolean operators. Kimes et al. (1999) followed up the Alves and Skole (1996) analysis and mapped six age classes (1-2, 3, 4-5, 6, 7-8, and ≥ 9 years) using multi-temporal Spot HRV data. Similarly, Lucas et al. (1993) mapped four age classes (<2, 2-3, 3-6, 6-14 years) using both MSS and TM, after noting that successional age classes could not be mapped with single data TM imagery. Temporal gaps in the multi-temporal sequences, caused by cloud cover, data losses, data cost, or lack of continuity between sensors, can potentially introduce errors in age estimates (Kimes et al. 1998). The magnitude of these errors is a function of the number of temporal gaps, length of the gaps, and the rates of secondary vegetation formation and clearing (Kimes et al. 1998).

The age of secondary forest stands have been predicted using neural networks with SPOT HRV and TM spectral and texture measures (e.g. Kimes et al. 1999 and Nelson et al. 2000). The results were not precise, with average age estimates in error from 1.59 years with TM (Nelson et al. 2000) and 2.0 years with SPOT (Kimes et al. 1999) and predicted age explaining only 37% and 38% of variability in age classes for the TM and

SPOT analyses, respectively. However, using two dates of SPOT HRV imagery improved age estimation considerably, with RMSE of 1.3 years and r^2 of 0.75 (Kimes et al. 1999). Since spectral variability across single aged stands is comparable to variability with age, TM spectral and textural data are not sufficient for separating secondary forest into single aged groups. This is not surprising given that rates of regeneration can vary depending on biophysical (e.g. edaphic and climatic) and land use controls. However, by aggregating ages of secondary vegetation into ranges, spectrally distinct classes can be identified (Moran et al. 1994a, Palubinskas et al. 1995, Steininger 1996). A potential shortcoming of the Kimes et al (1999) and Nelson et al. (2000) analyses is the use of reference data with unknown accuracy. Their reference data were based on multi-temporal post-classification analyses of Landsat TM and Spot XS data. While Kimes et al (1999) and Nelson et al. (2000) input classifications may have had high accuracies, all errors are propagated in time by the post-classification merging of the data. Therefore, some of the difficulty estimating stand age and variability within stand age classes was likely due to errors in their reference data which are difficult to quantify due to the stochastic independence of each analysis.

Several studies have focused on using Landsat TM data to separate age classes of forest regrowth. In some regions secondary vegetation stands can be spectrally separated into at most 4-5 spectrally distinct age classes, remaining spectrally distinct until an age of roughly 14 years (Boyd et al. 1996, Brondizio et al. 1996, Foody et al. 1996, Steininger 1996, and Helmer et al. 2000). Textural measures can increase overall accuracies significantly (e.g. >6% increase in overall accuracy and 0.06 increase in weighted Kappa coefficient) (Foody et al. 1996). In general, younger age classes

exhibited the most variability in spectral properties with age, and thus had the highest percentage of classification errors (Foody et al. 1996). Much of the observed variability is due to differences in species composition during the stand initiation phase of succession, potentially indicating distinct and separate successional pathways. Therefore, by stratifying the field data by stand age and successional pathway, higher classification accuracies were obtained with finer successional stage discrimination (Foody et al. 1996). Working near Manaus, Foody et al. (1996) demonstrated that intra-site differences in land use history (short term agriculture versus pasture use) can also have a significant impact on the spectral properties of regrowth stands across age ranges due to differences in species composition (Lucas et al. 1996). A pilot study (Salas and Zarin, unpublished) conducted using Landsat data from Amazonas and Mato Grosso further suggests that the seasonality of precipitation has a significant influence on the rate at which regrowth stands recover mature forest spectral reflectance characteristics in Amazonia.

An alternate approach for analyzing TM data is to transform the spectral bands using a Tasseled Cap transformation (Crist et al. 1986) into *greenness*, *wetness*, and *brightness* indices that may have more “ecologically meaningful interpretations” (Helmer et al. 2000). Several studies have indicated that the *wetness* index, for example, is useful for distinguishing secondary forests from old growth forest in temperate evergreen forests because it is sensitive to differences in structure (Cohen and Spies 1992, Fiorella and Ripple 1993, Collins and Woodcock 1996). While *greenness* had very little variability between shrubs, secondary forests, and undisturbed forests in Costa Rica, the *wetness* and *brightness* indices exhibited a substantial dynamic range between shrubs, young (<6 years), intermediate (6-17 years), and older (>17 years) secondary forest, and undisturbed

primary forest (Helmer et al. 2000). Significant changes in *brightness* (decrease), *wetness* (increase), and to a lesser degree *greenness* (increase) were observed over a 6-year period for young secondary vegetation; these changes were not observed for old stands of secondary vegetations (Helmer et al. 2000). Near Manaus, *brightness* index appeared to be more sensitive to differences in old stands (8-13 years), while the *greenness* index exhibited more dynamic range in younger stands (Steininger 1996). While topography introduced significant noise to the *greenness* and *brightness* indices, it had minimal impact on the *wetness* index, suggesting that it may be useful for mapping secondary vegetation in montane areas (Helmer et al. 2000).

These studies indicate that direct mapping of age of secondary forest stands with single date optical data is problematic due to the similar spectral properties across age classes. The degree of confusion across secondary vegetation age classes decreases as the range between ages classes increases (Kimes et al. 1999). Variability in spectral properties for a given age class can be due to clearing history (Nelson et al. 2000) which can influence the successional pathway and species composition (Foody et al. 1996, Lucas et al. 1996). In some cases, for example Lucas et al. (1993), separation of age classes was not possible with single date TM imagery. However, from an ecological perspective, this is not necessarily an overly troublesome result. Given that the spectral properties of secondary forest depend on the composition, structure, and optical properties of the vegetation and soil, in regions with open canopies, remote sensing is an important tool for improving our understanding of the processes during secondary succession by providing a potential mechanism to stratify secondary forest stands by

structure, and thus enable ecologists to examine differences in secondary forest development.

Persistence and Rates of Secondary Vegetation Formation

Secondary vegetation represents a large and increasing proportion of deforested areas in Amazonia (Skole et al. 1994, Moran et al. 1994). Rates of formation and clearing of secondary vegetation is estimated to be high in Amazonia, with estimates of annual turnover as high as 20% (Uhl et al. 1988). In other words, 20% of cleared areas transition to or from secondary vegetation annually. Multi-temporal satellite analyses provide a unique opportunity for spatially explicit mapping of agricultural lands and secondary vegetation turnover (Skole et al. 1994). Estimates of the persistence, or longevity, are needed to understand the impact of secondary vegetation on biogeochemical cycles, carbon sequestration, and net carbon fluxes. There have been relatively few multi-temporal studies using post classification change detection techniques to map age and dynamics of secondary vegetation in various regions of Amazonia (e.g. Alves and Skole (1996) and Nelson et al. (2000) in Rondonia, Lucas et al. (1993) near Manaus, and Sant'Anna et al. (1995) near Tapajos National Forest). This approach facilitates subsequent analysis of secondary vegetation persistence. For example, Alves and Skole (1996) used multi-temporal Spot HRV imagery for a site in Rondonia to estimate that while the total area of secondary vegetation increased from 1986 to 1992, the percentage of disturbed areas with secondary vegetation was highly variable, ranging annually from 22% to 48%. More than half of the secondary vegetation in 1986 was cleared within 6 years, and only a small proportion (14%) of the secondary vegetation in 1992 was older

than 6 years. Re-clearing of secondary vegetation can represent a large percentage of areas cleared for agricultural use; for example, over 40% of lands cleared for agriculture from 1988 to 1989 for a region of Rondonia came by re-clearing secondary vegetation (Skole et al. 1994). Steininger (1996) documented that, for a region near Manaus, ~50% of cleared areas in 1988 were covered with secondary vegetation in 1991, and at least ~10% of the secondary vegetation in 1988 was cleared by 1991; variability in formation rates and persistence was observed within this region, indicating significant differences in land use patterns across a small region. Additional multi-temporal studies are needed to better quantify the impact of secondary vegetation on the carbon balance of the Amazon.

Mapping Successional Stage

Since optical properties of secondary vegetation are a function of the optical properties of the constituents (leaves and branches) and their structure, which change during succession at varying rates, remote sensing estimation of successional stage seems more appropriate than age. There have been several studies that have used TM (Mausel et al. 1993, Li et al. 1994, Moran et al. 1994a, Palubinskas et al. 1995, Boyd et al. 1996, Brondizio et al. 1996, Foody et al. 1996, Sohn et al. 1999) and AVHRR (Lucas et al. 2000) to map differences in secondary succession with varying degrees of success.

One approach for mapping stage is to create a conceptual model based on known physical components and spectral properties of secondary vegetation to define *a priori* a set of successional stages (Brondizio et al. 1994, Moran et al. 1994). For example, Mausel et al. 1993, Brondizio et al. 1994, and Moran et al. 1994 showed that, based on

theoretical reflection and absorption characteristics of vegetation and soils and known patterns of vegetation development, three broad successional stages can be defined based on relative changes in TM reflective bands during development from pasture to mature forest status (see table 1.2). Based on field observations, the three stages were labeled as initial, intermediate, and advanced succession. Identification of advanced successional vegetation with TM can be difficult due to the spectral similarity with mature undisturbed forest with accuracies less than 75% (Li et al. 1994, others). However, by adding synthetic bands derived from principal components of TM reflective bands and vegetation indices and using a hybrid classifier that utilizes some textural information along with a maximum likelihood classifier, advanced secondary successional can be mapped with fairly high accuracies (>90%) (Li et al. 1994). Another alternative is to use the spectral pattern, defined as the cosine of the angles between multi-dimensional vectors, to discriminate successional stages. This approach minimizes atmospheric and topographic effects and was used successfully ($Kappa > 0.9$) to map 3 successional stages in a region of shifting cultivation in Mexico (Sohn et al. 1999). However, defining many separate or distinct classes or stages of secondary vegetation based on radiance measurements is difficult because the successional process acts along a continuum and, hence, any designation of stages or classes of development are expected to contain fuzzy boundaries between classes (Brondizio et al. 1994).

Estimating Rates of Succession and Successional Pathways

Spectral differences have been observed between young stands dominated by *cecropia* versus *vismia/miconia/bellucia* genera, with young *cecropia* dominant stands

exhibiting higher near-infrared and mid-infrared radiance values (Foody et al. 1996, Lucas et al. 1996). However, as *cecropia* becomes less dominant with age, spectral differences between these forest types decreases (Lucas et al. 1996). The structure of the upper canopy of young *cecropia* dominant stands is distinct with large, horizontal leaves creating a smooth and homogeneous upper canopy, which has fairly high near-infrared and mid-infrared radiance values (Lucas et al. 1996). While there are differences in how the spectral properties change during *cecropia* versus *vismia/miconia/bellucia* development, the spectral properties can overlap between these two forest types for different aged stands. However, TM based spectral data, coupled with age information, can provide accurate (weighted Kappa > 0.93) separation of successional pathways and successional stage during initial phases of succession (Foody et al. 1996). Temporal changes in successional stage have been used to quantify differences in rates of succession using post-classification analysis of an *a priori* defined set of classes (Mausel et al. 1993). Alternatively, some studies have shown that differences in spectral properties of same aged stands with different clearing histories were not sufficient to separate distinct clearing histories (Nelson et al. 2000).

Estimating Biomass of Secondary Vegetation

Red and near-infrared reflectance data have been used to estimate foliar biomass. Increases in the amount of foliar biomass containing leaf pigments result in a reduction in reflectance in the red region, with enhanced reflectance in NIR due to scattering from the leaf mesophyll (Mausel et al. 1993). However, as successional canopies develop, NIR reflectance can drop due to inter canopy shadowing. For

temperate forests, the relationships between red, near-infrared reflectance and biophysical properties (e.g. leaf biomass) have been shown to have a significant correlation up to an asymptote, especially when the red and near-infrared data are expressed as differences (e.g. VI or NDVI) to enhance their inverse relation with biophysical properties (Tucker 1979, Spanner et al. 1990). The relationship between optical vegetation indices (e.g. NDVI and EVI) and foliar biomass, expressed as LAI, is non-linear (Tucker et al. 1981) with saturation occurring at LAI between 3 and 5 (Asrar 1989). Estimates of biophysical properties of tropical forests are difficult due to high foliar biomass, coupled with large atmospheric attenuation from high water vapor content and the potential for very high aerosol content of tropical atmospheres (Singh 1987). The differential attenuation in the red and infrared regions hampers identification of canopy properties with vegetation indices (Singh 1987). For example, Sader et al. (1989) found that NDVI was not a useful predictor of foliar biomass or successional stage in Costa Rica. Nevertheless, increases in NDVI with age have been observed for secondary vegetation up to 6 years, after which NDVI drops and becomes indistinguishable from late succession and mature forest stands (Steininger 1996).

Radar backscatter, in theory, can provide estimates of foliar and woody biomass, as well as differences in canopy roughness based on micro-scale and meso-scale surface roughness effects. Differences in canopy roughness can be detected through analysis of meso-scale surface roughness as long as the “amplitude” of the canopy roughness is larger than the resolution of the imaging radar (Trevett 1986).

Multi-frequency, polarimetric SAR data at longer wavelengths can provide important information on stand structure and even biomass. There is a general

consensus that multiple frequency, polarimetric SARs can provide accurate estimates of biomass for successional forests up to a certain biomass level and that variability in radar backscatter saturates at higher biomass levels for longer wavelength SARs (summarized in Kasischke *et al.* 1997). There are very few polarimetric SAR data sets available for the tropics, especially for the Legal Amazon. However, during two Space Shuttle missions in 1994, the SIR-C instrument collected L- and C-band polarimetric SAR data of the Legal Amazon. Estimates of the saturation point of L-band backscatter from tropical forests vary from 40 tons/ha (Imhoff 1995) to 60 tons/ha (Luckmann *et al.* 1997). There has been considerable research in the use of AIRSAR for mapping biomass in temperate forests (e.g. LeToan *et al.* 1992, Ranson and Sun 1997, Dobson *et al.* 1992). These studies indicate that with AIRSAR data, it is possible to estimate biomass levels up to 200 ton/ha. There have been relatively few studies for tropical forests. Initial results of the saturation point for tropical forest indicate that biomass can be estimated to 200 tons/ha (Rignot *et al.* 1995, Hoekman and Quinones 2000) with an ability to differentiate up to 8 biomass classes with a high degree of precision (Hoekman and Quinones 2000). A 200 ton/ha biomass saturation point for P-Band inversions is high enough to cover a large portion of the expected range of biomass for secondary regrowth in the Amazon given that the majority of the regrowth stands are less than 15 years old (Skole *et al.* 1994, Lucas *et al.* 2000a) and the rate of biomass accumulation appears to range from less than 1 to 13 ton ha⁻¹ yr⁻¹ (e.g. Uhl 1987, Nepstad *et al.* 1991). While the use of P-band polarimetric data is extremely promising for estimating biomass of secondary vegetation in the Amazon, there has been very little research due to the lack of P-band data for the Amazon. Luckman *et al.* (1997) used measured stand characteristics and allometry to

estimate biomass for 13 stands of secondary forest in central Amazonia, with ages between 2 and 22 years. Of these 13 stands, eight had biomass levels above the assumed saturation point for L-band backscatter estimates, while none of the stands exceeded the 200 ton/ha saturation point for P-band. From this it is clear that a longer wavelength SAR system is needed to map secondary vegetation biomass in Amazonia. Currently there are no long wavelength polarimetric SAR systems on spaceborne platforms. Therefore, for the Amazon the only suitable SAR system for mapping secondary vegetation biomass would be an aircraft based multi-frequency (C, L, and P-band), multi-polarization SAR (e.g. JPL TOPSAR/POLSAR).

Monitoring Secondary Succession in Amazonia with Optical Remote Sensing: A Proposal for a Five Component System.

Although vegetation indices and various combinations of individual spectral bands can be used as a measure of secondary succession, structural properties of forests may also be characterized with multi-angle remote sensing measurements. Multi-angle remote sensing provides a unique opportunity for estimating differences in both meso- and micro-scale canopy roughness. Meso-scale roughness is derived from image texture (pixel to pixel variability), while micro-scale roughness is derived from differences in reflectance properties under different viewing geometries. Image texture is dependent on both canopy roughness and spatial resolution of remote sensing observations.

When measured from multiple viewing angles, assessment of structural properties of a forest canopy can be enhanced (Strahler and Jupp, 1990, Qi et al., 1995, Jupp and Walker 1997). Bi-directional properties of forest canopy are often unique and can be used

as indicators of forest structure, density, and composition. Once again using the Oliver (1981) conceptual model of succession, at different stages of development, secondary succession stands will have different clump sizes, leaf and stem angle distributions and sizes, crown geometry, and proportion of inter-canopy shadowing, all of which can affect remote sensing measurements (Asner et al., 1998). At the later growing stages, changes in structural properties may not affect the spectral properties as observed from a nadir looking sensor such as TM. However, each of these properties has profound influences on observations from oblique viewing angles, and therefore bi-directional properties. Successional stand structure can, consequently, be represented by multiple view angle measurements, which will be provided by sensors like ASTER, MODIS, and MISR sensors. Bi-directional reflectance distribution (BRDF) models have been created based on empirically and theoretically derived relationships between canopy properties and radiative properties of vegetation constituents (Goel, 1988, Myneni et al., 1989, and Strahler, 1997). BRDF model inversions can then be used to estimate canopy structural attributes (Goel and Thompson, 1984, Qi et al., 1995, Jacquemoud et al., 1995, Privette et al., 1996, and Knyazikhin et al., 1998). With recent availability of data from multiple view angle sensors at a moderate resolution, research on mapping the structure of secondary vegetation in the Amazon using BRDF model inversions should proliferate and provide useful techniques for monitoring.

Since secondary succession proceeds along a continuum of changes in stand composition and structure, and not as a series of discrete steps, remote sensing based characterization should shift away from discrete age classes or successional stages to parameterization of continuous variables, such as canopy roughness, geometry, or even

biomass, if possible. In the absence of discrete classes, evaluation or accuracy assessment of this type of approach will require methods that rely on fuzzy logic (Gopel and Woodcock 1994). This section of the chapter presents a proposal for an approach for routine monitoring of secondary vegetation in the Amazon, which uses a combination of “tried-and-true” and novel remote sensing techniques. The components of this monitoring system are designed specifically to provide quantitative data to aid our understanding of the response of Amazonian ecosystems to disturbance. While previous studies indicate that several successional age classes can be mapped, we propose using a different approach by developing coupled estimates of successional stage and regrowth rate. This would enable use of remote sensing technologies to assess not only the current stage of a successional stand but also the dynamics and future of regional biomass and carbon accumulation. We propose 5 components outlined here:

Component 1: Multi-temporal analysis for mapping extent, age and disturbance

intensity:

This component consists of a multi-temporal analysis of optical data (e.g. Landsat and SPOT) to map extent and age, with a set of rules to define disturbance intensity based on clearing frequency. These multi-temporal analyses would also provide quantitative data on the dynamics of formation and re-clearing of secondary vegetation. There are two broad approaches for multi-temporal analyses: post-classification change detection and changes in spectral characteristics. Although the post-classification approach requires high accuracy for the individual classifications, the spectral approach requires detailed calibration and atmospheric correction. However, from published results

it is clear that classification of cleared areas is relatively easy and can be done with very high accuracies (>97%). Therefore, mapping age can be achieved by tracking areas that have been cleared and then are no longer classified as cleared, so the more difficult step of separating secondary vegetation from forest is not necessary. In addition, multi-temporal analysis will also provide information on age of cleared areas, that can then be used to estimate below ground carbon fluxes (Morais et al. 1998).

Component 2: Development of scalable, BRDF estimates of canopy structure:

While ASTER, MODIS, and MISR data are all multidirectional, the resolution (15-30m) of ASTER is comparable to TM and fine enough to map stands of regrowth in the Amazon. To evaluate the influence of scale, MASTER data (MODIS and ASTER Simulator) could be used to investigate the use of BRDF models in inferring structural information of forest canopies. The candidate BRDF models include the Li-Strahler model (1985) and its modified versions (Li and Strahler, 1992), and 3-D model of Myneni and Asrar (1993). These models have also been selected as candidate models for mapping global leaf area index and fPAR by MODIS and MISR teams (Running et al., 1994, Myneni et al., 1997, and Knyazikhin et al., 1998). The inversion technique has been shown to be promising (Scarth and Phinn, 2000, Jupp and Walker, 1997) and we will apply it to MASTER at local scale and MODIS data at large scales. Airborne videography data would provide additional bi-directional measurements, due to a continuous acquisition of multiple frames by the system, and potentially provide more directional sampling than MASTER. The videography, MASTER, and MODIS data

would allow investigation for estimating the structural properties of forest canopies at a range of spatial scales from meters to kilometers.

The products from the BRDF modeling effort would include a set of forest parameters such as branch distribution, orientation, leaf optical properties and shadowing, all of which are structural characteristics of forest canopies. These parameters would be validated with ground *in-situ* measurements at the study sites and compared across a chrono-sequence of stands to assess rates of succession. These estimates of canopy structure could also then be compared with model predictions of succession stage.

Bi-directional properties of optical remote sensing are primarily dependent on the macro-level structures of forest canopies, which include forest openings, gap fraction, tree size, and branch distributions. Changes in any of these structural characteristics, which alter shadowing and mutual shading, would have substantial effects on remotely sensed bi-directional properties. Therefore, changes in structural properties can be inferred from directional measurements by sensors such as MODIS, ASTER, and MASTER. These bi-directional properties, however, also depend on the spatial resolution of remotely sensed imagery. Large pixel sizes represent averaged radiance measurements over larger areas and thus have high probability of including more components (shaded leaves, shadow, sunlit leaves, exposed soil/substrates, and branches and trunks), and, therefore, reflect a composite value of all components. When a pixel size is large enough to encompass a sufficient number of different components, the bi-directional properties may be “smoothed” and averaged out. In this case, bi-directional measurements may not be able to extract structural information. If a pixel is very small, on the other hand, the observed radiation may only reflect an individual component and,

therefore, the bi-directional properties may also be lost. We believe that there is an optimal spatial resolution at which structural information of a forest canopy can be inferred from bi-directional measurements. For this proposal, 5m resolution MASTER data, acquired with multiple paths over our sites to increase the number of angular samples, would be ideal. The fine resolution MASTER data would then be aggregated to match ASTER (15m), ETM+ (30m), and MODIS (500m and 1000m). By examining the bidirectional properties of the aggregated MASTER imagery, in comparison with ASTER, if available, ETM+, and MODIS data, an optimal resolution can be determined.

Component 3: Mapping structural classes of secondary vegetation:

This component focuses on development of algorithms for spectral retrieval of secondary vegetation structural classes using visible and infrared reflectance data. This approach requires the retrievals be based on highly parameterized relationships between spectral reflectance and ground-based measures of vegetation structure developed in component 2. Relationships between remote sensing spectra and vegetation structure should focus on the vegetation structural attributes that influence the spectral signatures (e.g. canopy closure and canopy roughness). The parameterization must be developed for every region studied. Accurate atmospheric correction and radiometric calibration is required for this approach. Estimates of successional stages and regrowth rates would be derived, at the stand level, from three types of MASTER spectral indices and a BRDF model inversion. These spectral indices would include a traditional vegetation index based on differences in blue, red and near-infrared reflectance (EVI), an index based on the relative reflectance between the successional and mature forest stands (successional

development ratio), and a pattern index based on spectral angles (successional development index). These estimates of successional state and regrowth rates would be carried out at a set of remote sensing/validation sites located across a climate gradient in the Amazon and on two distinct soil textures. Figure 1.2 illustrates a set of sites that would provide a gradient in climate conditions, across major soil texture differences, and would contain large differences in land use intensity (D. Alves, pers. com.). Scalability of the spectral indices and BRDF model to the scale of ETM+, ASTER, and MODIS would be tested by degrading the high resolution MASTER spectral data. Calibration and validation of these relationships will rely on using field estimates of succession state and structure, and, if available, LIDAR estimates of canopy height and vertical profiles.

In addition to the bidirectional property dependency on spatial resolution, vegetation indices also vary with spatial scale (e.g. Teillet et al., 1997). Spectral vegetation indices, like NDVI and EVI, computed at various spatial resolutions will represent different components of the forest. For example, if a pixel is very small, the measured reflectance may be due to only shaded branches, or shadows, or bare ground, depending on the spatial heterogeneity of the forest canopy. This inter-play between the scale of the sensors and canopy heterogeneity presents a challenge in interpretation of indices at variable spatial scales. If a spatial resolution is too large, detailed structural information may be lost due to a composite effect. Therefore, we believe that an optimal scale exists that would be best for forest structural analysis of regrowing forest in Amazonia and it can be derived by examining spectral indices using aggregated MASTER imagery in combination with MODIS and ASTER data.

Component 4: Mapping Recovery Rates:

Remote sensing data would be used to monitor relative changes in secondary vegetation structure (canopy closure and roughness). Components 2 and 3 would provide data on secondary vegetation age and structure. This component would focus on monitoring relative changes in spectral signatures, across a chronosequence of secondary vegetation stands, to estimate differences in recovery rates. Combining stand age information with changes in spectral properties would be used as an estimate of relative recovery rates. Radiometric and atmospheric normalization would be applied using the approach of Hall et al. (1991) to compensate for varying atmospheric conditions, changes in instrument calibration, differences in sensor response functions, and other temporal effects. Spectral-temporal changes and trajectories would then be mapped using change vector techniques (Johnson and Kasischke 1998) to quantify differences in succession and successional pathways.

Component 5. Assessment of Disturbance Specific Controls on Rates of Recovery:

Influence of the size and intensity of disturbance on recovery rates in Amazonia would be assessed by combining relative recovery rates based on spectral data with spatial and temporal information from multi-temporal analyses. The size (area cleared), proximity to seed source (e.g. distance to mature forest) and the land use intensity (e.g. period of pasture use, clearing frequency, number of fallow rotations) would be derived directly from the multi-temporal analyses and then analyzed in a GIS to develop a set of site specific rules of recovery rates based on land use.

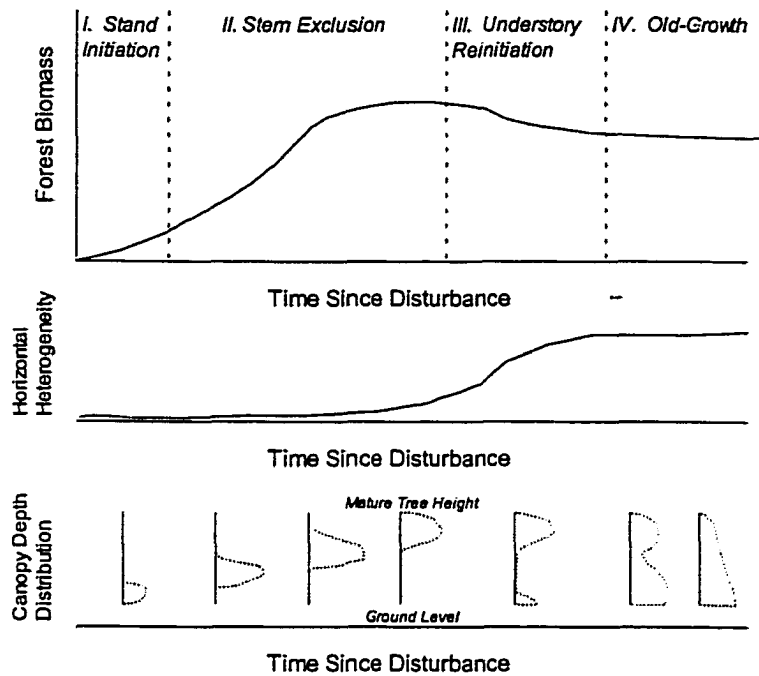


Figure 1.1 Conceptual diagram relating biomass recovery (Bormann and Likens 1979) to forest structural stages (Oliver 1981) following disturbance. The bottom chart shows the expected vertical profile of foliar biomass accompanying each stage. Each stage also has implications for horizontal heterogeneity and structure. Figure created by Mark Ducey (Department of Natural Resources).

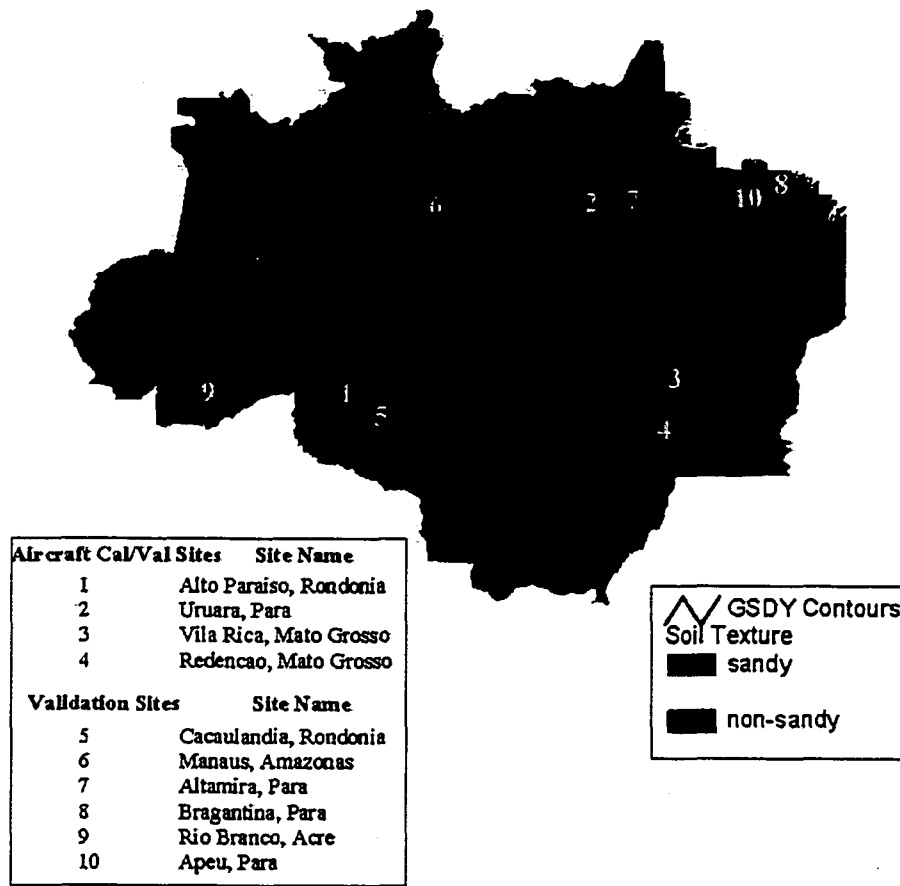


Figure 1.2. Locations of proposed aircraft Cal/Val field sites and the validation sites (in yellow) and growing season degree year (GSDY) contours (in blue) overlaying a coarse-resolution (1° by 1°) soil texture map of the Brazilian Amazon. Soil texture was defined based on porosity, matric potential at saturation, saturated hydraulic conductivity, and the slope of the retention curve (Meeson et al. 1995). GSDY was calculated as the mean monthly temperature (Jones 1994) for months with precipitation (Hulme 1995) greater than 100 mm.

Class #	RADAM Aggregated Vegetation Class	Pre-disturbance Area (10 ³ sq. km)	Area Deforested by 1986 (10 ³ sq. km)	Post-disturbance Area (10 ³ sq. km), [%loss]
1	Savanna/Savanna Estepica	726	7	719 [1.0]
2	Floresta Estacional Decidual	31	14	17 [45.2]
3	Floresta Estacional Semidecidual	55	8	43 [21.8]
4	Floresta Ombrofilia Densa	2,001	44	1857 [7.2]
5	Floresta Aberta	1,108	60	1048 [5.4]
6	Pioneiras/Campinarana	186	4	182 [2.2]
7	Savanna/Ombrofilia	192	17	175 [8.9]
8	Ecological Refugio	2	0	2 [0]
9	Savanna/Floresta Decidual Contato	216	17	199 [7.9]
10	Floresta Ombrofilia/Decidual Estacional	203	22	181 [10.8]
11	Pioneiras/Capinarana/Ombrofilia Contato	223	1	222 [0.4]

Table 1.1. RADAM vegetation classes for the Legal Amazon. Pre-disturbance area estimates are based on a digitized 1:1M scale maps with areas of disturbance replaced by surrounding vegetation class. Post-disturbance area estimates for 1986 are based on the Landsat Pathfinder deforestation data set overlaid on the pre-disturbance map.

	Visible Reflectance	NIR Reflectance	MIR Reflectance
Pasture/crop areas*	High	Variable, < SS1	High (dry soils)
SS1	Moderate	High	Moderate
SS2	Moderate, higher green/red ratio	Moderate	Low-Moderate
SS3	Low, with higher green/red than SS1, SS2	Low	Low
Mature Forest	Low	Lowest	Lowest

Table 1.2 Relative spectral properties of successional stages , as defined *a priori* by Mausel et al. 1993, Brondizio et al. 1994, Moran et al. 1994. SS1 is the initial succession stage consisting of areas with tall grasses and some woody/forest growth. SS2 is intermediate succession with larger trees, 8-12m tall, and beginning to develop a multi-canopy. SS3 is more advanced stage of succession with a maturing multi-canopy with some trees taller than 20m. * assumes imagery is acquired during the dry season after annual crops have been harvested.

CHAPTER 2

INTER-ANNUAL VARIABILITY IN DEFORESTATION AND REGROWTH IN THE TROPICS

Abstract

Estimates of land cover change dynamics for three sites in the Amazon (Alto Paraiso, Rondonia; Uruara and Rurupolis, Para) and four sites in Southeast Asia (Chiang Mai, Thailand; Kachin State, Myanmar; Upper Ca River, Laos; and Lower Ca River, Vietnam) were derived from multi-temporal Landsat TM data. The objectives of these analyses were to document the spatial and inter-annual variability in the rates of forest clearing, secondary vegetation formation, and persistence of secondary vegetation. Annual, or nearly annual, Landsat TM data from mid-1980s to late-1990s were classified into broad land cover classes (forest, non-forest, secondary vegetation, and water) using unsupervised classification with knowledge-based manual editing to facilitate high classification accuracies. Pasture, perennial crops, rotational agriculture, and abandonment into long-term fallow are the dominant land uses in these regions. Results indicate secondary vegetation was a large, rapidly changing pool. Variability in the observed annual rates of deforestation and secondary vegetation formation was high. The transition probabilities of both the formation and clearing of secondary vegetation decreased with age. Persistence of the secondary vegetation pool was also highly variable, likely indicating two distinct land use trajectories: rotational agriculture/pasture

maintenance versus abandonment. However, some of the observed variability was likely due to seasonality of the Landsat data acquisition and the period between subsequent classifications.

Introduction

Explicit estimates of annual rates of deforestation, secondary vegetation formation and persistence are needed to refine estimates of net carbon flux from tropical land use. The significance of secondary vegetation on carbon fluxes is a function of the extent of secondary vegetation, biomass accumulation rates, and persistence of the secondary vegetation (Skole et al. 1994). Fine spatial and temporal scale information on land cover change dynamics is critical since the “patterns and timings” of deforestation and abandonment impact biogeochemistry and hydrologic processes (Skole et al. 1994). Case studies using multi-temporal satellite data are needed to understand local-scale dynamics of deforestation, abandonment, and secondary vegetation turnover (Skole et al. 1994).

This chapter focuses on the following research questions:

- Are the annual rates of deforestation and abandonment to secondary vegetation significantly different from the decadal mean?
- How long does secondary vegetation tend to persist and, therefore, what fraction of the secondary vegetation pool represents rotational agriculture versus long-term abandonment?

Global Carbon Cycle

Ever since measurements of atmospheric CO₂ have been made on a regular basis (e.g. Keeling’s Mauna Loa records) global carbon cycle research has focused on trying to

balance the “budget”. Initially simple source/sink models were used to balance the budget based on reported fossil fuel consumption, estimated tropical land use changes, and modeled oceanic uptake. However, these sources and sinks could not account for the observed rise in atmospheric CO₂ concentration, leading to the search for the “missing sink”. With the availability of more detailed atmospheric and oceanic measurements collected at a global scale with a relatively fine temporal scale, new techniques and approaches have been used in an attempt to find the “missing sink” and balance the carbon budget. These new techniques have focused on better modeling of the net fluxes in either the oceanic or terrestrial carbon pools and the direct measurement of atmospheric constituents ([CO₂], O₂/CO₂, δ¹³C) to estimate fluxes of carbon between the atmospheric, oceanic, and terrestrial pools. The concentration of atmospheric CO₂ is designated by [CO₂].

Tans et al. (1990) used a global atmospheric circulation model to redistribute atmospheric CO₂ based on surface fluxes of CO₂ due to fossil fuel consumption, tropical deforestation, and oceanic uptake. They estimated the annual oceanic uptake, based on seasonal CO₂ partial pressure differences at the air-ocean interface and monthly climatological wind data, to be an average annual net sink of 1.6GTC (Giga-Tons of Carbon). They assumed that tropical land use contributes 1.0 to 2.5 GTC per year to the atmosphere. Their assumption for the tropical biotic source term was within the range of the 1994 IPCC estimates of 1.6±1.0 GTC per year (IPCC 1994). The atmospheric circulation model predicted that the atmospheric [CO₂] should exhibit a strong north-south inter-hemispheric gradient of 5.7 to 7.3 ppm. This estimate was significantly higher than the observed gradient of 3ppm based on the NOAA flask measurements (Tans et al.

1990). They speculated that the source of this discrepancy could either be their atmospheric transport model or an unaccounted for extra-tropical terrestrial sink in the Northern Hemisphere. Their analysis of ^{85}Kr and CFC tracer data indicated that inaccuracies in their transport model could account for differences of only 10% and not the two fold differences measured. Thus, they assumed that the “missing sink” was a terrestrial sink of 2.0 to 3.4 GTC in the northern hemisphere temperate zone. Siegenthaler and Sarmiento (1993) updated the Tans et al. (1990) oceanic uptake estimates by accounting for differences in ocean skin temperature and bulk water temperature, horizontal transport of carbon from the terrestrial biosphere to the ocean via rivers, and the north-south transport of carbon monoxide and its subsequent uptake in the southern oceans. From this they estimated that oceanic uptake was nearly 2.0 ± 0.6 GTC per year. As a result, they concluded that either there is a terrestrial sink of about 1.8 ± 1.3 GTC, or that the tropical source term of 1.6 ± 1.0 GTC is too high, or a combination of both. This highlights an important aspect of these constrained models, namely, that the magnitude of the inferred temperate sink is a function of the magnitude of the tropical source term. Another aspect of these analyses is that they rely on atmospheric transport models to spatially distribute atmospheric carbon. This spatial distribution is constrained by the atmospheric flask measurements.

A second approach is to use direct measurements of atmospheric or oceanic carbon content to estimate spatial and temporal patterns of carbon fluxes. This approach yields flux estimates that are not model dependent. Quay et al. (1992) estimated the net flux of CO_2 in the ocean and terrestrial biosphere using isotopic measurements of $\delta^{13}\text{C}$ (essentially the ratio of $^{13}\text{C}/^{12}\text{C}$) in the atmospheric CO_2 and dissolved inorganic carbon

from ocean surface waters. $\delta^{13}\text{C}$ varies depending on the source of the carbon and changes depending on the uptake mechanism due to isotopic fractionation. Therefore changes in this ratio provide an indication of the uptake mechanisms (Quay et al. 1992, Ciais et al. 1995a). Because terrestrial photosynthesis discriminates against the heavier isotope (^{13}C), atmospheric uptake can be partitioned between the ocean and the terrestrial biosphere (Quay et al. 1992, Sarmiento 1993, IPCC 1994, Ciais et al. 1995a). Quay et al. (1993) used this technique to estimate that from 1970 to 1990 the average annual oceanic uptake was 2.1GTC, while the average annual terrestrial uptake was negligible (0.1GTC).

Ciais et al. (1995a, 1995b) used a hybrid approach involving a two-dimensional atmospheric transport model (like Tans et al. 1990) with CO_2 and $\delta^{13}\text{C}$ measurements from NOAA's Climate Monitoring and Diagnostics Laboratory (CMDL) global flask network (like Quay et al. 1992) to estimate CO_2 partitioning as a function of latitude and time from 1990 to 1993. Their procedure relied on: estimates of the discrimination against ^{13}C by photosynthesis as a function of latitude and time using the SiB model; calculation of isotopic composition of respired soil carbon from various turnover pools using the CENTURY model; and estimated spatial distribution of $\delta^{13}\text{C}$ in ocean from ship cruise data. Their results indicate that the northern temperate zone was a large terrestrial sink (3.5 GTC) in 1992 and 1993, whereas the biosphere in the northern tropics (from equator to 30°N) was a large source (2.0 ± 1.3 GTC) of carbon. This tropical source estimate is considerably higher than the estimates of 0.9GTC by Houghton et al. (1987) and 1.6 ± 1.0 GTC by the IPCC. Ciais et al.(1995b) attributed this difference to either a problem with their intra-hemispheric transport between the tropical and temperate latitudes or that previous deforestation estimates were lower than the actual deforestation.

It is also interesting to note that they estimated that the southern tropics was a small terrestrial sink in 1992 and 1993. This is surprising because this latitudinal band contains Brazil and Indonesia. Estimates of CO₂ emission from tropical land use rank these two countries as the top two in terms of total emissions due to deforestation. The weak terrestrial sink in the southern tropical zone suggests that either the forests have a positive net ecosystem production (due to fertilization of undisturbed forest and/or secondary growth formation) or deforestation has been overestimated (Ciais et al 1995a).

Photosynthesis converts CO₂ and water into organic carbon and molecular oxygen (O₂). While combustion and respiration work in the opposite direction with the oxidation of organic compounds producing CO₂. Atmospheric [O₂] is a function of photosynthesis, respiration and combustion, and varies inversely with atmospheric [CO₂]. However, changes in atmospheric [O₂] are difficult to measure because they are very small compared with the overall atmospheric concentrations (Keeling and Shertz 1992). Changes in [O₂] can be estimated by changes in the ratio of O₂/ N₂ because [N₂] is relatively stable. Since O₂ is not chemically active in the ocean due to its low solubility, changes in atmospheric [O₂] can then be related to fluxes of CO₂ from the terrestrial biosphere (Keeling and Shertz 1992). The O₂ based estimate of net terrestrial exchange of CO₂ can be used to constrain the oceanic CO₂ uptake based on atmospheric measures of CO₂. Keeling and Shertz (1992) used this technique to estimate an annual oceanic uptake of 3.0±2.0 GTC and an annual net terrestrial sink of 0.2±1.7 GTC. Keeling et al. (1996) used O₂/ N₂ data from 1991-1994 to measure hemispheric gradients in CO₂ uptake. They estimated that on an annual basis from 1991 to 1994 the terrestrial biosphere was a net sink of 2.0±0.9 GTC, tropical land biota was not a strong source or sink, and the oceans

were a net sink of 1.7 ± 0.9 GTC. Using longer term trends in O_2/N_2 , they estimated that the measured slow down in the rate of increase in atmospheric CO_2 was due to either increased CO_2 uptake in the temperate land biota or the removal of a net tropical source of CO_2 due to decreased rates of deforestation.

Precise spatial reconstruction of the historical terrestrial sources and sinks of carbon is hampered by the relatively few number of CO_2 monitoring stations (Bousquet et al. 2000) and resolution of the hemispheric transport models (Rayner et al. 1999). Some inversion studies have compensated by aggregating latitudinal bands into broad regions. For example, Rayner et al. (1999) estimated annual mean land and ocean fluxes of carbon for northern hemisphere, southern hemisphere, and tropical regions. While the annual oceanic flux for the tropics was estimated to be highly variable and coupled with El Niño/Southern Oscillation (ENSO), the annual net flux for tropical land areas varied between a net source (over 0.5GTC) and sink (over 1 GTC) from 1980 to 1995 (Rayner et al. 1999). A recent inversion study using 20 years of atmospheric CO_2 data by Bousquet et al. (2000) indicates that, during the 1980s, the tropical land areas were largely responsible for the observed inter-annual variability in global carbon balance. However they also indicated that, during the early 1990s, the mid- to high-latitude land areas drove the observed inter-annual variability in carbon balance, and, from 1996-1998, the tropical, temperate, and boreal land areas contributed equally to the observed variability.

Variability in carbon storage has also been estimated for Amazonia using a transient process-based biogeochemical model (Tian et al. 1998). During El Niño years the undisturbed regions of Amazonia were estimated as a source of up to 0.2GTC and a

sink of up to 0.7GTC in non-El Niño years (Tian et al. 1995). These estimates are large compared with flux estimates based on land use change, which indicate a source ranging from 0.2GTC (Houghton et al. 2000) to 0.3GTC (Fearnside 1997). Our understanding of the carbon balance of the Amazon basin is confounded further by net carbon flux estimates based on eddy covariance measurements which indicate that the basin as a whole was a huge (1.2GTC) sink in 1987 (Fan et al. 1990) and large (0.5GTC) sink in 1992/1993 (Grace et al. 1995).

While these analyses seem to point to a significant temperate terrestrial sink for carbon, the carbon balance of the tropical biota is still uncertain and, therefore, it is still extremely important to quantify the annual net flux of carbon due to tropical land use. These data would serve several purposes. Annual, spatially explicit estimates of CO₂ emissions due to tropical deforestation and land use would help resolve some of the discrepancies resulting from these recent carbon models using annual atmospheric measurements. Annual deforestation data could be used to validate or identify problems with these carbon models, such as intra-hemispheric transport between the tropical and temperate zones or potential positive NEP in the tropical forests (Ciais et al. 1995a). In addition, in order to assess where carbon uptake is occurring over the long term, it is necessary to isolate inter-annual variability in carbon fluxes from long-term mean fluxes (Bousquet et al. 2000). The only way to properly validate these annual models is to have contemporaneous data on annual changes in carbon emissions due to tropical land use.

Estimates of Deforestation and Secondary Growth Formation due to Tropical Land

Use

FAO estimates that the average annual rate of tropical deforestation in the late 1980s and early 1990s was 15.4×10^6 ha (FAO 1993). The regional contributions of this global annual rate are 4.1, 3.9; 7.4×10^6 ha for Africa, Asia & Pacific, and Latin America & Caribbean, respectively. FAO estimated that for Continental Southeast Asia (Cambodia, Laos, Myanmar, Thailand, and Vietnam) the average annual deforestation rate from 1980 to 1990 was 1.3×10^6 ha. Early results from NASA's Landsat Pathfinder Humid Tropical Forest (LP HTF) project suggest the average annual rate from 1973 to 1985 was 1.4×10^6 ha. Since actual annual rates of deforestation may be highly variable, care must be taken for direct comparison of these estimates because of differences in the definition of deforestation, forest cover, and periods of the respective analyses.

Within the Latin America & Caribbean region FAO estimated that during the 1980s the average rate of deforestation for Tropical South America was 6.2×10^6 ha, with Brazil alone at 3.7×10^6 ha per year. Recent satellite analyses of the Brazilian Amazon indicate that from 1978 to 1988 the rate of deforestation was between 1.6 - 2.2×10^6 ha per year (INPE 2000, Skole and Tucker 1993). Estimates from the LP HTF project suggest that the average annual rate of deforestation in the Brazilian Amazon from 1986 to 1992 and 1992 to 1996 was 1.65×10^6 ha and 1.4×10^6 , respectively. INPE began mapping annual extent of deforestation in 1989 using 1:250,000 scale Landsat photoproducts (INPE 2000). Their estimates of annual rates revealed large differences in rates from 1989 to 1998, ranging from a low of 1.1×10^6 ha in 1991 to a peak of 2.9×10^6 ha in 1995. While INPE provides annual deforestation estimates, data on the extent and formation

and turnover rates of secondary vegetation are needed. An analysis of annual high resolution imagery (e.g. Spot XS or Landsat) could provide such data.

Role of Secondary Growth in Net Biotic Release of Carbon Due to Tropical Land

Use

It is commonly accepted that the rates of carbon accumulation during secondary succession are a function of many factors, including type of disturbance (e.g. method of clearing, temperature and frequency of burning), agricultural practices (intensity), size of disturbance, and climate (Bazzaz and Pickett 1980, Ewel et al. 1981, Uhl et al. 1988, Nepstad et al. 1991, Fearnside and Guimaraes 1996). During succession total biomass and soil organic matter increase toward a climax state. However, this climax state may differ from the pre-disturbance state (Botkin 1993). There have been numerous studies measuring rate of accumulation in above ground and/or below ground biomass in secondary forests following disturbance throughout the tropics (Fittkau and Klinge 1973, Edwards and Grubb 1977, Sabhasri 1978, Uhl and Jordan 1984, Andriess and Schelless 1987a, Uhl 1987, Saldarriaga et al. 1988, Uhl et al 1988, Nepstad et al. 1991, Kauffman et al. 1995a). For example, average annual rate of above ground biomass accumulation in abandoned pastures near Paragominas in the eastern Amazonia varied from 0.63 to 11.3 tons per hectare per year (Nepstad et al. 1991). These vast differences were attributed to land use. The rate of biomass accumulation was found to be inversely proportional to the intensity of land use prior to abandonment. Intense pasture maintenance results in “barriers to tree establishment” that influence the overall biomass accumulation (Nepstad et al. 1991). Nevertheless, an empirical model based solely on climatic controls can still

be a good, unbiased predictor of biomass accumulation rates in regions with non-sandy soils (Zarin et al. 2001).

Results from the NASA Landsat Pathfinder indicate extensive areas of forest fallow and secondary vegetation in Continental Southeast Asia and the Legal Amazon. For example, the extent of secondary vegetation in the Legal Amazon varied from 76,000 km², 31% of the deforested area, in 1986 to over 165,000 km², 41% of the deforested area, in 1996 (unpublished results from LP HTF). The impact of these large secondary growth pools on the net biotic flux of carbon has yet to be quantified. The dynamics of the secondary growth pool and the rate of biomass accumulation needs to be quantified in order to assess the impact of secondary growth on the global carbon cycle. Satellite analyses by Alves and Skole (1996) indicate that for a site in Rondonia secondary growth is a large (over 40% of the deforested areas) and a rapidly changing pool. Almost 60% of the areas in secondary growth in 1986 were recleared at least once by 1992, and over 55% of the deforested areas in 1986 were abandoned into secondary growth for some period of time by 1992 (Alves and Skole 1996). Remote sensing based change detection studies provide a unique opportunity for characterizing the dynamics of the secondary growth.

Methods

Landsat Classification

Multi-temporal Landsat Thematic Mapper images were obtained for three sites in Amazonia and four sites in Southeast Asia (see tables 2.1 & 2.2, figure 2.1). These

images were selected so that the acquisition period was consistent for a given site. The data for the Amazonia sites was targeted for mid-dry season. However, due to cloud cover, two images were acquired in the late dry-season/early wet-season. While the acquisition date for the sites in Southeast Asia was targeted for early dry season (November to January) to avoid leaf-off phenological conditions, half of the twenty-two images used in the Southeast Asia analysis were acquired after leaf drop. At each site, a base image was selected and rectified to Universal Transverse Mercator (UTM) map coordinates using control points derived from GPS data where available or from the spacecraft ephemeris ground control estimates. The remaining images were then co-registered to the base image using at least 35 manual ground control points (GCPs) with a target RMS of less than 0.5 pixels (all RMS errors were less than 0.7 pixels). The sites in Southeast Asia are generally mountainous, causing significant topographic effects in the TM imagery. To reduce the topographic effects two synthetic bands were created prior to classification. These bands were simple band ratios of the TM band 5 over 4 and band 4 over 3.

An unsupervised classification procedure was applied to avoid having to specify *a priori* the spectral characteristics of our thematic classes. Of the several clustering algorithms that exist, the ISODATA technique was utilized in this study. Using a minimum spectral distance decision rule for assignment of pixels, images were clustered using ISODATA with a specified convergence threshold of 95% and 45 clusters. The convergence threshold is the percentage of pixels that do not change clusters between iterations even with a small shift in cluster means. Pure clusters were assigned a class

value and removed from further clustering. Class assignment was based on several field surveys of the study sites and the inherent TM spectral properties of the land cover classes. "Mixed" clusters were re-clustered iteratively by masking areas of pure clusters and re-running ISODATA. Manual editing was applied to remove mis-labeled clusters. Final classifications had 7 thematic classes (forest, cleared, natural non-forest, water, cloud, cloud shadow, and secondary vegetation) for the Amazonia sites and 5 thematic classes (vegetated, cleared, water, cloud, and cloud shadow) for the Southeast Asia sites. The sites in Southeast Asia are upland regions of moderate to severe topography with shifting cultivation by indigenous hill-tribes as the dominant form of land use. After many years of shifting cultivation, the upland landscape in these areas consists of a broad range of villages, paddies, swiddens (areas containing active agriculture), fallows ranging from scrub/grasses to secondary forests, and mature forest (Sabhasri 1978). The combination of topographic influences and a continual range in vegetation made it difficult to separate secondary vegetation from forest, so these classes were combined into a single "vegetated class" for the Southeast Asia analyses. Very little of the landscape goes un-used and cleared areas are mostly areas that were cultivated during the wet season. Boolean operators were used to create a mask consisting of the sum of all areas of that were classified as water, cloud, cloud shadow, and natural non-forest (Amazonia only) in any year. This mask was applied to all final classifications to remove areas where we do not have land cover data in all of the inventories.

Change Detection

While there are several strategies for change detection, post-classification change detection facilitates the generation of land-cover transition matrices, thereby providing spatially explicit information on “from to” class changes (Khorram et al., 1999).

Transition matrices can be easily created because the images are co-registered and every pixel is assigned to a land-cover class. While other change detection strategies, for example image enhancement or differencing, provide information on the location, spatial patterns, and amount of change, these techniques do not provide land cover transition information because the images are not classified. Land-cover transition matrices were used to determine both the amount and spatial patterns of deforestation and secondary vegetation formation. Pixel level transition sequences were labeled using Boolean operators. For example, a site that was deforested in 1990 and then contained secondary vegetation from 1993 through 1995 would have a transition sequence from 1989 to 1995 of “FDDSSS”, where F, D, and S represent forest, cleared, and secondary vegetation classes, respectively. Cohorts of new secondary vegetation and clearings were tracked throughout each time series to quantify persistence of each class. Histograms of the transition sequences were analyzed to quantify the land cover dynamics. For example, all areas of new deforestation in 1992 were identified by the transition sequence “FFFD...” and new secondary growth areas in 1993 were identified by “XXXXS...” where X can be either the F or D classes.

We applied a significant assumption regarding permitted transition sequences. It was assumed that if a pixel was classified as disturbed (cleared or secondary vegetation class) in an earlier image, it could not revert to mature forest in later images. This

assumption was made in order to map areas of older secondary vegetation that become spectrally indistinguishable from mature forest and thus would be mis-classified as mature, undisturbed forest in subsequent imagery. Classification errors can have a significant impact on post-classification change detection studies because classification errors propagate with each additional classification added to the transition. In Amazonia, while accuracy in separating cleared areas from secondary vegetation and forest is typically quite high (98-99%), spectral confusion between secondary vegetation and mature, undisturbed forest is most problematic (Kimes et al.1999). However, from the transition sequences we know if a particular pixel was disturbed in the past and, thus, must be secondary vegetation instead of undisturbed forest. Therefore, by incorporating an historical land cover condition using Boolean operators into our transition sequences we improved the overall accuracy of the transition sequences and mapped areas of older secondary vegetation that otherwise would have been missed.

Accuracy Assessment

Traditional statistical accuracy assessment (Congalton 1991) and spatial shape analysis techniques were used to evaluate the results. It was not feasible to collect appropriate (in space and time) reference data for a statistically valid accuracy assessment of all Landsat TM classifications. However, reference data were collected in 1998 at Alto Paraiso, Brazil and in 1996 and 1997 in Chiang Mai, Thailand sites with a camera and GPS to document the location and land cover conditions. Additional field visits in Brazil, Laos, Thailand, and Vietnam were used to calibrate the analysis. The accuracy was computed for the forest, cleared, and secondary vegetation classes for Alto Paraiso and

for forest and non-forest classes for Chiang Mai. The overall accuracy of the 1998 Alto Paraiso, 1996 Chiang Mai, and 1997 Chiang Mai classifications were 98%, 88%, and 85%, respectively. Tau (Ma and Redmond 1995) and Kappa (Hudson and Ramm 1987) statistics were also calculated to evaluate overall accuracy relative to a random assignment of classes. Tau/Kappa statistics for the 1998 Alto Paraiso, 1996 Chiang Mai, and 1997 Chiang Mai classifications were 98%/94%, 83%/75%, and 80%/71%, respectively. Summaries of the statistical accuracy assessment are provided in Appendix B.

Aside from classification errors, mis-registration and atmospheric conditions can reduce the accuracy of change detection studies (Wickware and Howarth, 1981). The potential impact of mis-registration was examined by performing a spatial analysis of the changed areas (Salas et al. 2001). Changed areas were clumped into groups of contiguous pixels by change class. Calculation of the perimeter/area (P/A) ratio of the individual change clumps provides an indication of the shape of the changed area. Higher P/A values represent changed areas with a shape closer to linear, and hence could represent mis-registration. This ratio was used for estimating the proportion of total area changed that may be attributed to edge effects or mis-registration. For a given pixel size p the area of a group of pixels is given by $A_n = np^2$ where n is the number of pixels. Since the perimeter for a horizontal or vertical line of pixels is $P = 4np - 2(n-1)p$, the corresponding P/A would be

$$P/A = \frac{4np - 2(n-1)p}{np^2} = \frac{2(n+1)}{np}$$

For a set of pixels that do not share an edge (a single pixel or a diagonal line of pixels) the P/A is $4/p$. While RMS error may be unreliable for estimating the precision of co-registration (Verbyla and Boles 2000), we assume that our co-registration errors are sub-pixel given that all of our RMS errors were less than 0.7 pixels. Visual inspection of the change images did not reveal any indications of large mis-registration effects. Based on this assumption, change detection errors due to mis-registration should be manifest as thin, single pixel bands of changes with P/A ranging from low of $\frac{2(n+1)}{np}$ to a maximum of $4/p$. However, change areas with P/A in this range are not necessarily spurious changes due to mis-registration, but rather could be indications of small land cover changes. The distribution of clump sizes and P/A values for all changes observed from 1989-1990 for Chiang Mai and 1996 to 1997 for the Ruropolis and Uruara sites are provided in figure 2.2a, 2.2b, and 2.2c, respectively. The P/A ratio was calculated for each contiguous area of change, herein called a "clump". We then compared the observed P/A ratio for each clump with the theoretical P/A for a line of pixels, given by the equation above, with the same number of pixels in the observed clump. If the observed P/A was higher than the expected P/A for a linear strip (area above the curved line in Figure 2.2), then the change was flagged as a potential error due to mis-registration. Based on the P/A spatial analysis, less than 10% of the total changes observed at the two Amazonia sites could be due to mis-registration and at most 21% at the Chiang Mai site. However, since some land use changes can create thin areas of disturbance surrounding areas of deforestation (e.g. see work of Laurance et al. 1997), analysis of the types of observed changes would be useful for separating spurious changes due to mis-registration

from actual edge effects due to human disturbance. While this was not done for this study, future analyses will focus on using the spatial shape of changes, coupled with the thematic change data, to identify forest degradation due to edge effects that include biomass decline and fire encroachment along the edges of deforested areas.

Results and Discussion

Amazonia Sites: Alto Paraiso, Ruropolis, and Ururara

The total area disturbed, defined as the sum of cleared and secondary vegetation classes, increased steadily from the mid/late 1980s to late 1990s at all three sites (Figures 2.3a, 2.3b, and 2.3c). Area of disturbance increased from 20% in 1989 to over 41% of the total area in 1998 for Alto Paraiso, a 105% increase in total area disturbed over this 9-year period. At Uruara, the disturbed area increased from 9.8% in 1986 to 24.5% in 1999, a 149% increase over the 13-year period. At Ruropolis, disturbed area increased from 9.1% in 1987 to 19.9% in 1998, a 119% increase over the 11-year period. While the area weighted intensity of disturbance was different at these sites, the average annual expansion was similar, ranging from 10.8%/yr to 11.7%/yr. The percentage of disturbed area as secondary growth varied dramatically on an annual basis from 28% to 63% at Alto Paraiso, 37% to 64% at Uruara, and 57% to 71% at Ruropolis. Early dry-season imagery tended to have a higher proportion of secondary vegetation than late dry-season imagery (Figure 2.4). The influence of the timing of the Landsat imagery was more apparent at the Alto Paraiso site, which has a more pronounced dry season with typically less than 40mm of precipitation in the peak dry months of June and July, than at the

Uruara and Ruropolis sites, which seldom have pronounced dry months with less than 40mm (Legates and Wilmott 1990, Huffman et al. 1997).

The average annual rates of disturbance for the Alto Paraiso (1989-1998), Ruropolis (1987-1998), and Uruara (1986-1999) were 11,400ha, 12,000ha, and 6,800ha, respectively. On an area-weighted basis, average annual disturbance rates were more than double at Alto Paraiso and Uruara when compared with Ruropolis. Annual rates of disturbance varied significantly (figures 2.5a-c). There is no apparent synchronicity of higher and lower rates between sites, nor with the INPE (2000) basin-scale data. For example, in 92-93 and 94-95 rates were high at Alto Paraiso and relatively low at Ruropolis and Uruara. At the basin scale there was an almost three-fold difference between low rates in 1990/1991 ($11,130 \text{ km}^2 \text{ yr}^{-1}$) and high rates ($29,059 \text{ km}^2 \text{ yr}^{-1}$) in 1995/1996 (based on INPE 2000). Whereas, this large difference was not evident at these sites indicating spatial heterogeneity in patterns and magnitude of deforestation rates across the basin, which is consistent with the findings of Sanchez et al. (1997). While much of the annual variability is due to differences in annual disturbance rates, the large difference between 92-93 and 93-94 at Alto Paraiso is likely an artifact of the seasonality of the image acquisitions due to the timing of clearing and burning activities. In Rondonia much of the clearing takes place in July-August, so the images from June 22, 1992 and October 7, 1993 span two clearing seasons, whereas between the October 7, 1993 and June 4, 1994 images there was no peak clearing period.

The rates of formation and clearing of secondary vegetation were often higher than deforestation rates and exhibited more inter-annual variability. There were periods with high formation and low clearing rates, for example 1991 and 1993 at Alto Paraiso,

and, conversely, periods with low formation rates and high clearing rates, for example 1993 at Alto Paraiso and 1997 at Ruropolis (see figure 2.6). Secondary growth dynamics appeared to be higher for transitions across years with dry versus wet season imagery, which is likely due to the timing of land cover changes relative to the Landsat image acquisitions across years in the time series. The impact of the “timing” effect will be dependent on the actual land use. Pastures that are not well maintained are often called “dirty pasture” due to the presence of shrubs and herbaceous plants that have over grown the pasture grasses. Farmers typically do not cultivate or introduce pasture grasses immediately following clearing of mature forest. Secondary vegetation formation typically occurs soon after the initial clearing event. On average, only 30% of new clearings remained devoid of secondary vegetation during the first 2 years following initial clearing (table 2.5). Therefore, while rates of secondary vegetation change were observed to be more variable than deforestation rates, we expect the two processes to be coupled.

Post-disturbance land use can have a significant impact on the carbon balance of the landscape. While it is clear that secondary vegetation is widespread across these sites and the tropical region as a whole, the persistence of the secondary vegetation is not well known. Cohorts of new secondary vegetation following cleared class were tracked through the multi-temporal analyses to quantify how frequently the stands were re-cleared and what percentage of stands persist beyond a short rotation period. The results are presented in tables 2.3a,b, and c and in figure 2.7. On average only 57% of secondary vegetation stands ($n=16$, std. dev. = 16.6%) persisted for longer than one year. In other words, over 43% of secondary vegetation stands were re-cleared in the first year. Only

25% of the stands ($n=9$, std. dev. = 12.5%) persisted for at least 5 years, with less than 10% lasting longer than 8 years indicating that most of this pool is part of a rotational system and not due to long-term abandonment. The 1990 and 1993 Alto Paraiso cohorts of secondary vegetation appeared to have different survivorship characteristics with a much higher level of persistence. For example, only 7% of the 1990 cohort was re-cleared in the first year and over 36% persisted for at least 8 years. These two years also had relatively small cohorts of secondary vegetation (see figure 2.6) and are derived from imagery that was acquired later in the dry season (see table 2.2). Secondary vegetation persistence at the Alto Paraiso site was compared with the other two sites to see if there were regional differences between Rondonia and Para. Based on an analysis of variance (d.f. = 15, F-test with threshold of $\alpha=0.25$), there were small differences in persistence after the first year, but these differences were not apparent for the 3-year old stands. The results on secondary vegetation persistence presented here address only one component of new secondary vegetation. There are vast areas of new secondary vegetation that is observed that appear to come directly from the mature forest class (denoted "F" above). There are several land use changes conditions that could cause this apparent "F" to "S" transition, including but not limited to logging and multi-year clearing. Future analyses will focus on characterizing these land use changes using transition sequence analysis of persistence coupled with a spectral analysis of the secondary vegetation class.

Southeast Asia: Chiang Mai, Upper and Lower Ca River, and Kachin sites.

These four sites contain a broad range of natural forest types, ranging from low stature dry dipterocarp forests that have low canopy cover to dense hill evergreen forest

with very high canopy cover, and secondary forests and fallow formations due to a long history of land use in the uplands of Southeast Asia (Sabhasri 1978). Analysis of spectral separation based on transformed divergence measures (Swain and Davis 1978) indicated that separation of disturbed areas (e.g. secondary forests and fallow areas) from mature forests in this region of moderate to severe topography would be difficult. Therefore, rather than direct mapping of disturbed areas, we focused on accurate designation of cleared areas and then tracked areas that later shifted to our broad forest class during the multi-year analysis. Areas of disturbance were then defined as all areas that changed classes during the inventory plus areas that remained in cleared class throughout the inventory. While use of such broad land cover class may not be ideal for complete characterization of the landscape, assessments of clearing of forests and creation and persistence of fallow areas can be achieved using post-classification change detection methods.

Based on the percentages of the study areas impacted by change (see table 2.4), land cover changes were more intense at the Chiang Mai and Lower Ca River sites than the Upper Ca River and Kachin sites. Over 300,000 ha, or 48% of the study site, were disturbed between 1989 and 1997 at the Chiang Mai site. The site in Myanmar appeared to have the least intensive land cover changes with less than 8% (16,200ha) of the study area disturbed between 1989 and 1996. However, care is needed for direct comparison of these sites because of different inventory frequencies. The less frequent the inventory, like the 3 images over the 7 year period at the Kachin site, the more likely that land cover changes will be missed, potentially resulting in an under-estimate of area of change. We had more images at the Chiang Mai (annual TM images) and Upper Ca River (6 images

over 9 years) sites than the Lower Ca River (4 images over 8 years) and Kachin sites. The impact of frequency of observation on area estimates is described in more detail in a later section.

Throughout the time series, total cleared areas increased slightly at all sites except for the Kachin, Myanmar site which had a small loss in cleared area of 140ha, less than 0.1% of the study area from 1989 to 1996 (see table 2.3). While at the other 3 sites the overall net expansion of cultivated areas was small on an annual basis, ranging from $0.03\%yr^{-1}$ to $0.14\%yr^{-1}$, large areas were cycled in and out of cultivation, a characteristic of shifting cultivation in Southeast Asia. In aggregate, the clearing rates for these four Southeast Asia sites did not exhibit the large inter-annual variability seen at the Amazonian sites with average clearing rates between 0.6 to 1.1% (Figure 2.8a). The largest change was an almost doubling of clearing rates from 1994 to 1995. However, there was a large degree of inter-annual variability in clearing rates at the Chiang Mai and Lower Ca River sites. At Chiang Mai for example, the clearing rate for 1995 was almost 4 times the 1990 rate.

Although it is difficult to map areas of fallow in the uplands of Southeast Asia directly with Landsat TM imagery due to the spectral confusion with mature forest, new areas of fallow were identified as areas that were cleared and were subsequently in the "broad forest class" in a later image. Large areas of fallow were identified at each site (table 2.3). For example, over 245,000ha of fallow were created from 1989 to 1997 in Chiang Mai, representing almost 39% of the study area. Note that the total area of secondary forest and fallow areas will be larger than the percentages listed in the table as these percentages only represent new areas identified during the inventory period.

While the aggregate rates of fallow formation were in a similar range as the clearing rates (0.6% to 1.2%), the inter-annual variability was higher. Contrary to clearing rates, each site had a large degree of inter-annual variability in the rates of fallow formation, with rates shifting as much as 400% between subsequent inventories (figure 2.8b). Once again the Chiang Mai and Upper Ca River sites exhibited the largest amount of variability. The persistence of fallow areas at the Chiang Mai site is depicted in figure 2.9a. Almost 50% of the fallow areas were in a short (3 years or less) rotation system, with only 33% in a long rotation system (greater than 7 years). The bulk (78%) of the cleared areas are cultivated for less than 3 years, with only 2% of the areas remaining in cultivation beyond 7 years (figure 2.9b). These persistence data indicate that the dominant cultivation in this area is shifting cultivation with a short cultivation/short fallow rotation.

The impact of this short rotation land use system in Chiang Mai on net clearing rates is evident in figure 2.10 where years with net increases in cultivated area are followed by decreases in cultivated areas. However, this land use pattern is not as apparent at the other sites likely due in part to differences in land use but also due to temporal gaps between images that dampen the short annual fluctuations. The influence of a “dampening factor” was assessed by comparing differences in decadal and sub-decadal rates. For each site, mean decadal rate was calculated using the first (1989) and the last (1996, 1997, or 1998) image in the time series. Sub-decadal rates were calculated using all temporal combinations of the images in time series. The ratio of the sub-decadal rates to the decadal rate was then calculated at each site (figure 2.11). With the exception of two cases, shorter census periods reflected higher clearing rates. Clearly the revisit

frequency of the Landsat observation influences estimated clearing rates since long revisit periods do not capture the dynamics between these cleared and broad forest classes. In addition, extrapolation of net forest loss based on short period rates can lead to a severe over-estimate of long-term losses.

Our results indicated that clearing and fallow rates were higher at the Chiang Mai and Lower Ca River sites. However, it is not clear if these differences were due to actual land use differences or just an artifact of differences in observation frequency. Based on the relationship between frequency of observation and estimated clearing rates in figure 2.11, it is clear that, at an annual-scale, the clearing and fallow rates at the Upper Ca River and Kachin sites are actually higher than those presented in figure 2.8.

Conclusions

An analysis of multi-temporal Landsat TM data for seven case study sites in the tropics was presented. This analysis focused on documenting inter-annual variability in rates of clearing and secondary vegetation formation and an assessment of persistence of secondary vegetation. Rates of clearing and secondary vegetation formation varied considerably on an annual basis in both the Amazon and Southeast Asia regions, indicating a large departure of annual rates from the decadal mean. Within region variability was also high as exhibited across the case study sites. The secondary vegetation pool is large and appears to be covering an increasing proportion of disturbed areas in Amazonia and Southeast Asia. However, the high transition probabilities observed for young stands indicates that secondary vegetation is an important component of the local land use practices dominated by rotational agriculture and pasture use and

that a small percentage of the secondary vegetation persists for longer than 8 years. The high 1-year transition probabilities for secondary vegetation and new clearings is likely due to a combination of rotational agriculture and the multi-year process of pasture formation. Therefore, consideration of land use practices, including clearing periods and vegetation phenology, is needed for post-classification change detection analyses to avoid spurious or misleading results. Due to the highly dynamic nature of land use in these areas, gaps in annual time series of Landsat observations can introduce large uncertainties in the estimates of clearing and secondary vegetation formation rates.

Analysis of the pixel level transition sequences, coupled with an *apriori* understanding of land use practices, can be used to move beyond land cover classification to map land use processes directly. While post-classification change detection with broad land cover classes can provide useful data on land cover change and rotational agriculture practices, better discrimination of vegetation structure and stature is needed to examine carbon dynamics. Use of remote sensing derived continuous variable, such a vegetation density or fractional cover, characterization of the landscape, coupled with post-classification derived changes in land cover, would provide a clear indication of the impacts of land use change on the above-ground carbon balance of these landscapes. Nevertheless, these results suggest the potential for large inter-annual variations in the net flux of biotic CO₂ due to land use change in Amazonia and Southeast Asia.

Table 2.1 Landsat Thematic Mapper data used for Southeast Asia analysis.

Chiang Mai, Thailand	Kachin, Myanmar	Ca River, Laos	Ca River, Vietnam
Feb 3, 1989	Jan 16, 1989	Mar 2, 1989	Apr 4, 1989
Jan 29, 1990	Mar 8, 1993	Nov 29, 1992	Nov 20, 1991
Feb 17, 1991	Dec 13, 1996	Dec 8, 1995	Oct 21, 1992
Feb 4, 1992		Nov 27, 1997	Dec 8, 1995
Feb 22, 1993			Nov 27, 1997
Feb 24, 1994			May 15, 1998
Dec 10, 1994			
Mar 18, 1996			
Mar 5, 1997			

Table 2.2 Landsat Thematic Mapper data used for Amazonia analysis.

Alto Paraiso	Uruara	Ruropolis
Jul 8, 1989	Aug 23, 1986	Jun 30, 1987
Aug 12, 1990	Jun 23, 1987	Jul 11, 1988
Jun 12, 1991	Jul 18, 1988	Aug 8, 1989
Jun 22, 1992	Jul 20, 1991	Jul 11, 1991
Oct 7, 1993	Jul 22, 1992	Jul 13, 1992
Jun 4, 1994	Jun 15, 1996	Oct 10, 1995
Jul 25, 1995	Jun 18, 1997	Jul 8, 1996
Jun 25, 1996	Aug 3, 1999	Jun 25, 1997
Jun 28, 1997		Jun 12, 1998
Jul 17, 1998		

Table 2.3a Persistence of secondary vegetation at Ruropolis site. Each entry is the percentage of the secondary vegetation cohort that has persisted by age of cohort. Therefore, only 63% of the new secondary vegetation created in 1988 was not cleared by 1989. Only 5% of the 1998 secondary vegetation cohort persisted for 10 years.

	<i>1yr</i>	<i>2yr</i>	<i>3yr</i>	<i>4yr</i>	<i>5yr</i>	<i>6yr</i>	<i>7yr</i>	<i>8yr</i>	<i>9yr</i>	<i>10yr</i>
1988	63	---	39	26	---	---	14	9	7	5
1989	---	53	32	---	---	16	9	7	5	---
1991	48	---	---	22	13	9	7	---	---	---
1992	---	---	41	22	14	11	---	---	---	---
1995	48	28	20	---	---	---	---	---	---	---
1996	37	25	---	---	---	---	---	---	---	---
1997	56	---	---	---	---	---	---	---	---	---

Table 2.3b. Persistence of secondary vegetation at Alto Paraiso site. Each entry is the percentage of the secondary vegetation cohort that has persisted by age of cohort.

	<i>1yr</i>	<i>2yr</i>	<i>3yr</i>	<i>4yr</i>	<i>5yr</i>	<i>6yr</i>	<i>7yr</i>	<i>8yr</i>
1990	93	85	64	61	53	45	41	36
1991	76	41	38	31	24	21	17	---
1992	44	39	30	21	18	14	---	---
1993	90	68	52	45	36	---	---	---
1994	52	26	19	12	---	---	---	---
1995	50	36	23	---	---	---	---	---
1996	62	34	---	---	---	---	---	---
1997	38	---	---	---	---	---	---	---

Table 2.3c. Persistence of secondary vegetation at Uruara site. Each entry is the percentage of the secondary vegetation cohort that has persisted by age of cohort

	<i>1yr</i>	<i>2yr</i>	<i>3yr</i>	<i>4yr</i>	<i>5yr</i>	<i>6yr</i>	<i>7yr</i>	<i>8yr</i>	<i>9yr</i>	<i>10yr</i>	<i>11yr</i>	<i>12yr</i>
1987	56	---	---	43	24	---	---	---	11	8	---	5
1988	---	---	68	35	---	---	---	16	11	---	7	---
1991	48	---	---	---	22	15	---	9	---	---	---	---
1992	---	---	---	35	21	---	12	---	---	---	---	---
1996	49	---	21	---	---	---	---	---	---	---	---	---
1997	---	38	---	---	---	---	---	---	---	---	---	---

Table 2.4 Disturbance area for Indochina sites. Total area disturbed was calculated by summing up all areas that were identified as cleared in classifications. Net changes in cleared area were calculated as the net change in cleared area from 1989 to final year in the time series. Area of new fallow was calculated as areas of disturbance that were not in cleared class at the end of the time series. Note that areas with the highest % of new fallow areas are the sites with the most complete time series of images.

<i>Site (area in 1000ha)</i>	<i>Total Area Disturbed (ha)</i>	<i>Net change in cleared areas (ha)</i>	<i>Inventory Period</i>	<i>Area of new study area fallow (ha)</i>	<i>Percent of in new fallow</i>
Chiang Mai, Thailand (632)	303,200	3680	1989-1997	245,000	39%
Upper Ca River, Laos (134)	17,400	310	1989-1997	11,000	8%
Lower Ca River, Vietnam (121)	44,800	1220	1989-1998	36,900	30%
Kachin, Myanmar (231)	16,200	-140	1989-1996	10,800	5%

Table 2.5 Persistence of new clearings at Alto Paraiso. Each entry is the percentage of the new clearing cohort that has persisted by age of cohort. New clearings cohort represents all areas where mature forests were cleared during the previous year. SO, for example, the 1990 cohort consists of all areas cleared after the 1989 image and before the 1990 images were acquired. Of the 1990 cohort, only 52 percent remained as cleared class in 1991. In other words, 48% of the new clearings contained secondary vegetation by 1991.

	<i>1yr</i>	<i>2yr</i>	<i>3yr</i>	<i>4yr</i>	<i>5yr</i>	<i>6yr</i>	<i>7yr</i>	<i>8yr</i>
1990	52	33	29	15	12	12	11	11
1991	56	48	27	23	22	21	21	---
1992	84	16	8	6	4	4	---	---
1993	50	30	15	11	11	---	---	---
1994	64	16	11	11	---	---	---	---
1995	56	34	32	---	---	---	---	---
1996	40	31	---	---	---	---	---	---
1997	47	---	---	---	---	---	---	---
AVG	56	30	20	13	12	12	16	11

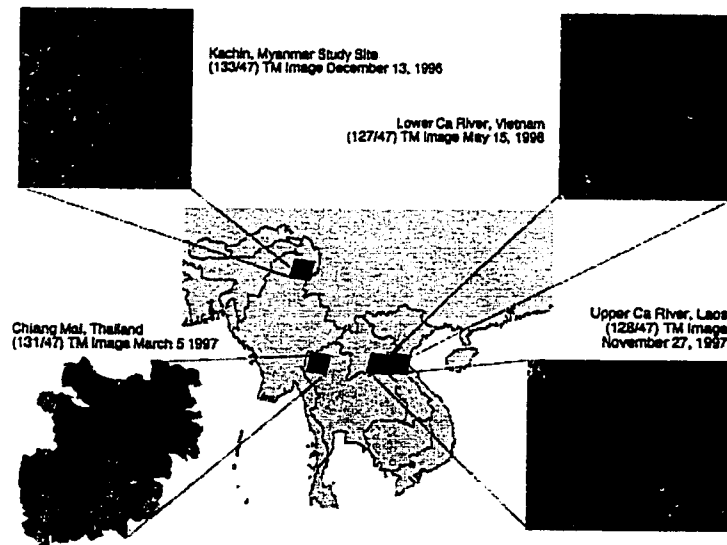
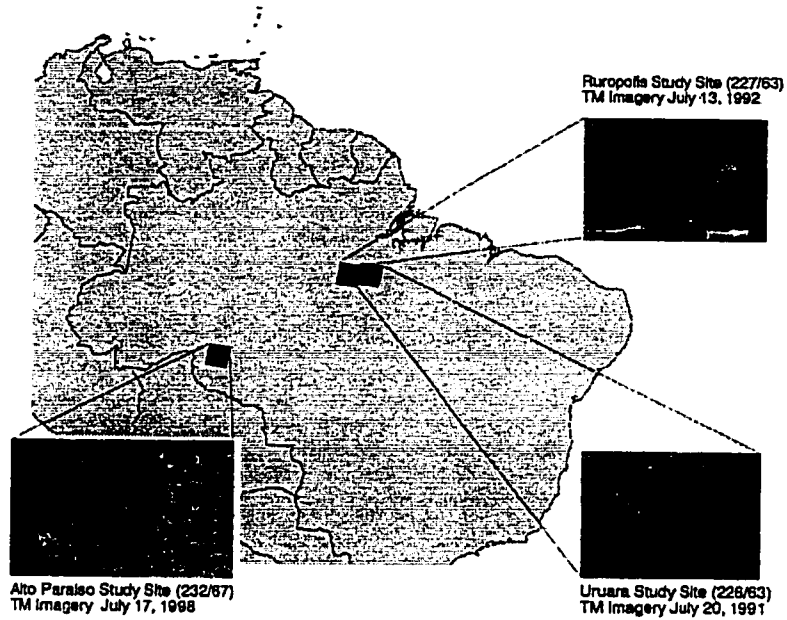


Figure 2.1 Location of study sites in (a) Amazon and (b) Southeast Asia

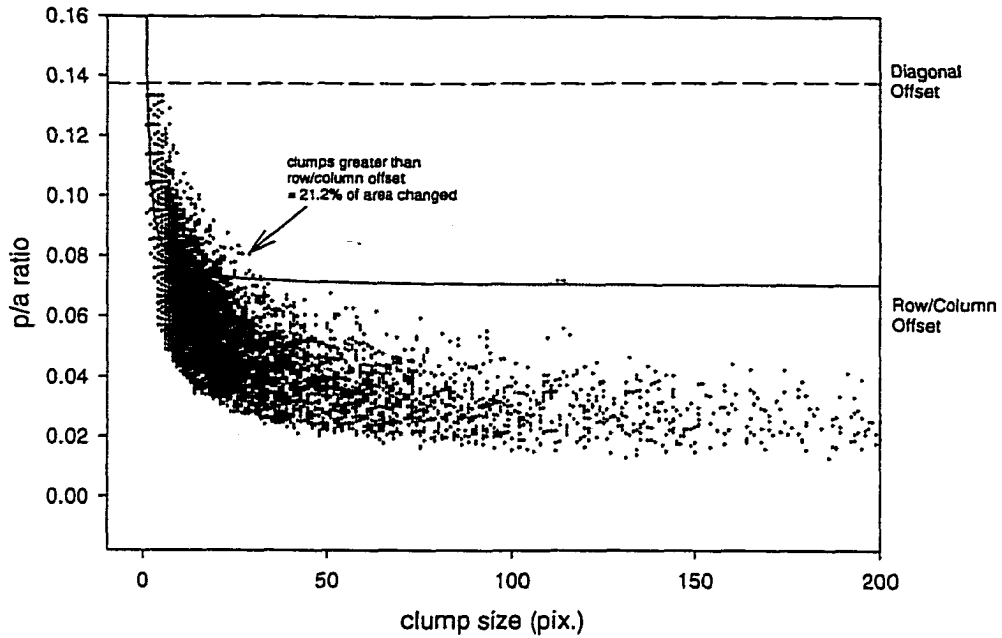


Figure 2.2a Perimeter-to-area ratio for land cover changes 1989-1990 at Chiang Mai site. Clumps are defined as contiguous areas of the same change class. All clumps with P/A ratios above the row/column-offset value could be the result of a single-pixel offset. Clumps with P/A values above the curve could be due to single-pixel mis-registration or to edge effects due to forest disturbance along the edge of existing clearings.

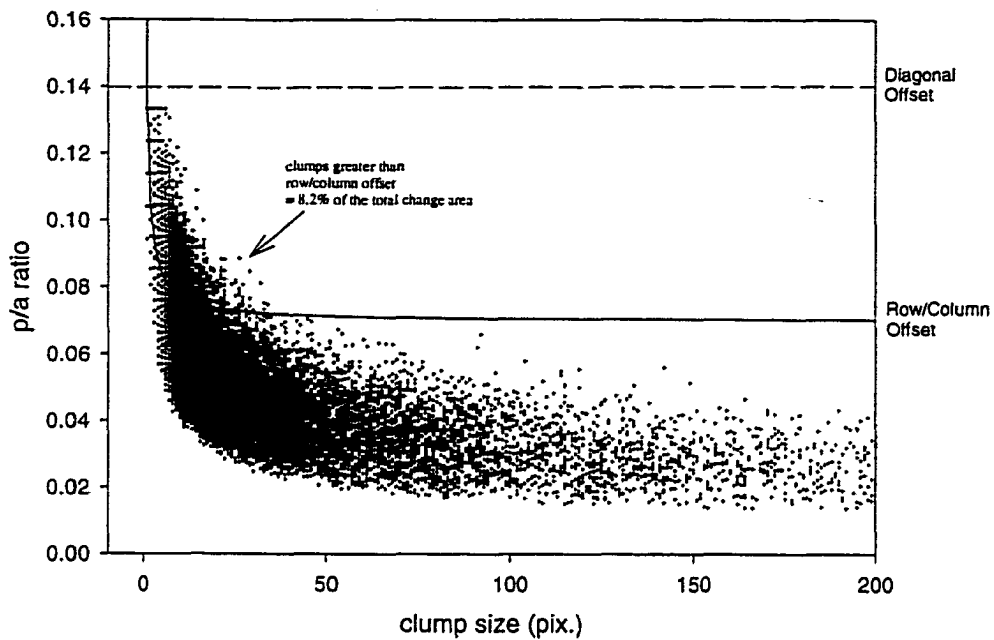


Figure 2.2b. Distribution of perimeter-to-area ratio for 1996-97 changes at Ruropolis. Clumps are defined as contiguous areas of the same change class. All clumps with P/A ratios above the row/column-offset value could be the result of a single-pixel offset. Clumps with P/A values above the curve could be due to single-pixel mis-registration or to edge effects due to forest disturbance along the edge of existing clearings.

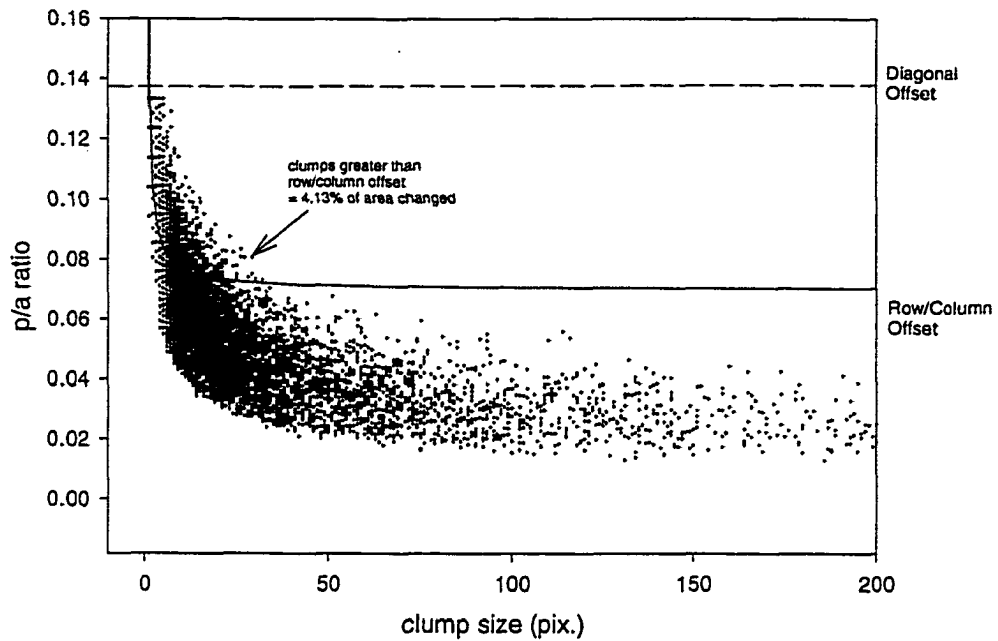


Figure 2.2c Perimeter-to-area ratio for land cover change 1996-1997 at Uruara site. Clumps are defined as contiguous areas of the same change class. All clumps with P/A ratios above the row/column-offset value could be the result of a single-pixel offset. Clumps with P/A values above the curve could be due to single-pixel mis-registration or to edge effects due to forest disturbance along the edge of existing clearings.

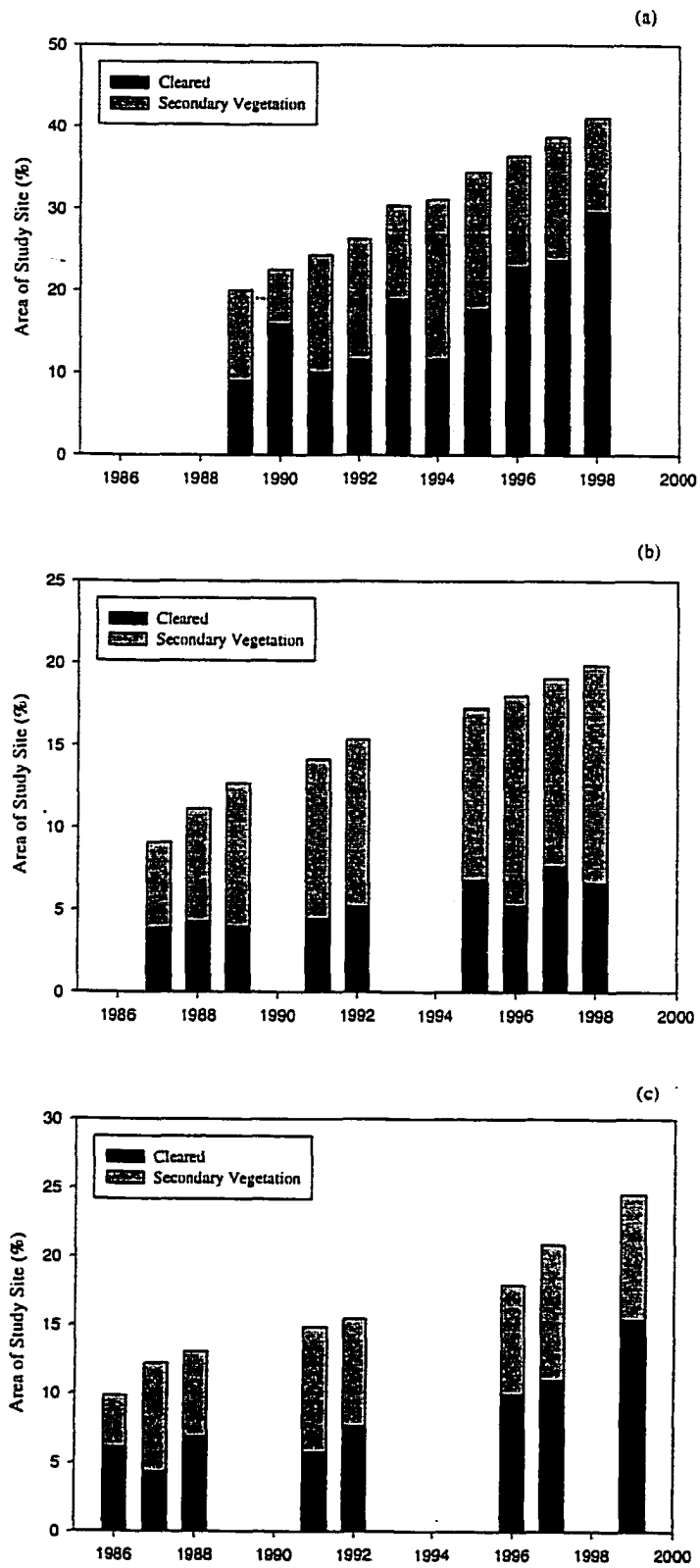


Figure 2.3 Area of disturbance for (a) Alto Paraiso, (b) Ruropolis, and (c) Uruara.

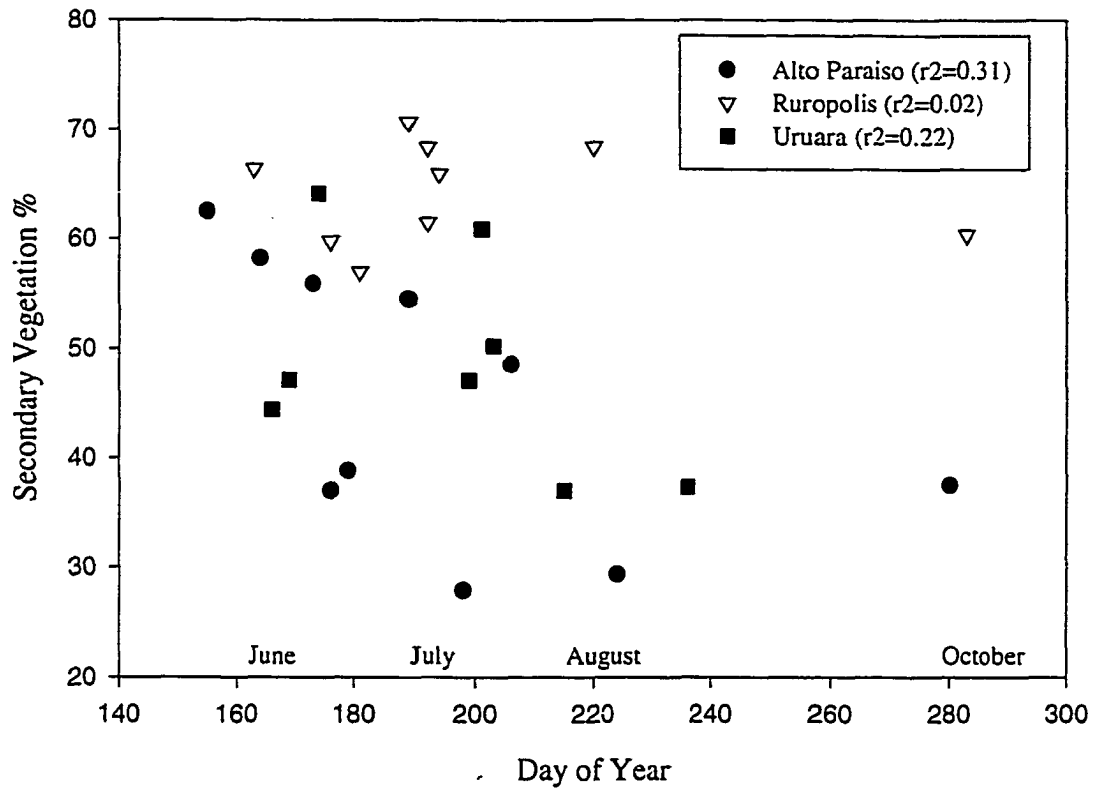


Figure 2.4 Influence of timing of Landsat acquisition on the proportion of secondary vegetation. Alto Paraiso has a very pronounced dry season from June through August, with higher precipitation returning in September. By October the dry season has ended. Omitting the October data point, the correlation between day of year and proportion of secondary vegetation is remarkably high ($r^2=0.48$), indicating a strong seasonality in vegetation characteristics of the disturbed landscape. Ruropolis and Uruara have a less pronounced dry season and exhibit lower correlation between DOY and proportion of secondary vegetation.

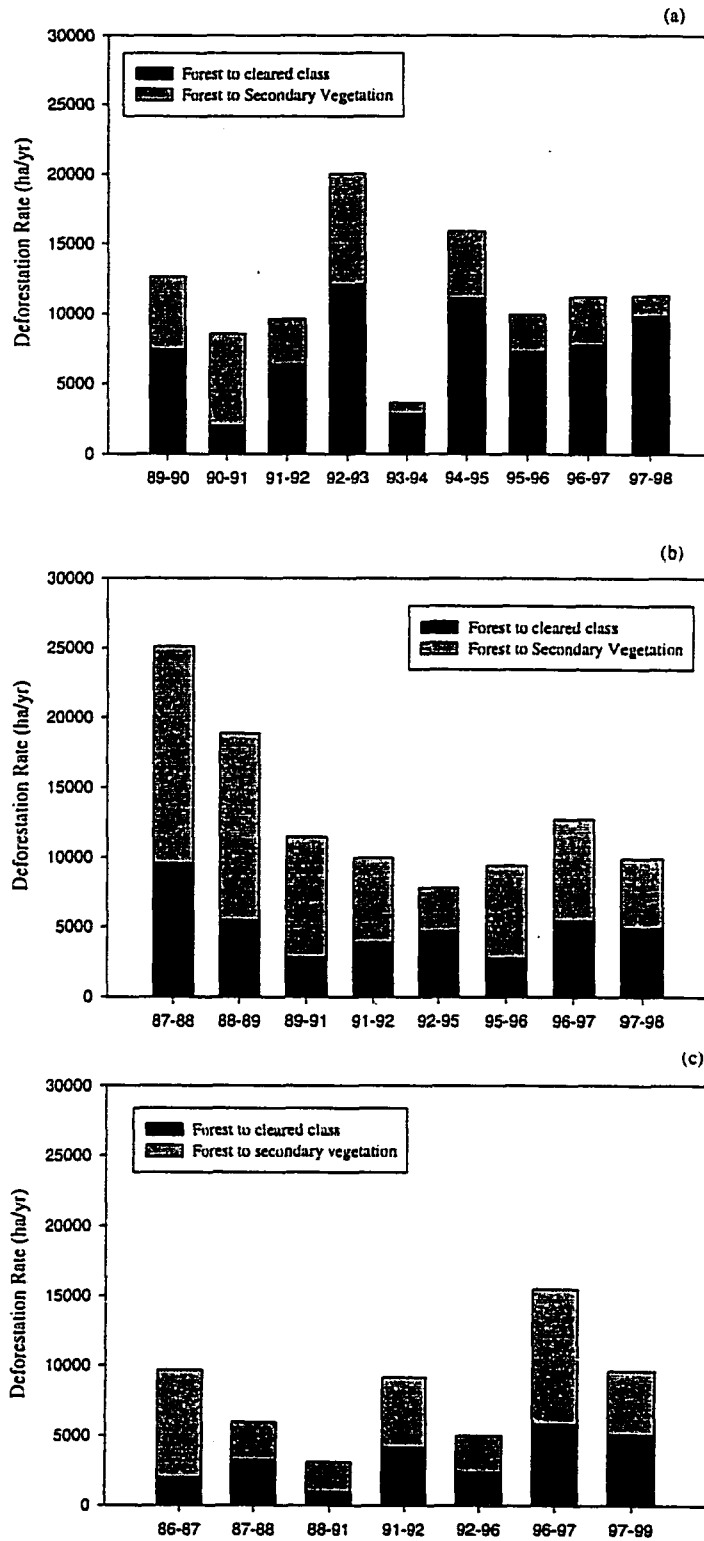


Figure 2.5 Rates of deforestation for (a) Alto Paraiso, (b) Ruropolis, and (c) Uruara. Decadal average rates were approximately 12,000, 11,400, and 6,800 ha/yr for these 3 sites, respectively.

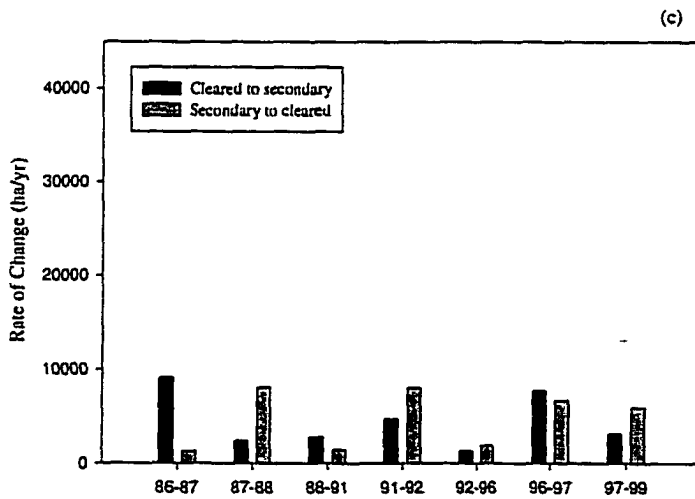
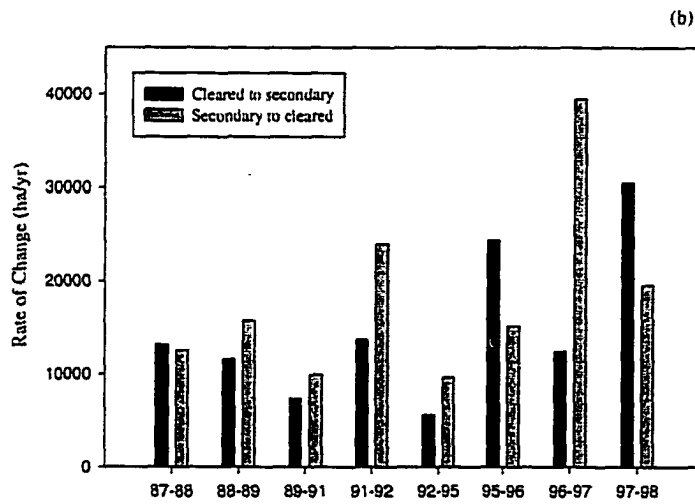
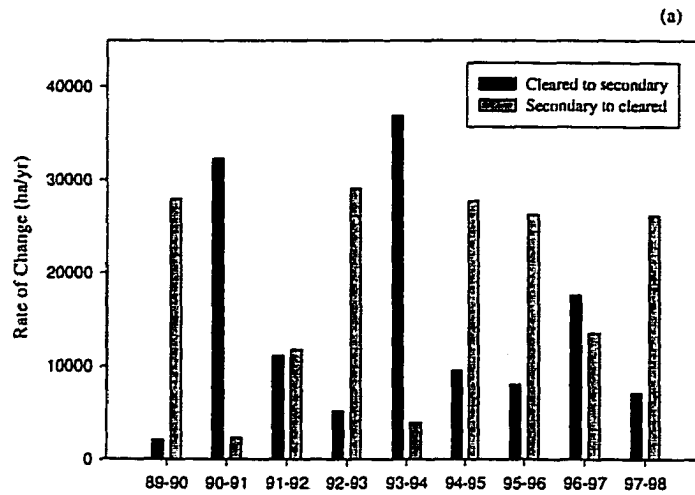


Figure 2.6 Rates of secondary vegetation formation and re-clearing for (a) Alto Paraiso, (b) Ruropolis, and (c) Uruara.

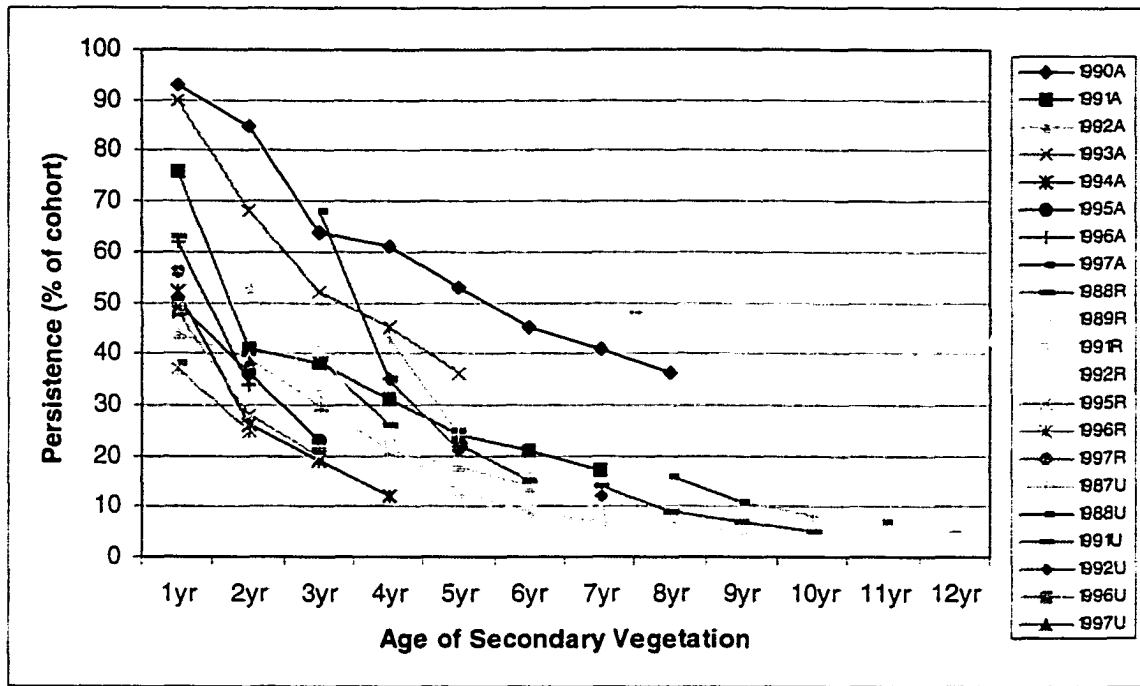


Figure 2.7 Persistence of all secondary vegetation cohorts at Amazon sites. Most cohorts follow a similar survivorship trajectory except for the 1990A and 1993A, which are the cohorts created at the Alto Paraiso site in 1990 and 1993, respectively. In general, a small percentage (<25%) of secondary vegetation persists beyond 5 years. There are several levels of survivorship in these curves. During the first year there is a large drop in survivorship, likely due to rapid re-clearing for pasture maintenance. Once the secondary vegetation persists beyond 1 year, the shape of the survivorship function becomes less steep. The 2 to 5 year period highlights the use of secondary vegetation as fallow in a rotational agricultural system. At the 5 to 6 years period the slope appears to become even smaller, likely indicating abandonment of agricultural and pasture areas. We contend that these differences in slope indicate differences in the use of secondary vegetation.

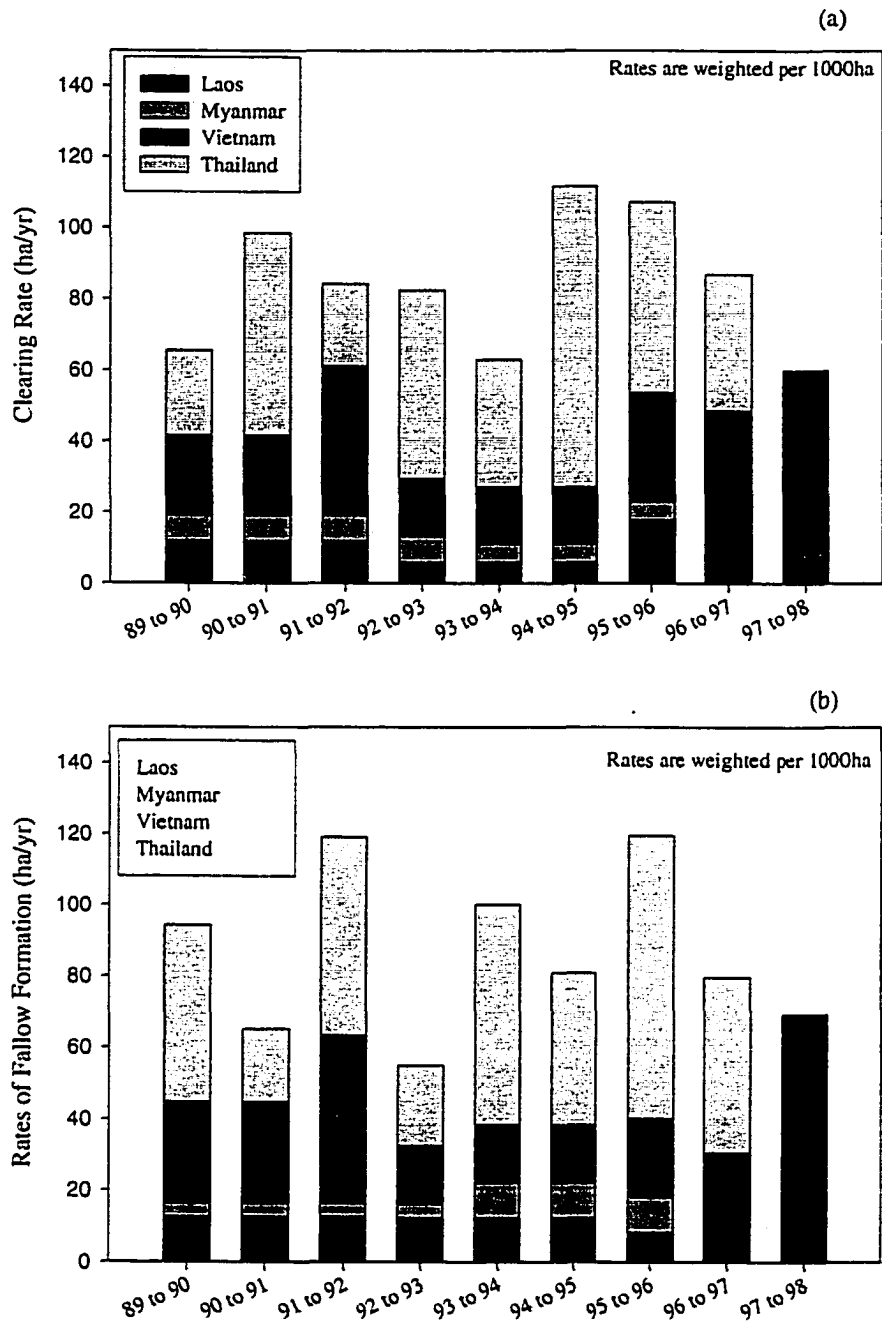
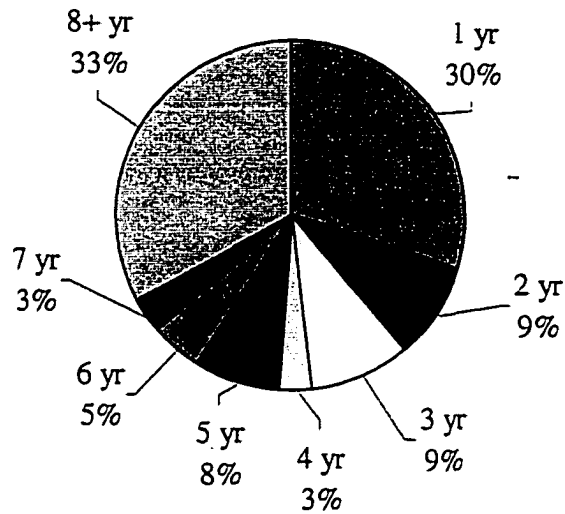


Figure 2.8 Rates of (a) clearing and (b) fallow formation across Indochina sites. Rates of clearing and fallow formation are variable during this time period. Chiang Mai, Thailand site fluctuates between high rates of clearing, followed by high rates of fallow formation.

(a)



(b)

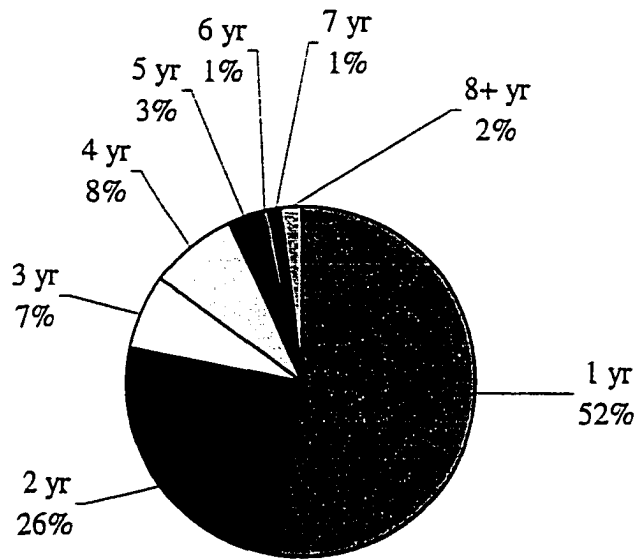


Figure 2.9 Persistence of (a) fallow and (b) new clearings in Chiang Mai. Almost 50% of fallows are re-cleared within the first 3 years. One third of the fallow areas persist longer than 7 years. Over one half of new cleared areas are cultivated for a single year and then are left to fallow. These transition probabilities indicate a short cultivation/ short fallow system.

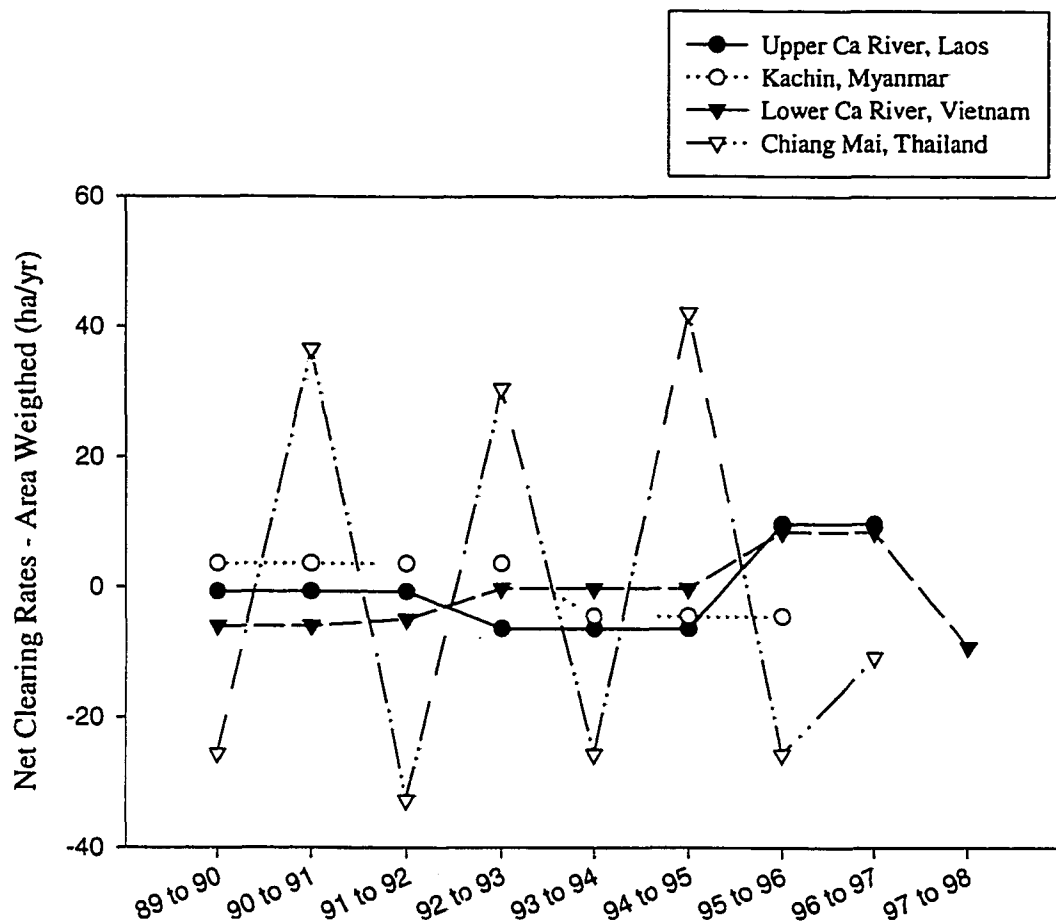


Figure 2.10. Net clearing rates for Southeast Asia sites. These clearing areas represent areas in cultivation. Chiang Mai site fluctuates between an expansion in cultivated areas and a decline in cultivated areas.

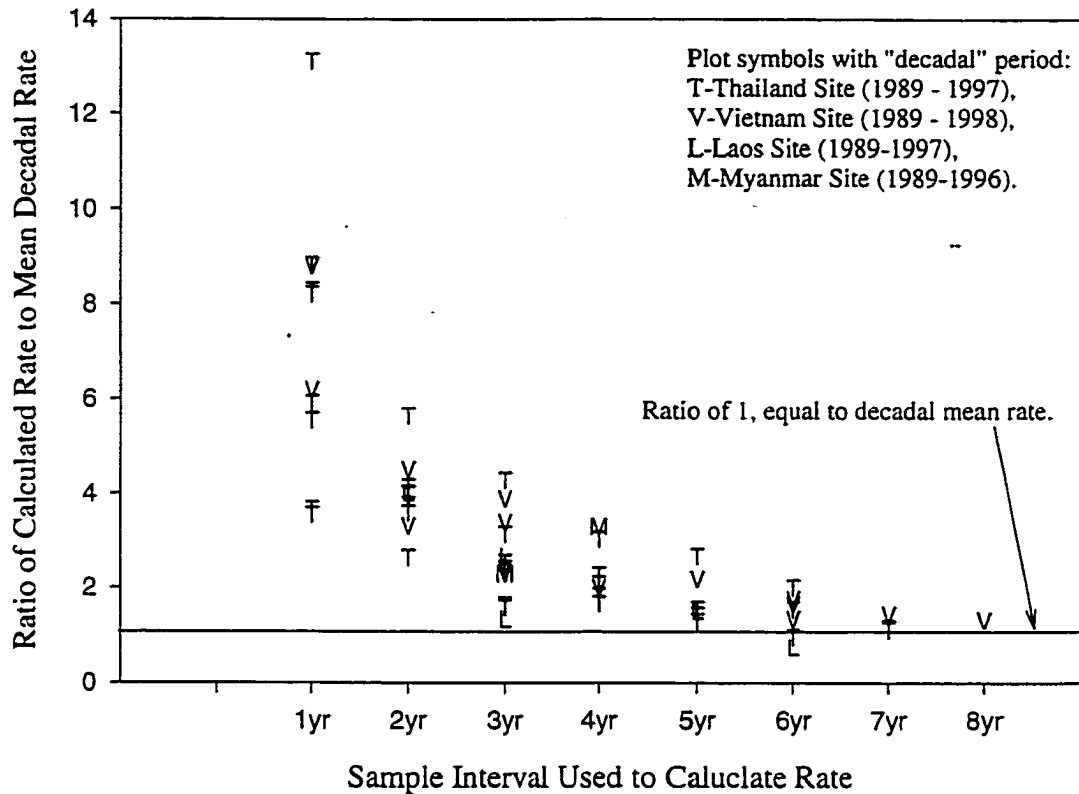


Figure 2.11 Influence of observation frequency on rates estimation. At each site, mean "decadal" clearing rates were calculated using the first (1989) and last (1996/7/8) image in our time series. Sub-decadal rates were also calculated using all combinations of images in our time series and compared to decadal rates. This figure indicates that long revisit periods do not capture the land cover change dynamics of these land use systems, and extrapolation of net losses of forest/fallow areas based on short periods can overestimate long term losses.

CHAPTER 3

ASSESSMENT OF JERS-1 SAR FOR MONITORING SECONDARY VEGETATION IN AMÁZONIA: I. SPATIAL AND TEMPORAL VARIABILITY IN BACKSCATTER ACROSS A CHRONO-SEQUENCE OF SECONDARY VEGETATION STANDS IN RÔNDONIA.

Abstract

Quantification of the direct impact of land use in the tropics on net biotic carbon flux relies on estimates of rates of deforestation, pre- and post-disturbance biomass, and fate of the cleared land. While existing remote sensing applications are providing estimates of the rates of deforestation and the fate of the cleared land (pasture, croplands, or secondary vegetation), techniques for estimating biomass of natural systems with remote sensing are needed. Synthetic aperture radar presents a unique opportunity for imaging tropical forests under most cloud conditions and potentially provides information on vegetation biomass. Earlier studies have developed models for estimating above-ground biomass from JER-S SAR data. In this paper we examine the temporal and spatial variability of mean normalized radar cross-section across a chrono-sequence of secondary vegetation stands and clearings in Rondonia, Brazil. We also assess the influence of the observed temporal and spatial variability in normalized radar cross-section for estimating biomass of secondary vegetation stands. Results indicate that quantitative estimates of biomass using single date JERS-1 imagery is difficult because of temporal variability in

backscatter due to intrinsic texture, system noise, and environmental effects. However, JERS-1 data are still useful for distinguishing of secondary vegetation stands at different stages of development. Merging JERS-1 SAR data with Landsat TM derived age estimates improved characterization of clearings and secondary vegetation in Rondonia by providing information on the relative differences in secondary vegetation development and residual slash with age.

Introduction

Land Use and Inter-annual Variability of the Global Carbon Cycle

With the availability of more detailed atmospheric and oceanic measurements collected globally with a fine temporal scale, new techniques and approaches have been used to understand the global carbon cycle. These new techniques have focused on modeling of the net fluxes in either the oceanic or terrestrial carbon pools (Tans *et al.* 1990 , Siegenthaler and Sarmiento 1993) or on using direct measurements of atmospheric constituents ($[CO_2]$, O_2/CO_2 , $\delta^{13}C$) to estimate fluxes of carbon between the atmospheric, oceanic, and terrestrial pools (Quay *et al.* 1992, Keeling *et al.* 1996). Ciais *et al.* (1995a, 1995b) developed a hybrid approach using a two-dimensional atmospheric transport model (like Tans *et al.* 1990) with $[CO_2]$ and $\delta^{13}C$ measurements from NOAA's Climate Monitoring and Diagnostics Laboratory (CMDL) global flask

network (like Quay *et al.* 1992) to estimate CO₂ partitioning as a function of latitude and time of year from 1990 to 1993.

While all these analyses seem to point to a temperate terrestrial sink for carbon, it is still extremely important to quantify the annual net flux of carbon due to tropical land use. Annual, spatially explicit estimates of CO₂ emissions due to tropical land use and land cover change would help resolve some of the discrepancies from the recent carbon model results based on annual atmospheric measurements. Annual deforestation data could be used to validate these carbon models or identify problems within the models, such as intra-hemispheric transport between the tropical and temperate zones or potential positive net ecosystem productivity (NEP is the carbon balance for the ecosystem) in the tropical forests (Ciais *et al.* 1995a). In order to validate these annual models contemporaneous data on the inter-annual variability of tropical deforestation and regrowth rates are needed to estimate annual fluxes of carbon from the tropical biota. Furthermore, the models based on the annual [CO₂], O₂/CO₂, δ¹³C measurements indicate that the southern tropics was not a strong biotic source or sink of carbon in the early 1990s. Annual measurements of deforestation and regrowth can be used to assess if high rates of abandonment and low rates of deforestation during this time period could explain the dampening of the biogenic source of carbon inferred from the atmospheric measurements (Skole *et al.* 1998).

Land use in the tropics is an important biotic component of the global carbon cycle and has a direct impact on the above and below ground organic carbon stocks of the tropical biome. Conversion of forests to pasture and agriculture results in a net source of biotic CO₂ to the atmosphere, while forest fallow and abandonment into secondary

vegetation represent a net sink of biotic CO₂. The magnitude and timing of these fluxes are a function of the extent of the conversion, the fate of the cleared lands, and carbon stocks of the pre- and post-disturbance landscape. The magnitude of the net biotic flux of carbon from the tropics is not well understood. In order to further our understanding of the impact of land use in the tropics the processes of deforestation and abandonment need to be studied further. While average decadal rates of deforestation on a regional scale are now being quantified more accurately (Skole and Tucker 1993, Townshend *et al.* 1995, INPE 1999), quantitative estimates of the net biotic flux on a decadal average suffer from lack of information on pre- and post-disturbance biomass and the fate of the disturbed lands (e.g. crops land, pasture, or fallow).

Remote Sensing Land Use and Land Cover Change in Tropics

Remote sensing is a useful tool for monitoring changes in tropical land cover because it can provide systematic and synoptic coverage of large areas. Optical remote sensing has been used extensively to map the extent and rates of deforestation (Tucker *et al.* 1984, Malingreau and Tucker 1988, and Skole and Tucker 1993) and, recently, the extent and temporal dynamics of secondary vegetation (Alves and Skole 1996, Mausel *et al.* 1993, Skole *et al.* 1994, Adams *et al.* 1995, Steininger 1996, Foody *et al.* 1996). Now that the spatial extent and rates of tropical deforestation are being accurately quantified, techniques for measuring pre- and post-disturbance biomass, rates of secondary vegetation formation and turnover, and rates of biomass accumulation for secondary vegetation are needed to improve the accuracy of carbon flux estimates. Recent results from NASA's Landsat Pathfinder project have revealed that there are extensive areas of

secondary vegetation throughout Continental Southeast Asia and Amazonia. Over 30% of the deforested area in the Brazilian Amazon was in some form of secondary vegetation in 1986 and 1992 (Houghton *et al.* 2000), areas of approximately 77,000 km² and 98,000 km² in secondary vegetation in 1986 and 1992, respectively. The impact of these large secondary vegetation pools on the net biotic flux of carbon has yet to be quantified. The dynamics of the secondary vegetation pool and the rate of biomass accumulation needs to be understood in order to assess the impact of secondary vegetation on the global carbon cycle.

Although traditional optical remote sensing techniques can distinguish between cultivated areas, pastures, and secondary vegetation, they are limited in terms of mapping various stages of fallow and secondary forests (Sader 1987). On the other hand, since synthetic aperture radar (SAR) backscatter from a vegetated target is a function of the dielectric properties of the vegetation and soil, surface roughness, and size and orientation of the scatterers (e.g. leaves, branches, and trunks) in relation to the imaging system (Ulaby *et al.* 1981), SAR data have considerable promise in characterizing changes in vegetation structure and biomass of the fallow and secondary vegetation areas (Sader 1987, Dobson *et al.* 1992, Rignot *et al.* 1995). In addition, SAR has a significant advantage over optical systems for monitoring land cover and land cover change due to its ability to image the surface under most cloud conditions.

There has been considerable research on the use of synthetic aperture radar data for estimating above ground biomass. Multiple frequency, polarimetric SARs can provide accurate estimates of biomass for successional forests up to a certain biomass level. Radar backscatter tends to saturate at higher biomass levels for longer wavelength SAR

systems (summarized in Kasischke *et al.* 1997). Estimates of the saturation point of L-band backscatter from tropical forests vary from 40 T/ha (Imhoff 1995) to 60 T/ha (Luckman *et al.* 1997a, Curran and Kuplich 1999). Ranson and Sun (1994) and Rignot *et al.* (1995) have shown that P-band backscatter can be used to estimate biomass for forest stands ranging from 150 T/ha (temperate forest) to 200 T/ha (tropical forest), respectively.

Rates of biomass accumulation vary dramatically due to different climatic, edaphic and land use controls. If we assume an average annual biomass accumulation rate of 6 to 9 T/ha (based on Alves *et al.* 1997) for secondary vegetation in Amazonia, then variations in L-band backscatter would saturate after 6-10 years (approx. 50-60 T/ha), whereas P-band radar backscatter would not saturate for 17-25 years (approx. 150 T/ha). There have been several studies that either mapped secondary vegetation stand age directly or used household surveys to estimate stand ages for sites throughout Amazonia. These studies provide insight into the utility of certain sensors for monitoring secondary vegetation. Luckman *et al.* (1997a) measured stand characteristics and used allometry to estimate biomass for 13 stands of secondary vegetation in central Amazonia, with stand age ranging from 2 to 22 years. Of these 13 stands, eight had biomass levels above the assumed saturation point for L-band backscatter estimates, while none of the stands exceeded the saturation point for P-band. Brondizio *et al.* (1994) studied the age class distribution of secondary vegetation stands in eastern Amazonia and found that only 20% of the area in secondary vegetation was less than 6 years old. Alves and Skole (1996) used multi-temporal SPOT XS imagery to characterize dynamics in rates of deforestation, secondary vegetation formation and turnover in Rondonia, Brazil. Of all the secondary

vegetation in 1986, 42% remained as secondary vegetation through 1992 and represented only 14% of the total area in secondary vegetation in 1992. Our analysis of 11 years of annual Landsat TM imagery indicates that in 1998 over 60% of all the secondary vegetation stands near Ariquemes, Rondonia were 6 years or younger (Chapter 1). Yanasse *et al.* (1997) used C-band and L-band SIR-C data to discriminate secondary forest stand ages up to 6 years old for a site in Tapajos. While P-band radar would be superior, L-band systems should be able to estimate the differences in biomass for a large portion of secondary vegetation stands throughout Amazonia.

The rate of carbon accumulation during secondary succession is a function of many factors, including type of disturbance (e.g. method of clearing, temperature and frequency of burning), agricultural practices (intensity), size and shape of disturbance, and climate (Bazzaz and Pickett 1980, Ewel 1983, Uhl *et al.* 1988, Nepstad *et al.* 1991, Fearnside and Guimarães 1996). There have been numerous studies measuring rates of accumulation in above ground and/or below ground biomass in tropical secondary forests following anthropogenic disturbance (e.g. Fittkau and Klinge 1973, Edwards and Grubb 1977, Sabhasri 1978, Uhl and Jordan 1984, Andriess and Schelhaas 1987, Uhl 1987, Saldarriaga *et al.* 1988, Uhl *et al.* 1988, Nepstad *et al.* 1991, Kauffman *et al.* 1995). In Amazonia, for example, average annual rates of above ground biomass accumulation in abandoned pastures and agricultural areas varied from less than 1 T/ha/yr for areas under long-term intensive pasture use (Nepstad *et al.* 1991) to over 12 T/ha/yr for light to moderate use areas (Alves *et al.* 1997, Nepstad *et al.* 1991, Uhl *et al.* 1988). Although there have been isolated field studies of above- and below-ground biomass accumulation rates in tropical secondary vegetation, the relative contributions of land use, climate, and

edaphic controls on rates of forest aggradation is not well understood. Therefore, estimation of changes in above-ground biomass and structure of secondary vegetation with remote sensing would be extremely useful for augmenting field based studies due to the synoptic nature of remote sensing applications.

In this paper we examine the potential of using multi-temporal JERS-1 SAR data for quantifying differences in rates of recovery of secondary vegetation for a site in central Rondonia. First, we characterize the temporal and spatial variability of JERS-1 normalized radar cross-section, defined as the fraction of backscattered power to the transmitted power and herein called sigma naught, across a chrono-sequence of secondary vegetation stands. Then, we test the biomass density, herein called biomass, retrieval scheme presented by Luckman *et al.* (1998) for mapping biomass at the landscape scale, and evaluate the impact of using multi-temporal JERS-1 SAR data for estimation of biomass. A quantitative understanding of sensitivity of estimating biomass changes with JERS data will highlight the effectiveness of this sensor for monitoring rates of regeneration in Amazonia. In an effort to estimate the impact of residual slash on the overall radar backscatter from secondary vegetation stands, we also examine the temporal changes in mean sigma naught with age of clearings. While Luckman *et al.* (1998) asserted that the biomass retrieval scheme is generalizable for sites across the Amazon provided sigma naught estimates are cross-calibrated to fit their model, our hypotheses concern the use of a model of similar shape with an asymptotic relationship between sigma naught and biomass. Our conclusions provided in this paper are intended to be relative, and would not change despite the use of directly-fit values of model parameters specific to our site in Rondonia. In a companion paper (Salas *et al.* in this

issue) we develop a series of statistical models to evaluate, in an operational context, what level of changes in biomass one might be able to identify with JERS-1 SAR data for a given confidence level. These models assess both the impact of number of JERS images on coefficient of variation of mean biomass estimates and how size of the secondary vegetation stands influence the confidence interval of the biomass estimates.

Methods

Multi-temporal TM Classifications

Annual Landsat TM from 1989 to 1998 (see table 3.1) were obtained through the NASA's Landsat Pathfinder project (Townshend *et al.* 1995). The first image in the time series was used as a base image and registered to north-up UTM projection using the coordinate estimates from the spacecraft ephemeris. TM data from subsequent years were co-registered to the base image using a first order transformation, based on between 30-35 manual ground control points, with RMS errors less than 0.6 pixels.

The co-registered TM data were classified using an unsupervised (ISODATA) clustering technique, followed by a manual, knowledge based assignment of the 45 clusters into 7 thematic classes (forest, cleared, natural non-forest, water, cloud, cloud shadow, and secondary vegetation). Mixed clusters were masked out and re-clustered to enhance class separability. Areas of water, cloud, cloud shadow, and natural non-forest were masked out of the classifications.

Mapping Age of Individual Secondary Vegetation Stands and Clearings

Land cover changes were quantified using post classification change detection, resulting in a transition sequence for each pixel. For example, a pixel that was deforested in 1990, abandoned to secondary vegetation in 1993, and then remained as secondary vegetation through 1996 would have a transition sequence from 1989 to 1996 of “FDDSSSS”, where F, D, and S represent forest, non-forest, and secondary vegetation classes, respectively. The histograms of all possible transition sequences were analyzed to quantify the land cover change dynamics. Initial analysis of the magnitude of the number of land cover change transitions between 1989 and 1996 and their spatial patterns revealed a highly dynamic landscape (Salas *et al.* in prep). Likely some of this dynamic is the result of edge effects due to sub-pixel mixing, artifacts from mis-registration, and classification errors, but based on the size of many of these changes this is also highly dynamic landscape where land use patterns result in rapid changes in land cover (Alves and Skole 1996, Skole *et al.* 1994).

For this study, we segmented clearings and stands of secondary vegetation into two sets of age classes based on whether or not we knew when the areas were initially cleared from forest and, for the secondary vegetation classes, how long the area remained as non-forest. Table 3.2 contains the class transitions we used for this analysis. To insure that the land cover of the secondary vegetation and the clearings did not change between the 1996 TM acquisition and the JERS acquisitions later in 1996, the 1997 TM classification was used to remove those areas that changed land cover between the 1996 and 1997 TM inventories. All other transition combinations not listed in table 3.2 were masked out. Individual fields or stands were identified and labeled in a GIS by running an

8-neighbor clump algorithm. A 3x3 low pass filter was used to identify boundary pixels for each clump. These boundary pixels were then removed to minimize the impact of single or sub-pixel mis-registration between the multi-temporal SAR data and the TM-based land cover database, and to remove boundary effects at the edge of intact forest and clearings/secondary vegetation stands that cause increased backscatter at the near boundary and radar shadows at the far boundary (Leckie and Ranson 1998). All stands or fields smaller than 0.75ha were subsequently removed from the analysis to minimize the variance of the mean stand sigma naught due to speckle. Our resulting map of secondary vegetation contained 182 stands, ranging from 1 to at least 8 years old.

Accuracy assessment of Secondary Vegetation and Clearing Age

An accuracy assessment on the 1998 classification was performed with 166 field reference points collected in October 1998. The overall classification accuracy was 98.2% with producer's/user's accuracies of 100%/97.97% and 83.3%/100.0% for the non-forest and secondary vegetation classes, respectively. However, to estimate the overall classification accuracy of the land cover change statistics, estimates of accuracy from additional time periods are needed. This study area is also a field validation site for NASA's Landsat Pathfinder Humid Tropical Forest project. The Landsat Pathfinder accuracy assessment for this area for the 1993 TM scene used 103 reference points with an overall accuracy of 84%, a user's accuracy over 96% and a producer's accuracy over 90% for the non-forest class. Areas that were cleared previously and not classified as deforested must, therefore, be secondary vegetation, hence the accuracy of the deforested class controls the accuracy of the transitions. Although we have not performed an annual

accuracy assessment for each classification, we estimate the overall accuracy of the 8 year (1989 through 1996) post classification change detection to range between 72% (based on 1993 Pathfinder accuracy results) to 85% (based on the 1998 results). The objective of our TM image classification was to create the most accurate possible maps of deforestation and vegetation regrowth. Therefore, we performed rigorous manual editing by heads up digitizing on the full resolution TM data. While the methods used for the Landsat Pathfinder analysis were similar in using multiple clustering, the manual editing step was performed at 1:250K scale with hardcopy overlay for the Pathfinder analysis to facilitate timely completion of the over 2000 images for the Landsat Pathfinder Humid Tropical Forest project (see Chomentowski *et al.* 1994 for more details on Pathfinder processing). As a result of these slight differences in processing detail, the overall accuracy should be closer to the 85% estimate derived from the 1998 assessment.

JERS-1 SAR data pre-processing

The Japanese Earth Resources Satellite 1 (JERS-1) was launched and operated by National Space Development Agency of Japan (NASDA) from February 1992 until October 1998. Onboard the JERS-1 satellite was an L-band (1.275 GHz) synthetic aperture radar (SAR) with horizontal co-polarization (HH). The JERS-1 SAR imaged with a 35° look angle and a ground resolution of 18m in both range and azimuth with a 44 day revisit cycle. Table 3.3 lists the eight level 2.1 products (3-looks with 12.5m pixels) used for this study. Figure 3.1 contains a subset of the 1996 TM image and a 3-date RGB composite of the 1996 JERS images from October, August, and July, respectively. These data were obtained through our participation in NASDA's Global

Rain Forest Mapping Project (see Rosenqvist *et al.* 2000 for details on GRFM). JERS-1 SAR data were used for our analysis of secondary vegetation because the lower frequency of L-band is more sensitive to above-ground biomass than C-band data available from ERS or Radarsat, the only other satellite based SARs.

All eight images were co-registered automatically using image cross-correlation. To convert from 16-bit digital numbers (DN) to normalized radar cross-section, herein called sigma naught (σ°), values in dB the following formula was applied:

$$\sigma^{\circ} = 20 \log_{10}(DN) + F \quad (1)$$

where F is the NASDA provided correction factor (-68.5 dB for the images #1-7 and -68.3 dB for image #8). Equation (1) and the correction factors are taken from Shimada 1998. While it is possible to use the noise vector to improve the noise floor for JERS data (Chapman *et al.* 1999), it was not applied for this application. An estimate of noise equivalent sigma naught was derived from average DN values from a region of open water.

A range ramp in sigma naught values from mature forest stands was observed. While these data have been calibrated, there are still some residual artifacts due to significant antenna pattern variations, random gains in range, and slight incidence angle effect across the JERS footprint. The antenna pattern variations and random gain deviations have been observed before in data processed at NASDA (Rosenqvist *et al.* 2000). An empirical linear correction was derived from a 60 kilometer transect in range covering primary forest to normalize the impact of these combined range effects (Leckie

1990, Ranson and Sun 1994). The range ramp across this transect varied from less than 0.4dB to over 1.5dB (see table 3.3). The October 23, 1995 image was processed at the Alaska SAR Facility (ASF). ASF used a different antenna pattern correction algorithm that has been shown to perform a better correction (Chapman *et al.* 1999). The slight range ramp observed is attributed to the variations in incidence angle from near range to far range (34° to 43°) (Chapman *et al.* 1999). It is assumed that, while this linear empirical correction may not properly model incidence angle effect for non-forested areas across the landscape, the impact will be a second order effect due to the small range in incidence angles and, hence, is ignored. This noise due antenna pattern artifacts may be a result of the older SAR processor used at NASDA for these data.

To apply the biomass density retrieval scheme proposed by Luckman *et al.* (1998), we applied a cross-calibration correction procedure to normalize the gain of these 8 JERS images relative to the reference image used to derive the biomass model parameters. Mean and coefficient of variation statistics of σ^0 for a 228 hectare (≈ 14600 12.5m pixels) area of mature forest was extracted from all eight images. The cross-calibration gains were relatively small (<0.5 dB) and are listed in table 3.3.

Extraction of Stand and Clearing Sigma Naught Statistics and Confidence Limits

Radar imagery contains many sources of variability that contribute to the spatial and temporal variability in estimating mean sigma naught from a target. Our data pre-processing attempted to remove variability due to changes in calibration gains and antenna patter corrections for different incidence angles. However, to estimate the mean sigma naught from distributed target (stand of secondary vegetation or an individual clearing) other sources of variability must be considered, including speckle and the

intrinsic spatial heterogeneity of the target (Rignot and Kwok 1993). Canopy structure of secondary vegetation in the Amazon varies dramatically with and across age classes due to differences in species composition and growth rates. This type of spatial heterogeneity can be seen as meso-scale roughness in radar imagery, which is often expressed as image texture.

Physical scattering models predict that the sigma naught from randomly distributed scatters (incl. leaves, branches, and boles of the trees) will have a negative-exponential distribution whose mean value represents the true sigma naught of the target (Oliver 1991). Rignot and Kwok (1993) modeled the power (P) of a radar return at a given pixel location (i, j) for a region l would be:

$$P_{i,j,l} = [\langle I \rangle + T_{i,j,l} + n_i] S_{i,j} \quad (2)$$

where $\langle I \rangle$ is the expected backscattered power, $T_{i,j,l}$ is a random texture variable, n_i is system noise due to a mixture of noise sources (assumed to be additive and a function of slant range), and $S_{i,j}$ is an image speckle random variable. Since speckle and system noise can strongly modulated spatial statistics from space-borne SAR systems where the signal-to-noise ratio can be low, removal or estimation of speckle and system noise is necessary (Rignot and Kwok 1993). Noise equivalent sigma naught (NES0) was estimated from regions of open water within the images. For the eight images used in this study, NES0 ranged from -14.88dB to -17.16dB (see table 3.3). Estimates of the lower limit of sigma naught from secondary forests suggest that sigma naught values will exceed -11.0dB . Therefore, since NES0 estimates are at least 2.88dB less than the lowest

sigma naught values for secondary forests, system noise was assumed to be negligible.

Therefore equation (1) above can now be expressed as follows:

$$P_{i,j,l} = \langle I \rangle \cdot T_{i,j,l} \cdot S_{i,j} \quad (3)$$

The variance-to-mean square ratio of speckle can be estimated by $1/N$ where N is the equivalent number of looks (ENL) which is only a function of the imaging and processing system characteristics and not on the distribution of radar cross-section of the target (Rignot and Kwok 1993). Vieira (1996) estimated N for the NASDA level 2.1 product to be 2.8. For this study we analyzed only those stands and clearings that were at least 0.75 hectare. Given that the resolution of JERS is 18 meters, at least 23 independent samples were used to estimate mean sigma naught. Therefore, our maximum variance-to-mean square ratio due to speckle is 0.0155 ($1/ENL \cdot 23$). The influence of speckle on our mean sigma naught estimates will be small.

A source of variation in our mean sigma naught estimates comes from the intrinsic spatial heterogeneity of the targets (secondary vegetation stands and clearings). Luckman *et al.* (1998) following Oliver (1991), indicated that intrinsic texture (heterogeneity) variance (V_t) can be estimated by

$$V_t = \frac{\left(\frac{sd}{\mu}\right)^2 - \frac{1}{N}}{1 + \frac{1}{N}} \quad (4)$$

where $(\frac{sd}{\mu})$ is the coefficient of variation (CV) within the stand and N is ENL (Note;

in Luckman *et al.* 1998 the equation for V_t had an error in that the square of $\frac{sd}{\mu}$ was

missing). From equation (4) the expected CV value due to both speckle and texture was then calculated using

$$CV = \sqrt{\frac{V_t}{N} + V_t + \frac{1}{N}} \quad (5)$$

from which approximate 95% confidence limits in dB of two times the standard error of the mean were calculated using

$$10 * \log(1 \pm 2 * CV * \frac{1}{\sqrt{n}}) \quad (6)$$

where n is the number of pixels in the stand. Note that this method of calculating confidence limits does not account spatial correlation in sigma naught between neighboring pixels resulting from the pixel size being smaller than the resolution of the sensor. Including correlation between pixels in the calculation would increase the width of the confidence limits, but would not alter the pattern of relative values of confidence limits between even sized stands. To account for pixel-to-pixel correlation, we increased the confidence intervals based on the number of pixels within each stand.

Using equations (1), (4), (5) and (6) we calculated mean σ° and 95% confidence limits for each of the 182 stands of secondary vegetation and σ° for each of the 152 clearings.

Biomass Density Model

Luckman *et al.* (1998) developed a semi-empirical model for estimating biomass density of regenerating forests across the entire Brazilian Amazon using JERS-1 L-HH sigma naught data. The model coefficients were derived from field and radar observations for a site near the Tapajos River and then validated using independent field and JERS-1 data from Manaus. They concluded that noise due to speckle and image texture limits the utility of the above-ground biomass estimates to distinguishing four broad classes of regeneration state. We decided to use their model to quantify differences in broad biomass levels across the landscape and to track changes in biomass levels. Their model relates field estimates of biomass (B) to σ° by

$$\sigma^{\circ} = a - e^{-(bB+c)} \quad (7)$$

where a, b, c are constants that were empirically derived from field based estimates of biomass for 18 forested stands near the Tapajos River in the State of Para. Inverting this model to estimate biomass (B) from σ° yields the following equation

$$B = \frac{-\ln(a - \sigma^{\circ}) - c}{b} \quad (8)$$

Using equation (8) with our mean stand values and our confidence ranges, biomass for all 182 stands of secondary vegetation for each of the JERS images was estimated. We used the following values $a = 0.170$, $b = 0.053$, and $c = 2.146$ (taken directly from Luckman *et al.* 1998) for our calculations. While the biomass model saturates with respect to sigma naught at a biomass level around 60T/ha, equation (8) will provide biomass estimates beyond the sigma naught model saturation point. Therefore, for graphical purposes, we arbitrarily set maximum biomass estimates levels at 100T/ha.

Results and Discussion

Landscape Variability in Sigma Naught Across a Chrono-sequence of Secondary Vegetation and Clearings

Precipitation in this region of the Amazon is highly seasonal. There is a pronounced dry season from June through August during with less than 4% of the annual 2250mm of precipitation. Monthly mean precipitation derived from station measurements from 1978 through 1993 is provided in Figure 3.2. Unfortunately, daily precipitation for this region of Rondonia was not available for the time period of our JERS SAR data, therefore we examined image statistics to estimate relative variability due to surface moisture. Radar backscatter increases as soil moisture increases, often leading to decreased image contrast for landscapes in the Amazon with pastures and forest (Grover *et al.* 1999). Examination of our 4 JERS images from 1996 revealed that the July 13th image had the largest contrast between cleared areas and intact forest (>2dB difference) and that the October 9th and November 22nd images had the smallest contrast (figure 3.3). The July 13th image was assumed to have the least amount of soil moisture effects and,

hence, was used to characterize the mean sigma naught of our three broad land cover classes (forest, secondary vegetation, and cleared lands) across the landscape.

At the landscape scale, mean σ° increased with age of the secondary vegetation stands and decreased with age of clearings (see Figure 3.4). Across a three-year chronosequence of regrowth from 1 to 4 years the mean σ° derived from all stands ranged by 1.4dB (-10.4dB to -9.0dB). The range between the mean values from all the 4- to 8-year old stands was less than 0.3dB. This increase in σ° with stand age was expected as secondary vegetation stands tend to accumulate above-ground biomass with age. Rates of biomass accumulation for areas following light use in the region recover at an average annual rate ranging from 6.6 to 8.7 T/ha (Alves *et al.* 1997). On average 1-year old clearings had mean sigma naught of -8.8dB, higher than the 1- to 4-year old stands of regrowth. Mean σ° for the 3- and 8-year old clearings were over 3dB and 5db lower than the 1-year old, respectively, possibly reflecting a loss of residual biomass with age. Following forest clearing, slash is often left on site to dry out for up to two months after felling of the trees prior to burning. In Rondonia, clearing typically takes place in June and July, followed by burning in August and September. Estimates of burning efficiencies (amount of biomass consumed by the burn) range from 39% (Houghton 1991) to 51% (Kauffman *et al.* 1995). While the clearing process may be different for areas used for annual crops versus pasture, our clearing class contained both crop areas and pasture. The σ° data in figure 3.4 are from July 13, 1996, which was likely acquired before burning had begun for the 1996 dry season. All 1-year old clearings had been cleared by the June 24, 1996 TM scene used to map these new clearings. The large difference (2.5 dB) in 1-year and 2-year old clearings is most likely due to the first burn.

After the first burn, the biomass of slash declines more slowly due to decay processes with occasional repeated burning to establish and maintain pasture.

JERS σ° Statistics for Individual Clearings and Stands of Secondary Vegetation

Temporal variability in stand level σ° estimates can result from change in JERS-1 calibration, system noise, speckle, image texture, topographic effects influencing per-pixel scattering area estimates, and environmental conditions (Luckman et al. 1998). These first three potential sources of variability in σ° are unlikely to have much of an impact given our cross-calibration procedure and stand size limitations imposed for this analysis. This region of Rondonia is relatively flat, so topographic effect will likely be small. The influence of intrinsic image texture was characterized by equation (4). Variations in soil and plant dielectric properties and their relative contributions to stand level σ° will vary depending on the environmental conditions and the overall stand structure.

The mean and variance of σ° estimates for each clearing and secondary vegetation stand were spatially and temporally highly variable. While the clearing exhibited the same general trend that we observed on the landscape scale, namely a decrease in σ° with age, the variability within the same age classes was comparable to the temporal changes resulting from loss of residual slash following initial clearing (see Figure 3.5.). First year clearings had mean σ° values ranging from approximately -6.5dB to -12.0dB . Some clearings had higher σ° than the surrounding forest, most likely due to enhanced double bounce caused by the ground and slash interactions (Rignot *et al.* 1997, Saatchi *et al.* 1997). High response ($\sigma^{\circ} > -8.0\text{dB}$) was observed from the 1 and 2-

year old clearings in all four 1996 images. In the July 13th image, 12 of the 39 (31%) 1-year old clearings had σ° values greater than -8.3dB , the threshold for old regeneration and primary forest class in Luckman *et al.* (1998) biomass density retrieval scheme. These 12 clearings represented 36% of the total area for all 1-year old clearings. Of the 2-year old clearings, 20% (12% of the area) had mean σ° greater than -8.3dB , a lower percentage than the 1-year old population. On an area weighted basis more than 96% of the older clearings had mean σ° less than -8.3dB in all four 1996 images. The new clearings did not exhibit an appreciable decrease in sigma naught from the early dry season data to the later dry season images as would be expected once the slash for the clearing had been burned, indicating that environmental conditions may mask land use impacts on mean sigma naught. Normalization of soil moisture and micro-scale surface roughness effects would lead to better information on differences in clearing process. Further quantification of these differences would be useful for quantifying variability in clearing practice (amount of slash removed off site), burning efficiencies, and rates of decay of residual biomass.

While there is a general trend of increasing sigma naught with secondary vegetation stand age, there are significant temporal and spatial differences within age classes of secondary vegetation (figure 3.6). The intra-annual temporal differences in sigma naught from July 13th to November 22nd are apparent with higher sigma naught in the late dry season/early wet season images. The observed across stand variability within age classes was expected to a certain extent due to variability in amounts of residual slash, rates of biomass accumulation and differences in species composition. The

temporal variability is likely due to changes in environmental conditions (e.g. moisture content of soil and vegetation) resulting in large variations in mean sigma naught.

We converted mean σ° to biomass using equation (8) to look at trends in biomass estimates with age of the secondary vegetation stands (Figure 3.6). Biomass estimates were extremely variable and tended to increase with age of the stands. The biomass model from Luckman *et al.* (1998) was derived by fitting a sigmoid curve to field based estimates of biomass using a least squares fit. It is important to note that this sigmoid function reaches an asymptote at the biomass saturation point (Luckman *et al.* 1997a). Estimates of the saturation point for JERS L-HH biomass retrievals range from 40 T/ha (Imhoff 1995) to 60 T/ha (Curran and Kuplich 1999, Luckman *et al.* 1997a). Therefore, biomass estimates above the 40 to 60 T/ha range may be artifacts of the sigmoid function and not a reflection of differences in the actual above-ground biomass. Nevertheless, there are important trends in these results. The percentages of secondary vegetation stands at or above the saturation point increased with age. From the July 13th image, we see only one 1-year old stand above the saturation point, where more than 60% of the 8-year old stands were above the saturation point. Estimates from the October and November images had a larger percentage of the biomass estimates saturate. While the secondary vegetation stands may have accumulated some biomass between June and November, the large increase of saturated estimates is likely due to higher mean σ° , likely resulting from wetter environmental conditions and higher soil and vegetation moisture content (Curran and Kuplich 1999).

We examined the temporal stability of estimating biomass by comparing, on a stand-by-stand basis, biomass estimates for all 8+-year old stands from our July 13th,

1996 image with the three other 1996 estimates (Figure 3.7). In this figure we have drawn a line at 31 T/ha to represent the maximum biomass of secondary vegetation that Luckman *et al.* (1998) estimate can be separated from mature regrowth with a 95% confidence level. Once again the estimates vary dramatically across these four images and hence are not temporally stable. As stands age, the variance in mean σ^0 due to environmental conditions should decrease due to enhanced scattering from higher above-ground biomass. For example, Hashimoto *et al.* (1997) documented different seasonal variation in JERS-1 sigma naught for dirty pastures and two biomass classes of secondary vegetation in Rondonia, with ranges decreasing from over 2dB to 1dB. However, at the same time, as the stands develop there should be increased canopy heterogeneity as the overstory develops resulting in greater variance due to texture effects (Luckman *et al.* 1997b). A large percentage of the July 13th estimates that are below the saturation point exceed the saturation point for the other dates (Figure 3.7, quad 3). Secondly, there are many stands that exceeded the saturation point in the July 13th image (assumed to have the least soil moisture effects) and did not saturate for the later estimates (Figure 3.7, quad 2). A majority of the stand estimates were above the saturation biomass levels (quad 4). Based on the Alves *et al.* (1997) biomass accumulation rates of between 6.6 and 8.7 T/ha/yr, we would expect all the stands to have biomass levels exceeding the 31 T/ha saturation point. Of the 135 8+-year stands in our analysis, only 2 had biomass estimates below the saturation point for all four estimates, but if we only look at the July 13th data then 21 stands were below saturation point. The presence of some stands below this point indicate that either: a) the rate of biomass accumulation is well below the Alves *et al.* rates of 6.6 to 8.7 T/ha, b) the JERS estimates significantly

underestimate the actual biomass, or c) the TM classifications of vegetation regrowth areas are wrong. While dirty (not well maintained) pastures often have similar TM spectral properties to young secondary vegetation, especially for early dry season TM acquisitions, the probability is quite low that a dirty pasture would be classified as secondary vegetation in all 8 TM classifications because the farmers would need to maintain the pastures at some point in this period to still be able to use the land as pasture. Once the farmer maintained the field by burning the herbaceous vegetation the TM classification would have mapped the area as cleared.

Figure 3.8 illustrates the range in biomass estimates for all the 1-year old stands in 1996. While the percentage of regrowth stands above the saturation point in all 4 images is much lower (16%), 86% of the stands had at least one estimate above the saturation biomass level of 31 T/ha. From the July 13th image alone, 16% of the stands were above the saturation point. All of these 1-year old stands had been cleared from forest in 1994, were used for 1-year (1995) prior to secondary vegetation formation and therefore there could still have a large portion of residual slash remaining on site from the original clearing event in 1994.

Analysis of variance of spatial and temporal variability in stand sigma naught

We performed an analysis of variance (ANOVA) derived from mean stand σ^0 measurements from all four 1996 images to quantify the relative contributions of stand and temporal variability to the overall variance of the stand sigma naught. All 179 secondary-growth stands for which data were available from more than one scene were included in the analysis, yielding 685 observations. We assumed that the change in

above-ground biomass between the July 13th and November 22nd would have a negligible effect on the mean σ^o for any given stand. For this analysis we modeled the measured sigma naught in linear units (σ^o_{ij}) for a particular stand (i) at any given time (j) as

$$\sigma^o_{ij} = \mu + S_i + T_j + \varepsilon_{ij} \quad (9)$$

where μ is the average sigma naught across all stands and time periods, S_i is the expected difference of stand i from the average, T_j is the expected difference of a stand observed at time j from the average, and ε_{ij} is uncorrelated error due to noise. In performing the ANOVA, observations were weighted inversely proportional to their variance (calculated as $CV_{ij}^2 \sigma^o_{ij}$).

From this analysis we again see that the July 13th and August 26th images had lower mean sigma naught and the October 9th image had higher mean sigma naught values than the November 22nd images (Table 3.4), which is consistent with our expectations based on the mean landscape statistics (Figure 3.3).

A decomposition of the components of the variance in sigma naught is shown in Table 3.5. This decomposition is based on the unweighted contributions of the different parameters to estimated σ^o_{ij} values, and the corresponding residuals. Variation between stands that is consistent from image to image is indicated by the variability of the S_i values, and represents the majority of the variance. Variance between images that is consistent from stand to stand is indicated by the variability of the T_j values. The relatively small magnitude of this variation, and its minor contribution to the overall

variance, suggest the careful cross-calibration procedures employed here were successful in minimizing scene-wide impacts of calibration and environmental effects. In addition, changes in environmental conditions between images had a differential effect on the stands. However, the contribution of noise (ϵ_{ij} values) is large. The expected magnitude (in a root mean square sense) of the uncorrelated noise term is 74% of the expected magnitude of the difference of a stand from the mean. Because the error term is uncorrelated across a scene, it cannot be reduced through cross-calibration or the inclusion of a range of ground-truthed reference stands in the imaged area. Contributions to the overall error term include image texture, speckle, relative calibration, random system noise (Rignot and Kwok 1993), and within scene variability in environmental conditions (e.g. soil and vegetation moisture content). However in this case, the contribution of the error term is several times the contribution that would be expected from texture and speckle alone ($\chi^2=1807.7$, d.f.=503, $p<0.001$). Therefore, given the fairly high system signal-to-noise characteristics of these images, a large source of the noise term is likely due to the relative calibration and environmental conditions. There may also be a slight slant-range dependence that impacts the relative contribution of system noise across a single image. Since the relative calibration of JERS is approximately 1.0dB and the range in expected σ^0 is less than 2.5dB across a biomass range from 6 T/ha to the saturation point of 31 T/ha, calibration and differential effects on changing environmental conditions control the total noise contribution.

Soil moisture impact on mean stand sigma naught will be a function of soil moisture, soil roughness and amount of above-ground biomass. Stands with high biomass will likely be less sensitive to differences in soil moisture beneath the canopy in the

absence of standing water. Based on a threshold of $p < 0.05$, we estimate that, for 45% of secondary vegetation area, the variance in linear sigma naught within a stand estimate was within the expected range due to texture and speckle effects and, therefore, less sensitive to changes in environmental conditions. Looking at the temporal impact of background effects on stand sigma naught provides useful information on the overall scattering properties of the target. Sigma naught from a vegetated target is a function of the vegetation dielectric properties and structure, and sub-canopy surface conditions. Since within a given dry season the structure of secondary vegetation canopy will not change much and vegetation in this region do not experience water stress, differences in sigma naught are a function of sub-canopy conditions and water on vegetation surfaces (not withstanding variability due to system noise and relative calibration errors). The amount of temporal variability in mean sigma naught can be used to separate qualitative differences in stand scattering properties.

Conclusion

This study evaluated the spatial and temporal variability in L-HH sigma naught from secondary vegetation stands and clearings across a chrono-sequence of ages using JERS-1 SAR data. At the broad landscape scale, mean radar σ° increased with age of secondary vegetation, likely a result of higher above-ground biomass levels with age, and decreased with age of clearings, likely due to decreases in residual slash over time by burning and decay processes. However, at the stand level the sigma naught trends are more difficult to quantify. The temporal variability in mean stand σ° due to system

noise, relative calibration errors, environmental and site conditions is comparable to the expected dynamic range of σ° across the biomass values expected for secondary vegetation stands younger than 6 years old. The range of within age classes sigma naught was greater than the range across age classes. The source of this variability is likely due to a combination of differences in rates of regeneration, intrinsic stand texture, amount of residual slash, and soil and vegetation moisture conditions. Furthermore, differences in sigma naught signal between two stands at the same time, or between two observations of a single stand, is likely to include a sizeable noise contribution.

While quantitative retrievals of biomass with JERS need to be evaluated on a case-by-case basis, multi-temporal JERS data can be used to estimate qualitative differences in stand characteristics. An assessment of statistical variability in σ° with multi-date JERS relative to expected variance from texture, speckle, and system noise provides information on stability of the stand scattering properties for upland forest. While these differences may not relate directly to biomass, inferences about signal saturation can be made.

JERS-1 SAR data acquired during the dry season (June and July in this case) provided better contrast in general than the wet season data (October and November), but the best images cannot be selected based solely on acquisition date due to precipitation events during dry months. In addition to better characterization of secondary vegetation stand scattering properties, multi-date images improves the classification of clearings, secondary vegetation and forest by resolving some ambiguities due to the clearing process. Synergy of Landsat derived age information with JERS derived scattering properties provide a better characterization of the overall structure of clearings and

secondary vegetation stands in Amazonia. Further work is needed to quantify the implications of using JERS derived biomass estimates of secondary vegetation for mapping differences in rates of regeneration. The relationship between stand structure and radar texture needs to be researched further as a potential source of complementary information to mean stand sigma naught.

Acquisition Date	Season
July 7, 1989	Dry
December 2, 1990	Early Wet
June 12, 1991	Early Dry
June 22, 1992	Dry
October 7, 1993	Late Dry
June 4, 1994	Early Dry
July 25, 1995	Dry
June 25, 1996	Dry
June 28, 1997	Dry
July 17, 1998	Dry

Table 3.1 Landsat TM data used for multi-temporal classifications. While optical data suffer less from seasonality effects (excluding clouds), the images acquired during and at the end of the wet season tend to have a slightly higher proportion of secondary vegetation due to rapid growth of herbaceous vegetation.

Secondary Vegetation Classes			Clearing Classes		
Transition from	Age in	Code	Transition from	Age in	Code
1989 to 1996	1996		1989 to 1996	1996	
FFFFFFDS	1	1	FFFFFFFD	1	1
FFFFFFDSS	2	2	FFFFFFDD	2	2
FFFDSSSS	3	3	FFFFDDDD	3	3
FFFDSSSS	4	4	FFFFDDDD	4	4
FFDSSSSS	5	5	FFFD DDDD	5	5
FDSSSSSS	6	6	FFDD DDDD	6	6
FSSSSSSS	7	7	FD D D D D D D	7	7
DDDDDDDS	1	11	DDDD DDDD	8+	8
DDDDDDSS	2	12	SSSSSSSD	1	11
DDDDDSSS	3	13	SSSSSSDD	2	12
DDDDSSSS	4	14	SSSSSDDD	3	13
DDSSSSSS	5	15	SSSS DDDD	4	14
DDSSSSSS	6	16	SSSD DDDD	5	15
DSSSSSSS	7	17	SSDD DDDD	6	16
SSSSSSSS	8+	18	SDDDDDDD	7	17

Table 3.2. Class Transitions for estimating age and land use history for the secondary vegetation stands and clearings. Each entry for the transitions was derived from a single TM classification.

Image	Date	Season	Range Ramp	Cross-Calibration	NESO
1	2/27/1993	Wet	1.058 dB	0.11 dB	-16.35 dB
2	4/21/1993	Wet	1.182 dB	-0.35 dB	-16.37 dB
3	9/22/1994	Late Dry	1.538 dB	-0.44 dB	-16.29 dB
4	10/23/1995	Late Dry	0.374 dB	-0.37 dB	-14.88 dB
5	7/13/1996	Dry	1.516 dB	-0.33 dB	-17.16 dB
6	8/26/1996	Dry	0.954 dB	-0.09 dB	-15.04 dB
7	10/9/1996	Late Dry	1.340 dB	-0.14 dB	-15.75 dB
8	11/22/1996	Early Wet	0.948 dB	0.09 dB	-14.93 dB

Table 3.3 JERS-1 SAR level 2.1 data used. *Image 4 was processed by JPL, remaining 7 images were processed by NASDA. Cross-calibration differences were less than 0.5dB. The range ramp correct was derived using an empirical line model.

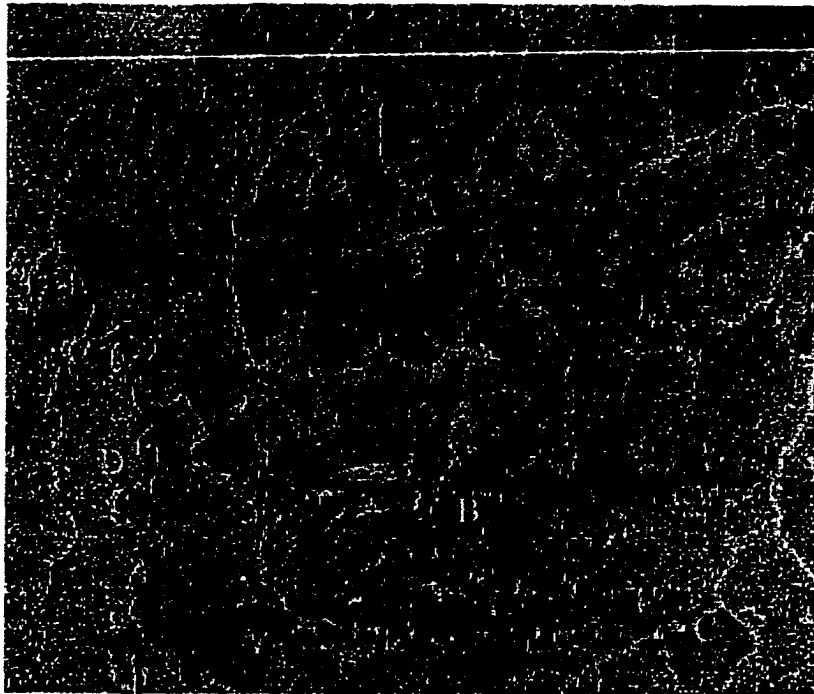
<i>Date</i>	<i>T_i</i>
July 13	-0.0030
Aug 26	-0.0031
Oct 9	0.0054
Nov 22	0.0007

Table 3.4 Estimated departure from average sigma naught for each of the four scenes in 1996, in linear units. The two dry-season scenes show lowest average sigma naught, consistent with expectation. The difference among images is statistically significant ($F=10.23$, $df=3$, $p<0.0001$).

<i>Source</i>	<i>Root Mean Square Value</i>	<i>Percent of Variance</i>
Stand variability (S_i)	0.0238	63.4%
Temporal variability (T_j)	0.0035	1.4%
Noise (ϵ_{ij})	0.0177	35.2%

Table 3.5 Magnitude of effects in the analysis of variance, and variance components as a percent of the total. While temporal variability (consistent within a scene) is small, noise from stand to stand is large, and similar in order of magnitude to the variability between stands within a scene.

(a)



(b)



Figure 3.1: (a) 3-date RGB composite of JERS SAR images from October 9, August 26, and July 13 from 1996, respectively. (b) TM image from June 25, 1996 in 4,3,2, RGB. The following areas are labeled: A) recently cleared land (after June 25th and before July 13th), B) older clearing, C) secondary growth (red color in TM image), D) undisturbed forest (cross-calibration site), E) dirty pasture. Note that in (a) the recent clearings have higher intensity with less heterogeneity than intact forest.

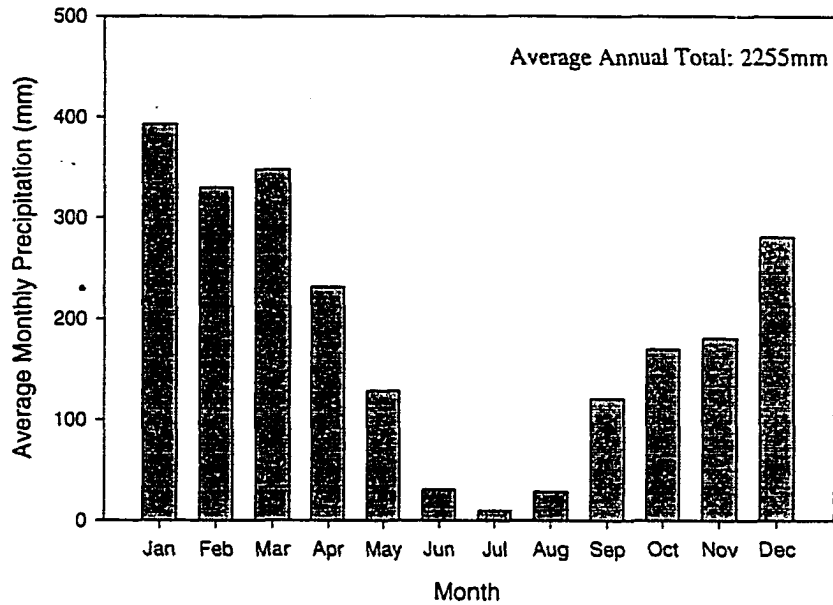


Figure 3.2 Mean Monthly Precipitation. Data are averages from station data acquired from 1978 to 1993. Source Division National Agua Energy Electric, Brazil. This region of the Amazon has a very pronounced dry season, running from June through August, with less than 3% of the total annual precipitation.

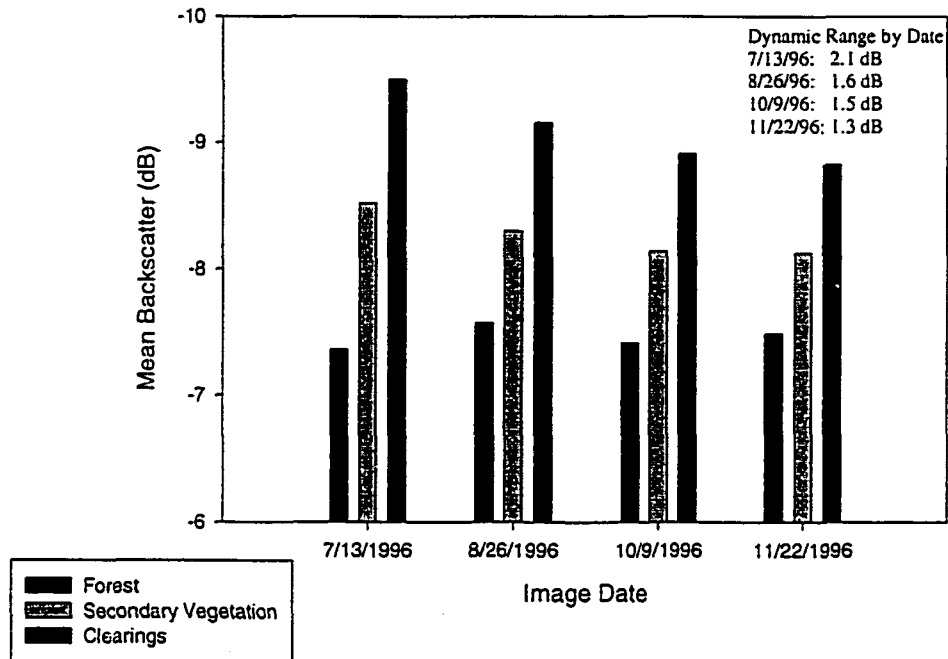


Figure 3.3 Landscape Statistics. The dynamic range, defined as difference between mean backscatter of forest and clearings, is provided. The image from 960713 has the largest contrast (dynamic range) between mean forest backscatter and mean clearing backscatter. The two images acquired late in the dry season and early in the wet season have the lowest contrast. From this it appears the July 13 image is driest.

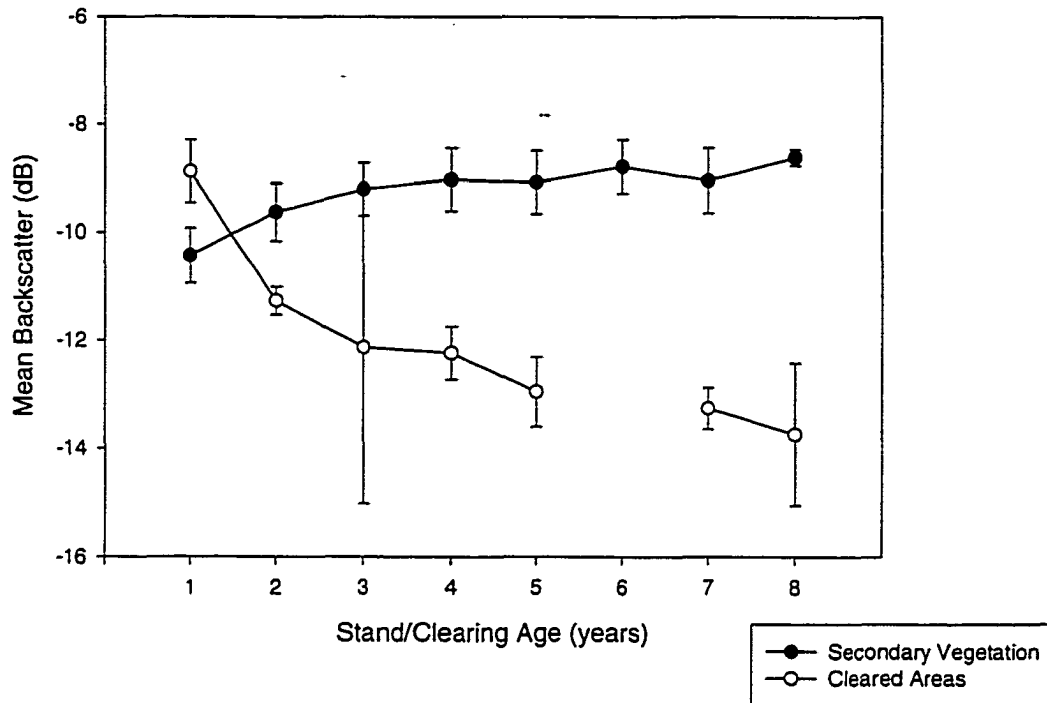


Figure 3.4. Mean backscatter across the landscape by age, calculated by averaging intensity means of all secondary vegetations stands or cleared areas. Error bars represent the 95% confidence levels ($\pm 1.96 \times \text{standard error}$). Statistics derived from July 13, 1996 image. Backscatter is higher for younger clearings and rapidly decreases with age. Backscatter is lower for young stands of secondary vegetation and increases with age.

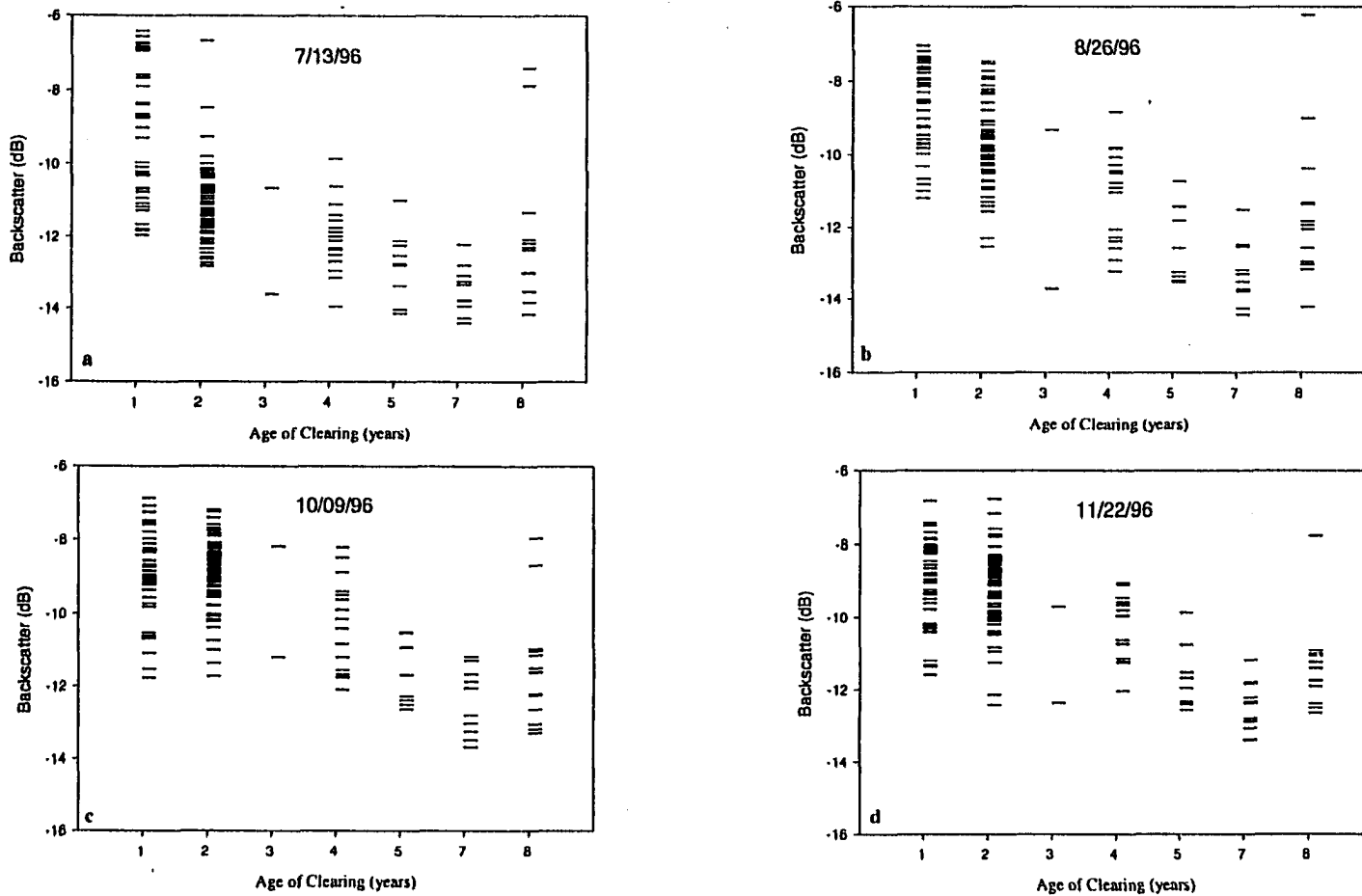


Figure 3.5. Mean backscatter by age of clearing. While there is a general trend of decreasing backscatter with age, there is also considerable range of mean backscatter within a single age cohort, as well as temporal differences. The October and November images tend to have higher mean values, likely because of higher dielectric properties of the target due to increased moisture content of soils and vegetation. Magnitude of the soil moisture effect depends on the soil texture, the surface roughness of the clearings, and amount of biomass.

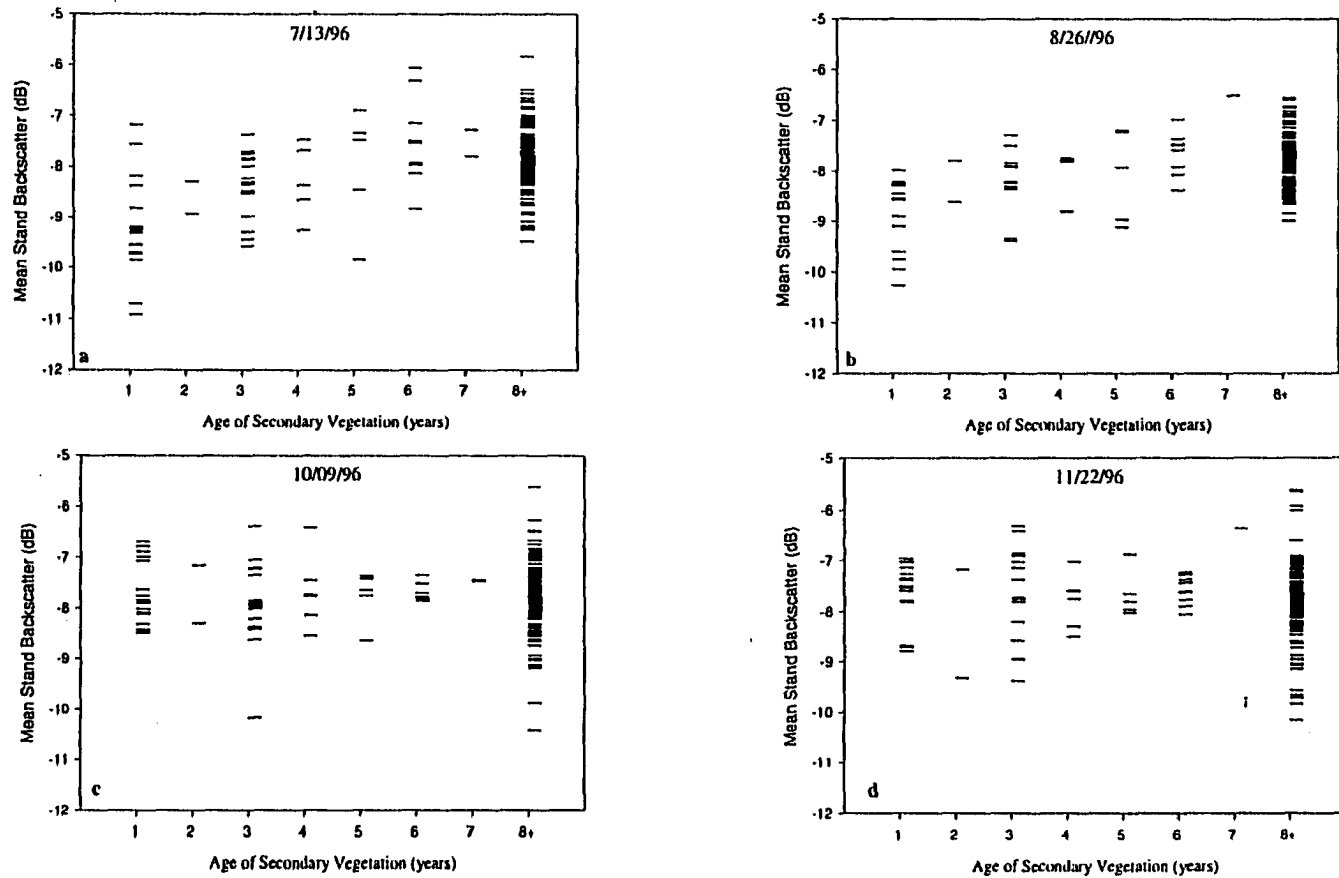


Figure 3.6. Mean stand backscatter by age of secondary vegetation. While there is a trend of increasing backscatter with age, there are significant temporal and spatial differences within age classes of secondary vegetation. The temporal differences in backscatter from July 3th to November 22nd are apparent with higher backscatter in the late dry season/early wet season images. The spatial variability within the same age classes is due to surface roughness, and land use effects, sensitivity of the backscatter characteristics with small changes in biomass, as well as variability in rates of biomass accumulation. The temporal variability is due to changes in environmental conditions (e.g. moisture content of soil and vegetation) resulting in large variations in mean stand backscatter.

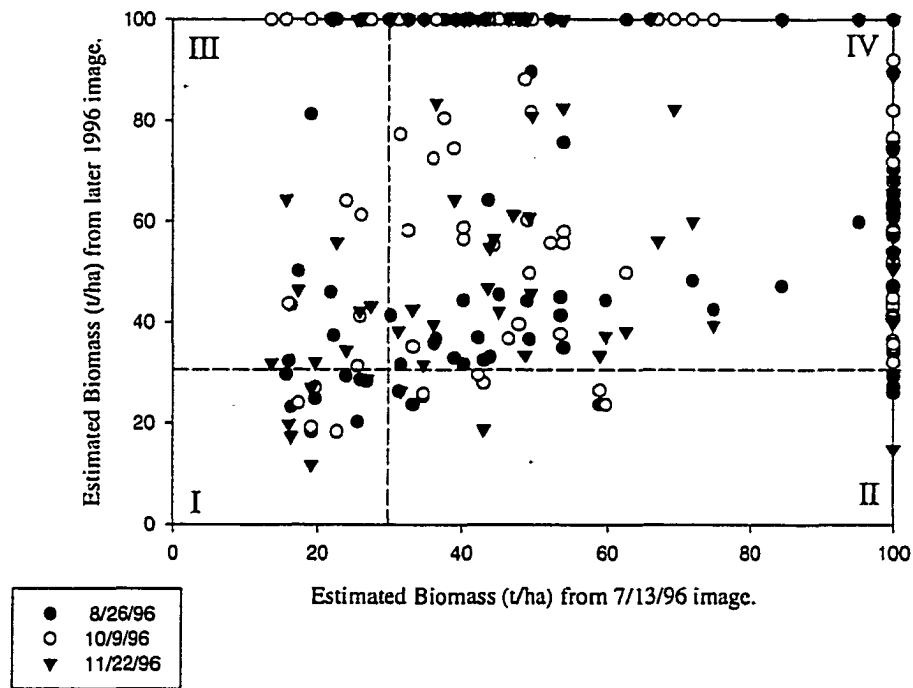


Figure 3.7. Relative biomass estimates for 8-year old stands of vegetation regrowth. The dashed lines represent a saturation point of approximately 31 T/ha. Four quadrants are labeled. Quadrant I: stands with no saturation in at least two periods. Quadrant II: saturation in July 13th but not for all 3 later estimates. Quadrant III: no saturation in July 13th but saturated at later date. Quadrant IV: saturation in both inventories.

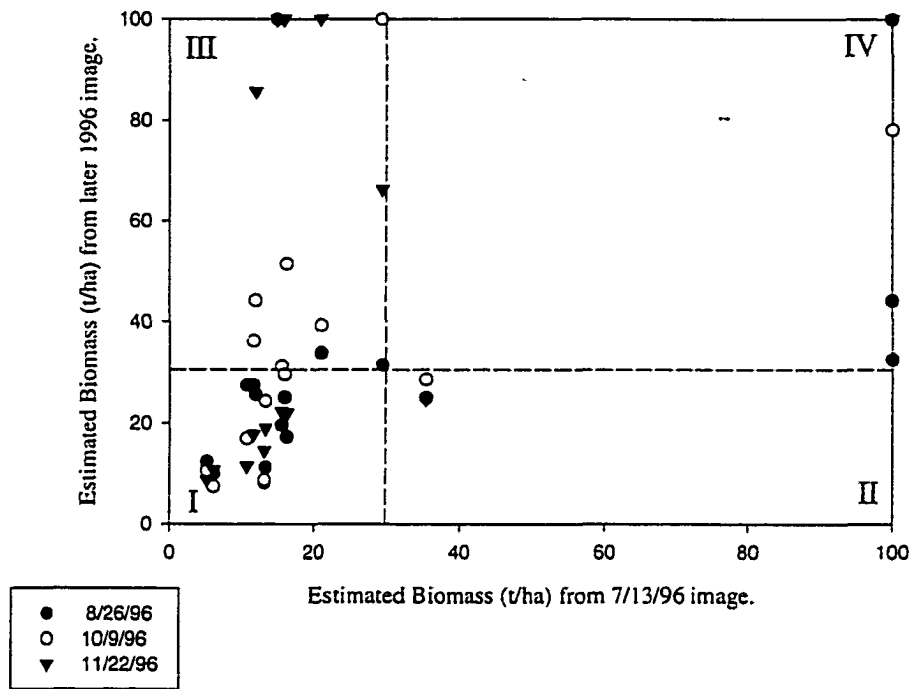


Figure 3.8 Relative biomass estimates for 1-year old secondary vegetation. The dashed lines represent a saturation point of approximately 31 T/ha. Four quadrants are labeled. Quadrant I: stands with no saturation in at least two periods. Quadrant II: saturation in July 13th but not for all 3 later estimates. Quadrant III: no saturation in July 13th but saturated at later date. Quadrant IV: saturation in both inventories.

CHAPTER 4

ASSESSMENT OF JERS-1 SAR FOR MONITORING SECONDARY VEGETATION IN AMAZONIA: II. SPATIAL, TEMPORAL, AND RADIOMETRIC CONSIDERATIONS FOR OPERATIONAL MONITORING.

Abstract

While the role of synthetic aperture radar in operational tropical forest monitoring has yet to be defined, it is nevertheless a critical technology for improving our understanding of deforestation and secondary vegetation in the tropics. In order to understand the role of this technology in operational monitoring a systematic evaluation, relative to other existing technologies, of its performance is required. In this paper we evaluate the spatial, temporal, and noise constraints of JERS SAR data for mapping and monitoring biomass of secondary vegetation in Rondonia, Brazil. Our results indicate that the variability in stand estimates of biomass is high and that the source of the majority of the variability is not from speckle and the intrinsic texture of the secondary vegetation but likely due to differences in environmental conditions resulting in differential background scattering properties. Multi-temporal analysis significantly improves biomass estimates to the point where it is possible to map changes in biomass. Slight reductions in the variability in estimates of normalized radar cross-section greatly improve biomass estimation.

Introduction

Land use within the tropical rain forest biome has a large impact on the net flux of carbon from the biota and is an important component of the global carbon cycle. Conversion of forests to pasture and agriculture results in a net source of biotic CO₂ to the atmosphere, while forest fallow and abandonment into secondary vegetation represent a net sink of biotic CO₂. The magnitude and timing of these fluxes are a function of the extent of the conversion, the fate of the cleared lands, and the carbon stocks of the pre- and post disturbance landscape. Understanding the processes of deforestation and abandonment will improve estimates of the magnitude of the net biotic flux of carbon from the tropics. Accurate, quantitative estimates of deforestation and secondary vegetation extent, rates of deforestation, land abandonment, and forest regeneration are critical for understanding the global carbon cycle. Remote sensing provides the only approach capable of providing this information accurately and timely, over large areas, at a uniform sampling scheme, and repeatedly over time. Optical remote sensing techniques have proven useful for quantifying deforestation and detecting secondary vegetation, but they have been hampered by persistent cloud cover in some regions and by a lack of sensitivity to biomass. There is a clear need for additional techniques to supplement the role of optical sensors for tropical forest monitoring. One most promising alternative to optical is synthetic aperture radar (SAR) because it is not affected by clouds and offers some sensitivity to biomass. Ultimately, these two remote sensing tools ought to be

working in a synergistic fashion to provide the best characterization of deforestation, abandonment and secondary vegetation.

Numerous studies have focused on the use of remote sensing for mapping the extent, temporal dynamics, age, and biomass of secondary vegetation in the tropics (e.g. Nelson *et al.* 2000, Alves and Skole 1996, Steininger 1996, Luckman *et al.* 1997a,b, Luckman *et al.* 1998, Foody and Curran 1994, Mausel *et al.* 1993, and Lucas *et al.* 1993). Multi-temporal Spot XS and TM data have been used to create maps of secondary growth age (Nelson *et al.* 2000, Alves and Skole 1996, Steininger 1996, and Lucas *et al.* 1993) and persistence (Nelson *et al.* 2000, Alves and Skole 1996). Vegetation indices using red and near-infrared reflectance saturate for separating forest secondary vegetation after a few years (Sant'Anna *et al.* 1995). However, vegetation indices that utilize mid-infrared and near-infrared data (Nelson *et al.* 2000, Steininger 1996, Boyd *et al.* 1996) and texture based classifiers (Nelson *et al.* 2000, Palubinskas *et al.* 1995) do not saturate as quickly and are better for detecting secondary vegetation in the tropics. Landsat TM spectral properties differ among the successional stages of secondary vegetation in the tropics (e.g. Sohn *et al.* 1999, Mausel *et al.* 1993, Moran *et al.* 1994, Steininger 1996, Foody *et al.* 1996). Over time, reflectance properties of secondary vegetation become indistinguishable from those of mature, undisturbed forest (Mausel *et al.* 1993, Boyd *et al.* 1996, Foody *et al.* 1996). Results from several studies using Landsat TM data indicate that secondary vegetation stands can be spectrally separated into 4-6 distinct age classes, with the oldest class remaining distinct from mature forest for ≈14-15 years (Sohn *et al.* 1999, Boyd *et al.* 1996, Foody *et al.* 1996, Steininger 1996). Neural net classification techniques have also been used to map secondary vegetation and estimate stand age with

single and two-date Spot XS and Landsat TM spectral and textural data (Kimes *et al.* 1999, Nelson *et al.* 2000).

C-band radar data are less useful than L-band data for mapping biomass of re-growing forest (Rignot *et al.* 1997, Saatchi *et al.* 1997 Yanasse *et al.* 1997). Single polarization (HH) L-band radar data have been used successfully to map deforestation and secondary vegetation and estimate ranges of biomass accumulation from radar backscatter (Luckman *et al.* 1997b, Luckman *et al.* 1998) and phase coherence (Luckman *et al.* 2000). There appears to be a general agreement that radar backscatter increases with increasing biomass and saturates at some biomass level. Estimates of the saturation point of L-band data from tropical forests vary from 40 tons/ha (Imhoff 1995) to 60 tons/ha (Luckman *et al.* 1997a). Ranson and Sun (1997) and Rignot *et al.* (1995) have shown that P-band backscatter can estimate biomass for forest stands up to 150 tons/ha (temperate forest) to 200 tons/ha (tropical forest), respectively.

The baseline for an operational forest monitoring system necessitates complete forest inventories as frequently as every five years (Ahern *et al.* 1998). Analysis of Landsat cloud cover metadata indicates that persistent cloud cover in the tropics would severely limit the ability to map annual changes using Landsat data. For example, from 1990 to 1994 less than 50% of the 228 WRS II footprints covering the Brazilian Amazon was covered by a low cloud cover (<20%) Landsat TM image. Clearly, due to persistent cloud cover, complete optical coverage is difficult, therefore, attempts at measuring rates of deforestation and secondary vegetation would benefit from SAR imagery, thereby ensuring complete coverage. Despite the lack of complete coverage with optical sensors, low cloud cover imagery is available for over 90% of the areas of current deforestation

in the Amazon. Numerous studies have demonstrated that SAR data can be used to detect deforestation (e.g. Rignot *et al.* 1997, Saatchi *et al.* 1997). A systematic evaluation of errors in estimating deforestation and secondary secondary vegetation relative to estimates derived from optical remote sensing platforms is needed to understand the role of radar in the context of operational forest monitoring. This evaluation should focus on the performance of multi-date SAR data for operational forest monitoring. While it is clear that SAR must play an important role in an operational tropical forest monitoring systems (cf. GOFCS Strategy Document), the role has yet to be defined. Knowing the level of performance of SAR for mapping land cover change is critical, especially for regions shrouded by persistent cloud cover where SAR may be the only viable alternative to optical sensors. While several studies have indicated that both optical (e.g. Skole *et al.* 1994, Steininger 1996, Foody *et al.* 1996) and SAR (Luckman *et al.* 1997a, 1997b, Curran and Kuplich 1999) data can be used to characterize differences in secondary vegetation, new research needs to focus on how differences in the rates of forest aggradation can be quantified to improve our understanding of the controls on carbon sequestration across the landscape.

In Chapter 3 we examined the spatial and temporal variability of mean normalized radar cross-section, herein called sigma naught, across a chrono-sequence of secondary vegetation stands and clearings. In order to evaluate the potential of using multi-temporal JERS-1 SAR data for quantifying differences in rates of recovery of secondary vegetation, we applied the biomass density retrieval scheme presented by Luckman *et al.* (1998) and evaluated the sensitivity of using multi-temporal JERS-1 SAR data for biomass density estimation. The temporal and spatial stability of the mean stand

sigma naught estimates were highly variable due to differential effects of changes in environmental conditions and variability of intrinsic heterogeneity (texture) of the stands. In this paper we develop a series of statistical models to evaluate, in an operational context, what level of changes in biomass density, herein called biomass, one might be able to identify with JERS-1 SAR data for a given confidence level. These models assess the impact of multiple JERS data takes and size of the vegetation secondary vegetation stands on the coefficient of variation of our biomass estimates. Performance of estimating biomass is evaluated based on the ability to quantify the presence and magnitude of biomass change over time.

Methods

In this section we provide a summary of the methods used in our analysis. Section 2.1 contains a brief description of how the individual secondary vegetation stands were mapped and how their ages were calculated. Sections 2.2 through 2.5 provide the details of the JERS data pre-processing, extraction of secondary vegetation stand level sigma naught statistics, and the biomass density model used, respectively. Section 2.5 describes the statistical methods and models used. The text provided in these 4 sections is paraphrased from our companion paper in this special issue, where more details on the image processing methods can be found. Our analysis is based on using multi-temporal TM data for mapping age and size of secondary vegetation stands and multi-temporal JERS data for generation of sigma naught statistics for a site in Rondonia, Brazil (figure 4.1).

TM analysis of secondary vegetation stand age and size.

Annual co-registered Landsat TM from 1989 to 1998 were classified using an unsupervised (ISODATA) clustering technique, followed by a manual, knowledge based assignment of the 45 clusters into forest, cleared, natural non-forest, water, cloud, cloud shadow, and secondary vegetation classes. Areas of water, cloud, cloud shadow, and natural non-forest were removed. These 10 classifications were then combined to create land cover changes map using post classification change detection. Initial analysis of the magnitude of the number of land cover change transitions between 1989 and 1996 and their spatial patterns revealed a highly dynamic landscape. For this study, we segmented the stands of secondary vegetation into two sets of age classes based on whether or not we knew when the areas were initially cleared from forest and how long the area remained as non-forest prior to secondary growth formation. Contiguous areas with the same land cover transition sequence over the 10-year period were identified and labeled using an 8-neighbor clump algorithm. A 3x3 low pass filter was then used to identify edge pixels, which were removed to minimize the impact of mis-registration between the multi-temporal SAR data and the TM-based secondary vegetation stand map. All stands smaller than 0.75ha were subsequently removed from the analysis to minimize the variance of the mean stand sigma naught due to speckle (see discussion below). We estimate the overall accuracy of the stand age maps to range between 72% and 85% (Salas et al. this issue). The location of the study area and an example of the stand age map are provided in figure 4.1.

JERS-1 SAR data pre-processing

We analyzed eight L-band (1.275 GHz), HH polarized, synthetic aperture radar (SAR) from the Japanese Earth Resources Satellite 1 (JERS-1). Table 4.1 lists the eight level 2.1 products (3-looks with 12.5m pixels) used for this study. These data were obtained through our participation in NASDA's Global Rain Forest Mapping Project (see Rosenqvist *et al.* 2000 for details on GRFM). These images were co-registered automatically using image cross-correlation and converted to normalized radar cross-section (sigma naught, σ°) values in dB with the following formula:

$$\sigma^{\circ} = 20 \log_{10}(DN) + F \quad (1)$$

where F is the NASDA provided correction factor (-68.5 dB for the images #1-7 and -68.3 dB for image #8). We applied an empirical linear correction, derived from a transect of primary forest, to account a ramp in sigma naught with range (Leckie 1990, Ranson and Sun 1994). The range ramp across this transect varied from 0.4dB to 1.5dB (see table 4.1). While, theoretically, this linear empirical correction may not properly model incidence angle effects for non-forested areas across the landscape or correct for non-linear effects of system noise with slant range, we assume that the residual noise correlated with range would be a second order effect due to the small range in incidence angles across our study area. We then cross-calibrated these data to normalize their gain differences. The cross-calibration offsets (table 4.1) were derived from mean and coefficient of variation statistics of σ° from 228 hectares of mature forest.

Extraction of Stand Sigma Naught Statistics and Confidence Limits

Speckle and the intrinsic spatial heterogeneity (texture) of vegetation impacts our ability to accurately estimate the mean sigma naught from stands of secondary vegetation (Rignot and Kwok 1993). The estimate of coefficient of variation caused by speckle and intrinsic texture can be estimated by:

$$CV = \sqrt{\frac{V_t}{N} + V_t + \frac{1}{N}} \quad (2)$$

where N is effective number of looks (ENL) and V_t is the variance due to texture (from Luckman *et al.* 1998), following Oliver (1991), and is calculated as

$$V_t = \frac{\left(\frac{sd}{\mu}\right)^2 - \frac{1}{N}}{1 + \frac{1}{N}} \quad (3)$$

where $\left(\frac{sd}{\mu}\right)$ is the actual coefficient of variation (CV) within the stand. Vieira (1996) estimated N for a single JERS-1 3-look pixel to be 2.8 Using the estimated CV we can estimate the 95% confidence limits in dB by

$$10 * \log\left(1 \pm 2 * CV * \frac{1}{\sqrt{n}}\right) \quad (4)$$

where n is the number of uncorrelated pixels in the stand. Note that (4) ignores all sources of variation except texture and speckle. An improved confidence limit, but still accounting only for texture and speckle, would be

$$10 * \log(1 \pm t_{0.05, n-1} * CV * \frac{1}{\sqrt{n}}) \quad (4a)$$

We used level2.1 data which has a spatial resolution of 12.5 meters. However, since JERS resolution is 18m, there is a significant amount of correlation between neighboring pixels that must be accounted for in calculating our confidence intervals. Using these equations we calculated mean σ^0 with the 95% confidence limits for each of the 182 stands of secondary vegetation.

Shimada (1996) estimated N for the NASDA level 2.1 3-look product to be 2.1. The discrepancy with the Vieira estimate could be due to differences in the SAR processor used to create the products. If N is closer to 2.1 then our overall confidence limits would be wider than reported here by a factor inversely proportional to the size of the secondary vegetation stand.

Biomass Density Model

Luckman *et al.* (1998) developed a semi-empirical model for estimating biomass density of regenerating forests with JERS-1 radar sigma naught data and asserted that the model is generalizable to other regions in the Amazon. We tested their model for quantifying broad differences in biomass of our secondary vegetation stands. Inverting their model to estimate biomass (B) from σ^0 , expressed in linear units, yields

$$B = \frac{-\ln(a - \sigma^0) - c}{b} \quad (5)$$

where a, b, c are constants that were empirically derived from field data from Tapajos region in Para State in the Amazon. We used the following values $a = 0.170$, $b = 0.053$, and $c = 2.146$ (taken directly from Luckman *et al.* 1998) for our calculations. Unfortunately, when $\sigma^0 \geq a$, the estimate produced by (5), or equivalently by (4), is undefined, since the model saturates with respect to sigma naught, not biomass density. This situation occurred frequently in all the scenes examined. Unfortunately, the model does not provide a natural or saturated biomass density level, but some value must be specified. To provide estimates in these cases, we used

$$B = \frac{-\ln(0.00005) - c}{b} = 146.4 \quad (5a)$$

which is slightly larger than the largest estimate calculated using (5), or 143.1 T/ha. Using these equations we then calculated the biomass for all 182 stands of secondary vegetation for each of the JERS images listed in table 4.1.

Statistical Methods and Models

Given the availability of multiple, contemporaneous images, confidence limits can be calculated for σ^0 (in linear units), σ^0 (in dB), and biomass in two different ways. First, the full-width (upper minus lower limit) of the 95% confidence limits for σ^0 (in linear units) may be calculated as

$$2E = 2t_{0.05,n} \frac{sd}{\sqrt{n}} \quad (6)$$

with the corresponding width for σ^0 in dB calculated using (4a). The full-width for biomass may be calculated by substituting $\sigma^0 + E$ and $\sigma^0 - E$ into (5) or (5a) as appropriate, and taking the difference. Note that this procedure specifically assumes that the all contributions to the variability in σ^0 and biomass, other than those from speckle and texture, are negligible.

Alternately, given J scenes, we might consider calculating the full-width of the 95% confidence limits for σ^0 in linear units as $2t_{0.05,J-1}$ times the standard deviation of the J estimates of σ^0 about their arithmetic mean. Confidence limit widths for σ^0 in dB and biomass may then be calculated as before. This procedure has the advantage that all sources of variation between scenes are accounted for, not just speckle and texture. Substantial differences between confidence limits calculated using (6), (4a), and (5a) in turn, and those calculated from the observed temporal variability in the estimates, must be regarded as evidence that speckle and texture are not the major controlling factors in the variability of the estimates. Confidence limits were calculated for both methods using only those 139 stands which were present in all 4 of the 1996 scenes, since confidence limits based on only 2 or 3 scenes would be more variable.

To quantify the contribution of factors other than speckle and texture to the variability in observed sigma naught, we performed a series of χ^2 tests on the sigma naught from the four 1996 scenes. Since σ^0 (in linear units) for a polygon is estimated as the mean sigma naught for all pixels in the polygon, and since the number of pixels in

a polygon is generally large, it follows directly from the Central Limit Theorem that the estimated σ^0 is approximately normally distributed about the true value. The quantity

$$se_{\sigma^0}^2 = \frac{sd^2}{n} \quad (7)$$

provides an unbiased estimate of the variance of σ^0 , under the null hypothesis that the variance of σ^0 arises from texture and speckle only. Recalling that a sum of squared, normally distributed variables is distributed as chi-squared, we may test the null hypothesis by comparing

$$\chi^2 = \sum_{ij} \frac{(\sigma_{ij}^0 - \hat{\sigma}_i^0)^2}{se_{\sigma_{ij}^0}^2} \quad (8)$$

to the critical values of χ^2 for $IJ-I$ degrees of freedom. In (8), i indexes I stands or polygons, and j indexes J scenes. Equation (7) is calculated separately for each polygon and scene. Stand area affects the value of chi-squared through the relationship between stand area and n , which affects $se_{\sigma^0}^2$. In Equation (8), each stand is treated as an equally weighted observation. The quantity $\hat{\sigma}_i^0$ is the least-squares mean of the σ_{ij}^0 values, which minimizes χ^2 . We calculated χ^2 for all 179 stands that were represented in more than one of the 1996 images combined, and for each stand separately. The combined χ^2 provides a powerful overall test of whether the observed variation between images could have arisen from texture and speckle alone. The χ^2 values for each stand individually provide a

direct measure of the magnitude of the observed temporal variation relative to the expected temporal variation under the null hypothesis.

Following the results of the χ^2 tests, we further examined the behavior of the coefficient of variation of the biomass predictions, based on the observed inter-temporal variability in predicted biomass. We further examined the implications of the magnitude of observed coefficients of variation for biomass predictions, for the coefficient of variation of estimates of change.

Results and Discussion

Effects of Factors Other Than Speckle and Texture

Confidence limits based on speckle and texture only, and confidence limits based on observed inter-temporal variation, are shown for σ^0 (in linear units), σ^0 (in dB), and biomass in Figure 4.2. First, considering the confidence limits based on speckle and texture alone, it is notable that many stands exceeded the “worst-case” scenario presented by Luckman *et al.* (1998, p. 135) of full-widths of 1.18 dB. In part, this is because 22% of the stands considered are less than the 1-ha size used by Luckman *et al.* (1998) in their assessment. The spatial scale of land-clearing and conversion activities is small in this region of Rondonia. Analysis of the distribution of secondary vegetation stands indicates that over 60% of the stands were smaller than 5ha (Figure 4.3a). On an area-weighted basis, over 45% of the area in secondary vegetation was in stands smaller than 5ha. Only one stand had estimates of textures variance, calculated using equation (3), higher than the maximum value of 0.2826 reported by Luckman *et al.* (1998). Regardless of the inter-

temporal variability that may or may not be reduced by better signal-to-noise ratio (SNR), texture and speckle impact on confidence limits will be high for a majority of the secondary vegetation stands in this region (Figure 4.3b).

Turning to the confidence limits based on observed inter-temporal variability, the difference in magnitude of the two sets of confidence limits is striking, regardless what variable is considered. Although the effect is somewhat exaggerated by the degrees of freedom used for t in (4a) and when evaluating the variability directly, most of the effect arises from the sheer variability in the images. As shown by Salas *et al.* (this issue), this inter-temporal variability does not arise from consistent variation from one scene to the next, which could be reduced by a different cross-calibration method. Indeed, despite careful cross-calibration, 125 of 139 stands show variability exceeding the 1.18 dB threshold identified by Luckman *et al.* (1998) when all sources of variation are considered. In practice, this translates into confidence limits for biomass that approach the range of biomasses calculated using (5) and (5a), or 0 to 146 T/ha. Confidence limits of such a great magnitude do indicate quite clearly that for many stands the biomass is almost completely undetermined by a single image.

The difference in magnitude between the variability arising from speckle and texture alone, and the actual variability, is most clearly described by the overall χ^2 test for all stands using the 1996 data ($\chi^2=1897.1$, d.f.=506, $p<0.001$). The ratio of χ^2 to d.f. indicates that the observed variance among scenes is, on average, 375% of that expected from speckle and texture alone. Clearly, other factors are contributing to the differences between scenes for many stands. Accounting for additive temporal effects that are consistent across scenes reduces χ^2 somewhat, but not to a practically significant degree

($\chi^2=1807.7$, d.f.=503, $p<0.001$). Such temporal effects include any environmental or sensing variations which affect all stands across a scene in a consistent, additive fashion. Given the relative unimportance of a consistent temporal effect, we must consider that this extraneous variability arises from some temporally variable factor, such as environmental conditions or sensor calibration, differentially interacting with the characteristics of the stands of interest. Seasonal differences in surface conditions can influence sigma naught values differently for pastures, secondary forests, and primary forest, with pasture exhibiting a large ($>2\text{dB}$) seasonal variability, secondary vegetation exhibiting a smaller ($\sim 1\text{dB}$) variability, and no effect on primary forests (Hashimoto et al. 1997).

Examining the χ^2 values for individual stands (Figure 4.4) allows us to gauge the consistency of the extraneous variability, relative to the variability introduced by speckle and texture. It is noteworthy that 76 of 179 stands showed χ^2 values less than the expected value (equal to the number of scenes in 1996 in which the stand was present, minus one), clearly indicating that the extraneous variability impacts some stands and not others. The lack of clear association between individual-stand χ^2 values and the least-squares σ^0 value might suggest, at first, that the extraneous variability is not associated with mean sigma naught, and therefore unrelated to biomass. However, recall that χ^2 measures variability relative to the variability imposed by speckle and texture, which is correlated with mean sigma naught and biomass. A more careful consideration suggests that the absolute magnitude of the extraneous variability, when it does come into play, is associated with the same factors that govern texture. There is clearly a relationship between texture and stand biomass due to changes in canopy structure during

development (Luckman et al 1997b). Since mean sigma naught from stands with higher biomass will be less susceptible to variations in environmental condition, such as soil moisture and dielectric properties of sub-canopy vegetation, the magnitude of the extraneous variability may be related to biomass.

Coefficient of Variation of Biomass Predictions

The parameters used in the biomass model were developed using field data from Tapajos, and tested with data from Manaus. Likely, the model would have different parameters if it were calibrated for our site in Rondonia because of differences in site conditions, soil properties, and species composition. Nevertheless, our results and conclusions would not change because of the non-linear relationship between sigma naught and biomass and, therefore, are intended to be relative.

A useful measure of the variability in predictions of biomass is the coefficient of variation of the predictions, calculated in a straightforward fashion as the standard deviation of the estimates from each scene, rescaled by their mean. The CV is plotted against the mean predicted biomass for each stand in Figure 4.5. A nuisance feature in developing this relationship between biomass and its CV was the presence of sigma naught values for which $\sigma^0 \geq a$. All stands that had at least one estimate where $\sigma^0 \geq a$ were omitted from this analysis. Fortunately, most of the stands omitted from this analysis were in the biomass range above which JERS-1 data are regarded as unsuitable for biomass estimation (Imhoff 1995, Luckman et al. 1997b, Curran and Kuplich 1999). The stands for which (5a) was unnecessary, all lie within this range. For these stands, it

is clear that the CV increases with increasing biomass. The solid curve fit to these coefficients of variation is described by

$$CV(\%) = 6.4983\sqrt{\text{biomass}} \quad (9)$$

For example, if the estimated biomass of a stand were 10 T/ha, based on a single scene, we would expect that estimate to have a CV of 20.5%. This implies approximate 95% confidence limits of 6 to 14 T/ha. By contrast, for a stand with an estimated biomass of 25 T/ha, we would expect a CV of 32.5%, implying 95% confidence limits of approximately 9 to 41 T/ha. Clearly, stands with small biomass are much better resolved – both in absolute and relative terms – than stands with large biomass.

Single vs Mult-temporal JERS observations for Estimating Changes in Biomass

To the degree that the variability indicated by Figure 4.5 reflects operational success in quantifying biomass, to what degree of accuracy can we quantify biomass differences (either from stand to stand within a scene, or within a stand over time)? If a stand imaged at one time has biomass B_1 , estimated with coefficient of variation CV_1 , and at a second time has biomass B_2 , estimated with coefficient of variation CV_2 , the standard error of the estimate of the difference will be

$$se_{B_2-B_1} = \sqrt{B_1^2 CV_1^2 + B_2^2 CV_2^2} \quad (10)$$

and the coefficient of variation of the estimated difference will be

$$CV_{B_2-B_1} = \frac{se_{B_2-B_1}}{|B_2 - B_1|} \quad (11)$$

The situation when estimating the difference between different stands at the same time is directly analogous. Using (11), and the relationship between biomass and its CV from a single scene as given in (9), we can plot the CV we would expect to obtain for the change in biomass of a stand, as a function of its initial biomass and percent growth (Figure 4.6). Several aspects are immediately apparent. First, if a single scene is used at each time of observation, changes in biomass as large as 30% between the two periods cannot be resolved reliably regardless of the initial biomass of the stand. Second, even considering a 100% change or doubling of biomass, a single scene at each time period provides insufficient information for a reliable resolution unless the initial biomass of the stand is < 10 T/ha. For example, if $B_1=10$ T/ha and $B_2=20$ T/ha, the CV of the change is 62%, or 6.2 T/ha. The approximate 95% confidence limits on the change would be 10 ± 12.4 T/ha. In other words, using a single scene at each time period, changes in biomass are unlikely to be well-resolved unless the change is very large, or the stand is nearly bare at one of the two time periods.

Fortunately, it is possible to improve on the resolution by using multi-temporal images. If J images are available at each time period, then

$$se_{B_2-B_1} = \sqrt{\frac{B_1^2 CV_1^2 + B_2^2 CV_2^2}{J}} \quad (12)$$

If we can suggest a target value of $CV_{B_2-B_1}$ for a given change, then we may estimate the required number of scenes as

$$J = \frac{B_1^2 CV_1^2 + B_2^2 CV_2^2}{(B_2 - B_1)^2 CV_{B_2-B_1}^2} \quad (13)$$

Using (9) as the relationship between biomass and the CV of its estimate, a solution to (13) is shown in Figure 4.7. The target value of $CV_{B_2-B_1}$ is taken as 50%, which is not an overly restrictive value. It implies approximate 95% confidence limits equal to plus or minus the actual change, or a 39 in 40 chance of obtaining the correct sign on the change. With this rather loose definition of acceptable accuracy, we see that moderate numbers of additional contemporaneous scenes at each time period do improve accuracy considerably. For example, with a 44-day repeat cycle, it is possible to obtain 8-9 images in a year. That additional information at each time period would allow identification of changes as small as 30% of initial biomass in stands with as little as 17 T/ha, and identification of a doubling in biomass up to the saturation point.

Impact of Noise on Estimating Biomass

The variability in our mean sigma naught for our stands was higher than could be accounted for due to texture and speckle alone. Potential sources of this variability include system noise, relative calibration errors, and environmental conditions (primarily surface moisture on vegetation and soil moisture). While estimating contributions of environmental conditions is unlikely with a single polarization instrument like JERS, better estimates of the scattering from vegetation alone may be possible with multi-

polarization sensors. Therefore, in an attempt to quantify impact of improved SNR (in this sense we consider noise all sources variability not due directly to biomass, including environmental conditions, system noise, calibration offsets, etc), we modeled the relative bias, coefficient of variation, and relative RMSE of estimating biomass with a 1.0 dB versus 0.5 dB normally distributed errors of mean stand sigma naught estimates. The model first assumes an actual biomass value and calculates the “true” σ^o by inverting equation (5), which was then converted to dB. Based on the “true” estimate of σ^o we calculated the probability density from our assumed distribution of σ^o based on our errors (0.5dB or 1.0 dB) and then recalculated biomass from the distribution. Numerical integration was used to estimate the expected value of bias (observed – “true” biomass), variance (observed biomass - average biomass)², and mean squared error (observed biomass - 'true' biomass)². From these we calculated the relative bias, CV, and relative RMSE as percentages. These steps were repeated across a range of biomass values to create Figure 4.8. The results highlight the inter-play between stand biomass and potential errors in estimating biomass. The observed positive bias can be explained by the non-linear (sigmoidal) relationship between sigma naught and biomass. A decrease in overall SNR of 0.5 dB would extend the range of biomass where there is little (<10%) bias, lower CV and lower RMSE. Clearly, any improvement in SNR will have a large impact on improving the success of estimating stand biomass given the sensitivity of these estimates confidence limits over the small dynamic range of sigma naught expected for biomass levels below the saturation point.

Conclusion

A statistical analysis of sigma naught statistics from a series of secondary vegetation stands was presented. These statistics were used to model and assess the impact of spatial and temporal variability in estimating stand biomass and changes in stand biomass with single and multi-date JERS SAR data. Many of the secondary vegetation stands in this study had confidence limits due to speckle and texture alone that exceeded the “worst-case” estimate provided by Luckman *et al.* (1998). While these differences are likely due to the smaller stands in this study, the size class distribution of stands across the landscape in Rondonia indicates that much of the secondary vegetation is contained in these smaller stands (<5ha). Nevertheless, speckle and texture are not the largest controlling factors on the variability of mean stand sigma naught estimates.

Extraneous factors, such as natural noise due to changes in environmental conditions, have the largest impact on the variance of biomass estimates. However, this variability due to these extraneous factors does not impact all stands of secondary vegetation, likely due to the presence of a biomass saturation point. The coefficient of variation of biomass estimates increases with stand biomass. With single data JERS imagery biomass cannot be estimated for most of the stands in this region of Rondonia. Multi-temporal observations improve the accuracy of biomass estimates sufficiently to enable identification of changes in biomass. Given the non-linear relationship between backscatter and above-ground biomass, a 0.5dB reduction in extraneous variability would significantly improve biomass estimation, especially for levels below 40-50 T/ha.

While it is clear that estimation of biomass from natural systems, like secondary vegetation in the Amazon, with a single polarization L-band SAR is extremely difficult, it

appears feasible to provide the carbon cycle community information useful for improving our understanding of carbon sequestration in secondary vegetation in Amazonia.

Improved techniques for estimating contributions of noise will further enhance this application because we then will be able to quantify stand-to-stand variability due to environmental conditions.

Table 4.1 JERS-1 SAR level 2.1 data used. *Image 4 was processed by JPL, remaining 7 images were processed by NASDA.

Image	Date	Season	Range Ramp	Cross-Calibration	NES0
1	2/27/1993	Wet	1.058 dB	0.11 dB	-16.35 dB
2	4/21/1993	Wet	1.182 dB	-0.35 dB	-16.37 dB
3	9/22/1994	Late Dry	1.538 dB	-0.44 dB	-16.29 dB
4	10/23/1995	Late Dry	0.374 dB	-0.37 dB	-14.88 dB
5	7/13/1996	Dry	1.516 dB	-0.33 dB	-17.16 dB
6	8/26/1996	Dry	0.954 dB	-0.09 dB	-15.04 dB
7	10/9/1996	Late Dry	1.340 dB	-0.14 dB	-15.75 dB
8	11/22/1996	Early Wet	0.948 dB	0.09 dB	-14.93 dB

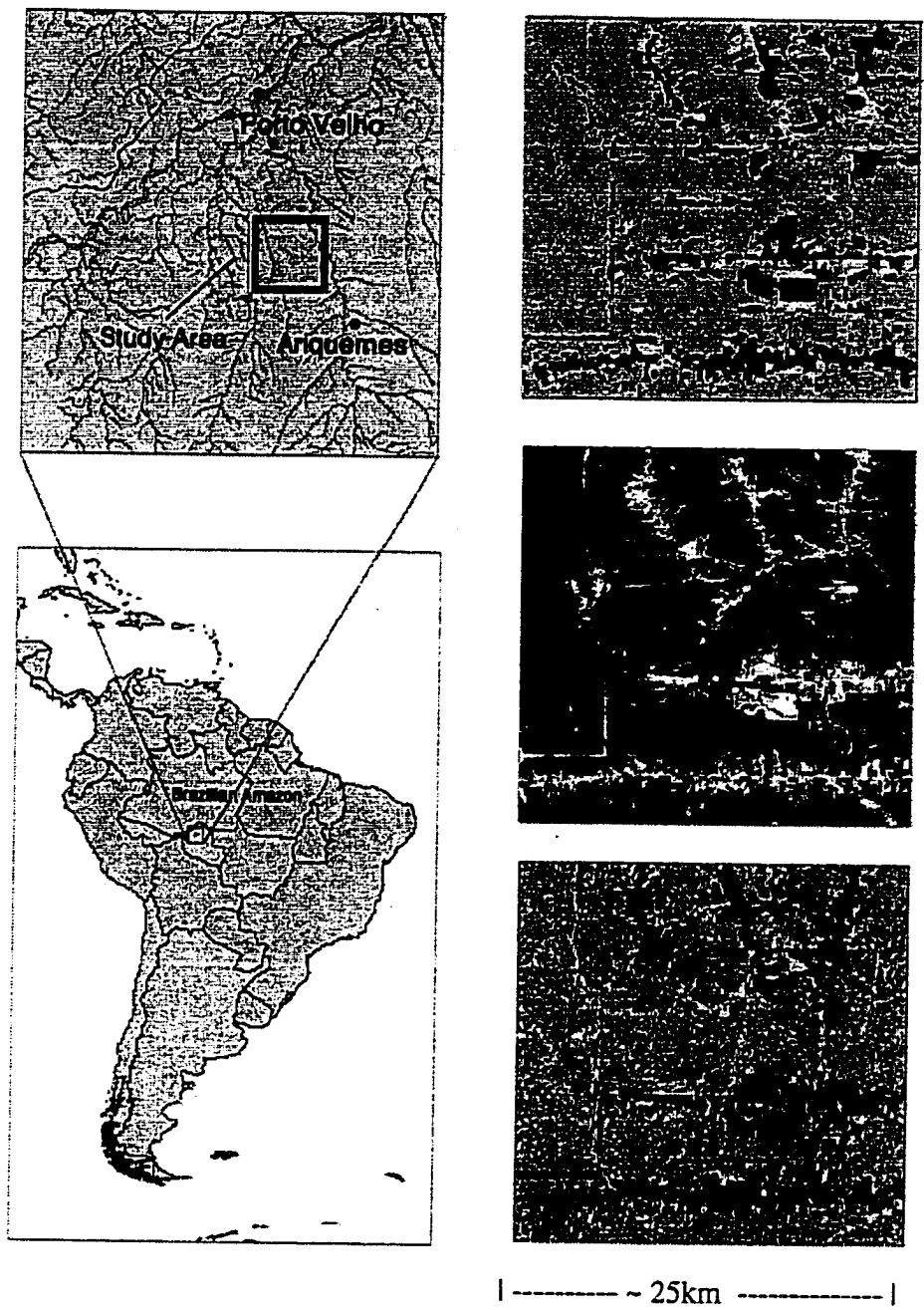


Figure 4.1. Location maps of the Rondonia site, and subsets of the secondary vegetation and clearing stand age map, June 25, 1996 TM image, RGB composite of October 9th, August 26th, and July 13th 1996 JERS images.

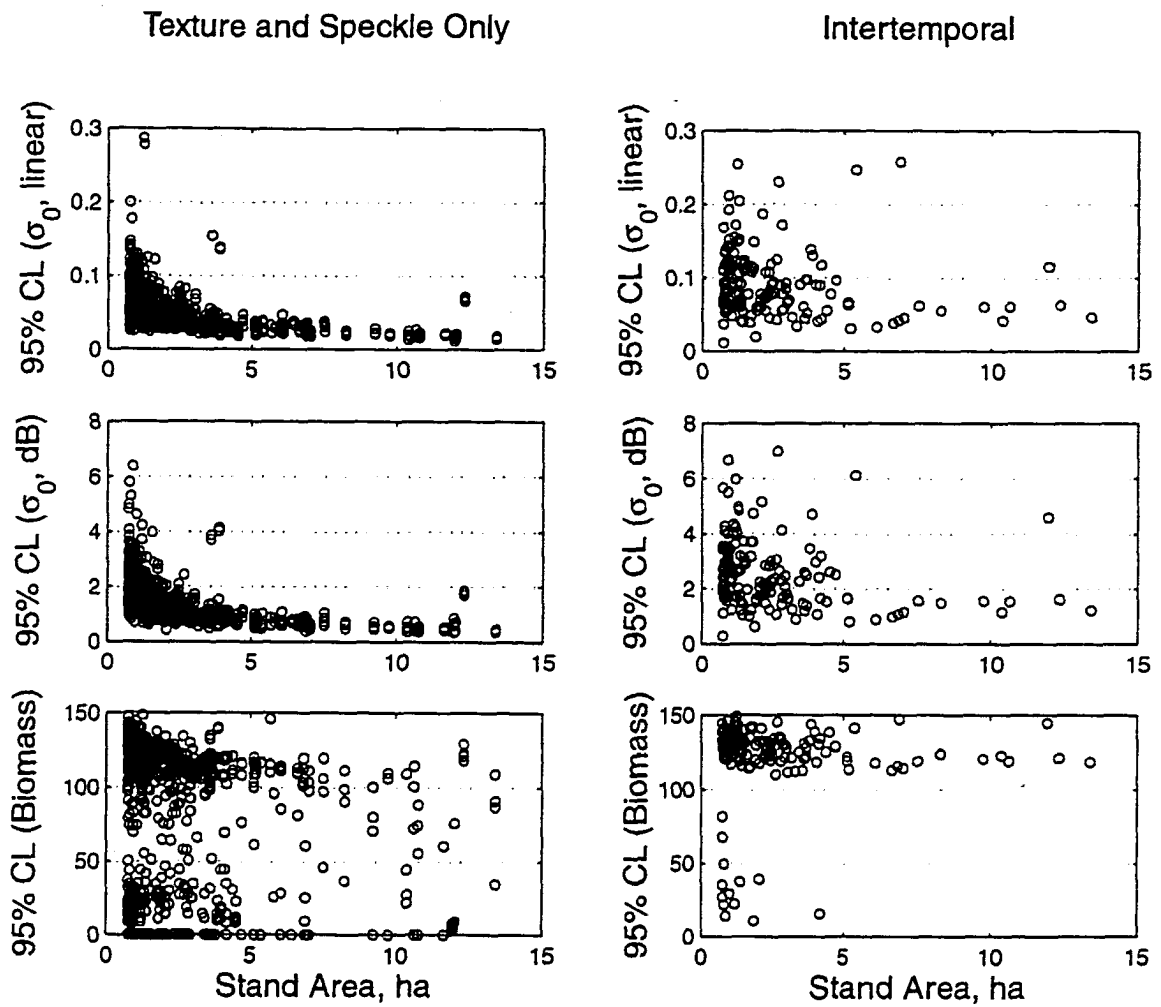


Figure 4.2. 95% confidence limits for σ^0 (linear units), σ^0 (dB), and biomass calculated based on speckle and texture alone (left column) and based on actual inter-temporal variation among images (right column).

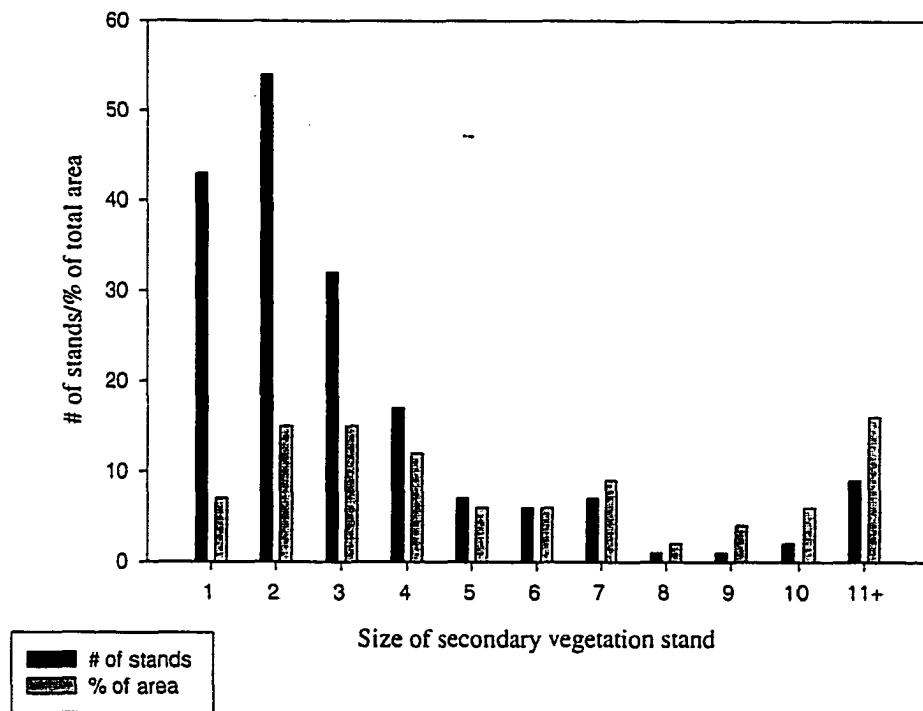


Figure 4.3a. Size class distribution of secondary vegetation stands, ranging from 0-1 ha to larger than 11 ha. Percentage of each class with respect to total area in secondary vegetation is also plotted. Note that there are many more stands in the smaller range (1 to 4 ha) than above 8 ha. Approximately 50% of the secondary vegetation are in stands less than 5ha. Stand sizes were calculated from multi-temporal TM analysis.

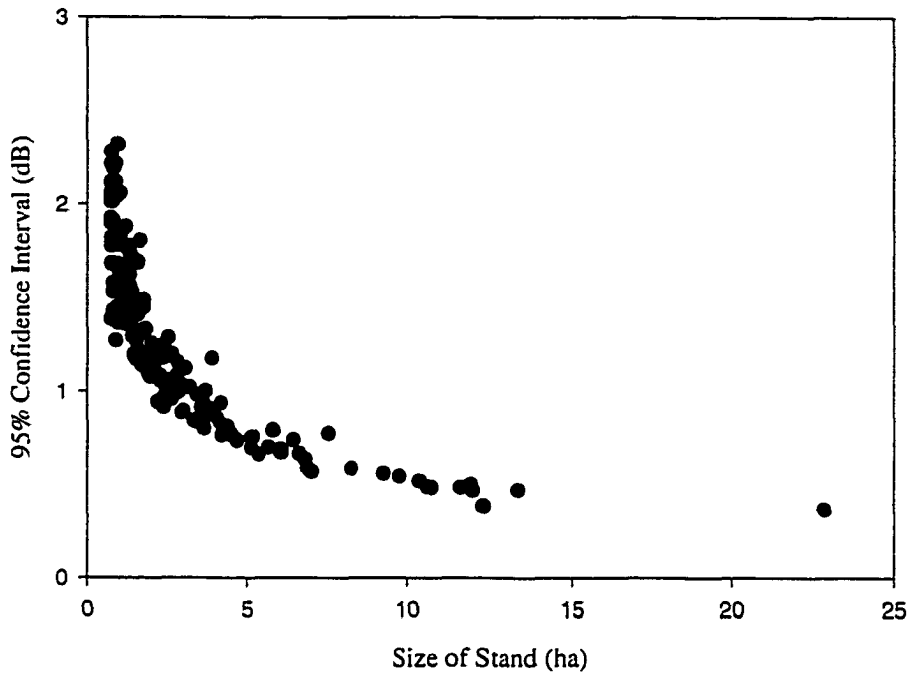


Figure 4.3b. Influence of secondary vegetation stand size on magnitude of 95% confidence interval in dB due to texture and speckle only. While the majority (122 of 179) of stands had confidence interval greater than 1dB, on an area weighted basis, 65% of the area of secondary vegetation was contained within stands with confidence intervals less than 1dB.

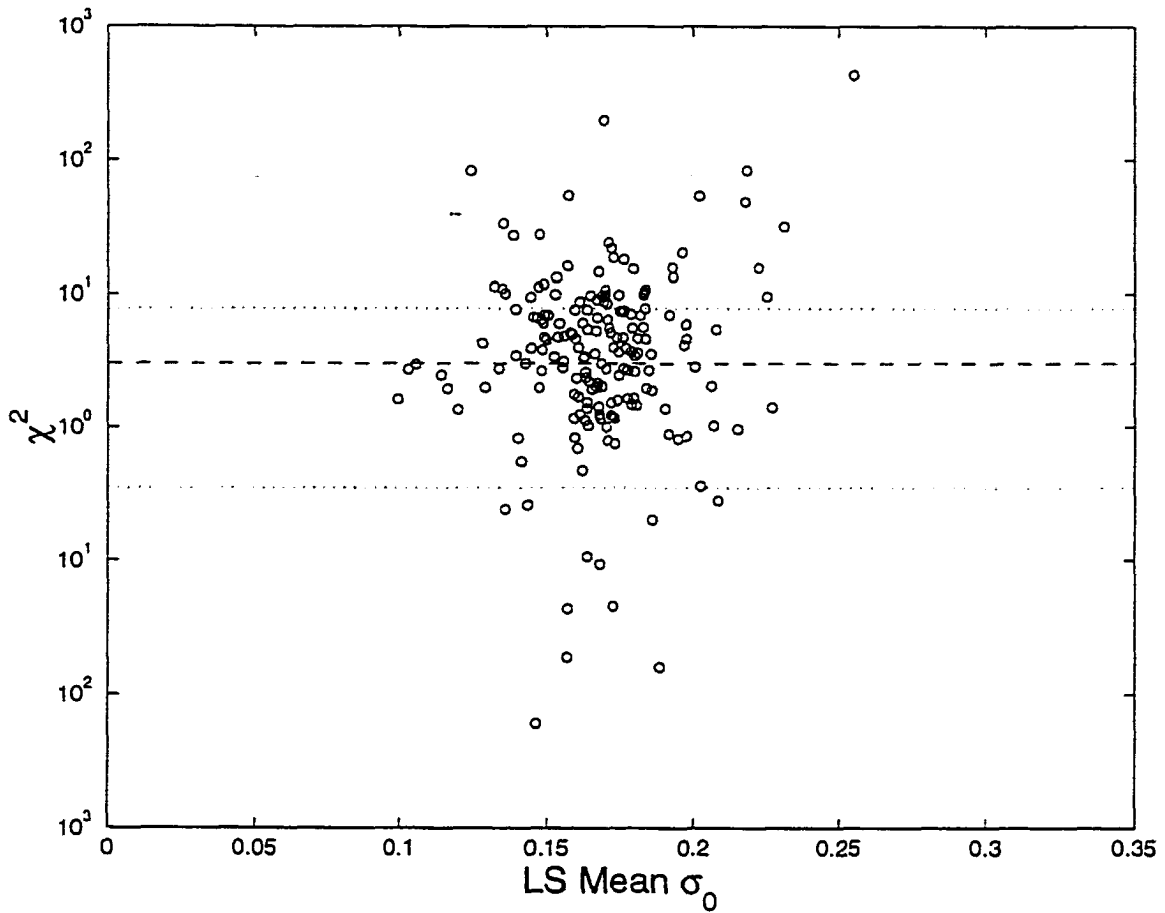


Figure 4.4. Individual-stand χ^2 values. The expected value of χ^2 is shown as a dashed line; dotted lines show the upper and lower critical values for a one-tailed error rate of 0.05. If texture and speckle were the dominant sources of variability, the points would cluster around the expected value, with 5% of the points outside each of the two dotted lines.

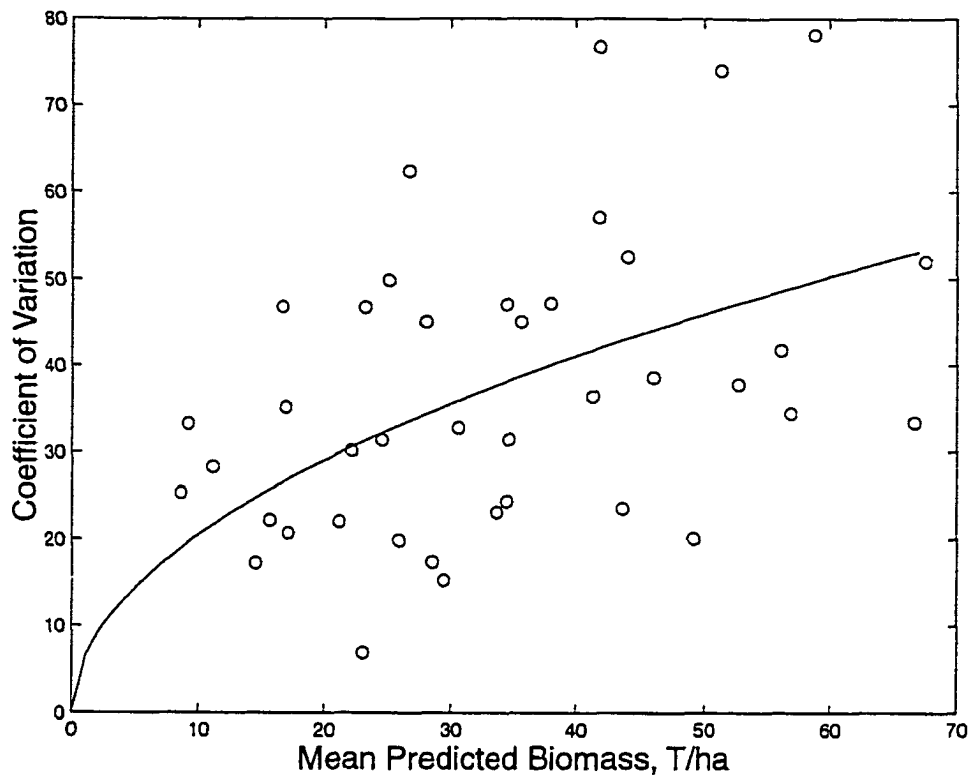


Figure 4.5 Coefficient of variation for biomass estimates (in percent), as a function of predicted biomass. This figure and curve are derived from only those stands with no instances of $\sigma^o > a$. Most of the stands had at least one instance when $\sigma^o > a$.

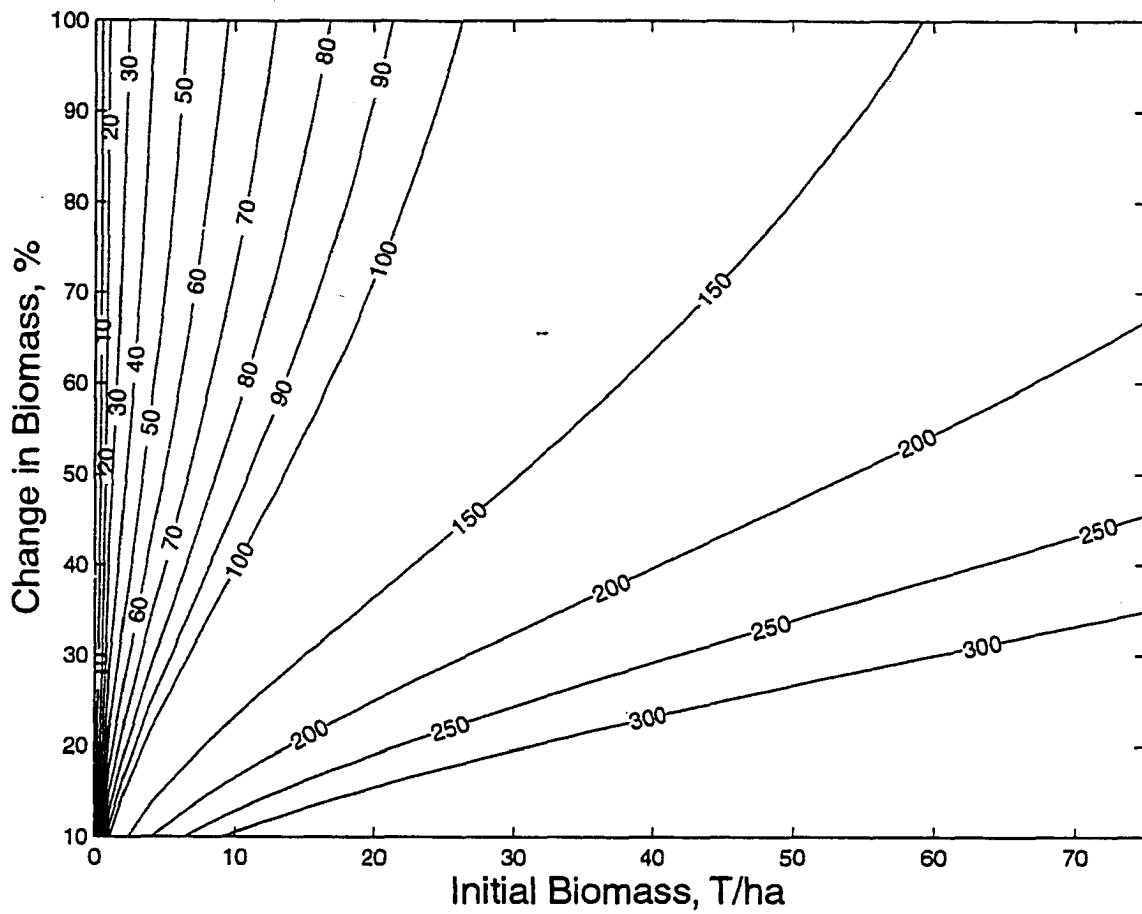


Figure 4.6. Coefficient of variation (%) for estimates of change in biomass, using a single scene at each time period, as a function of initial biomass and percent change.

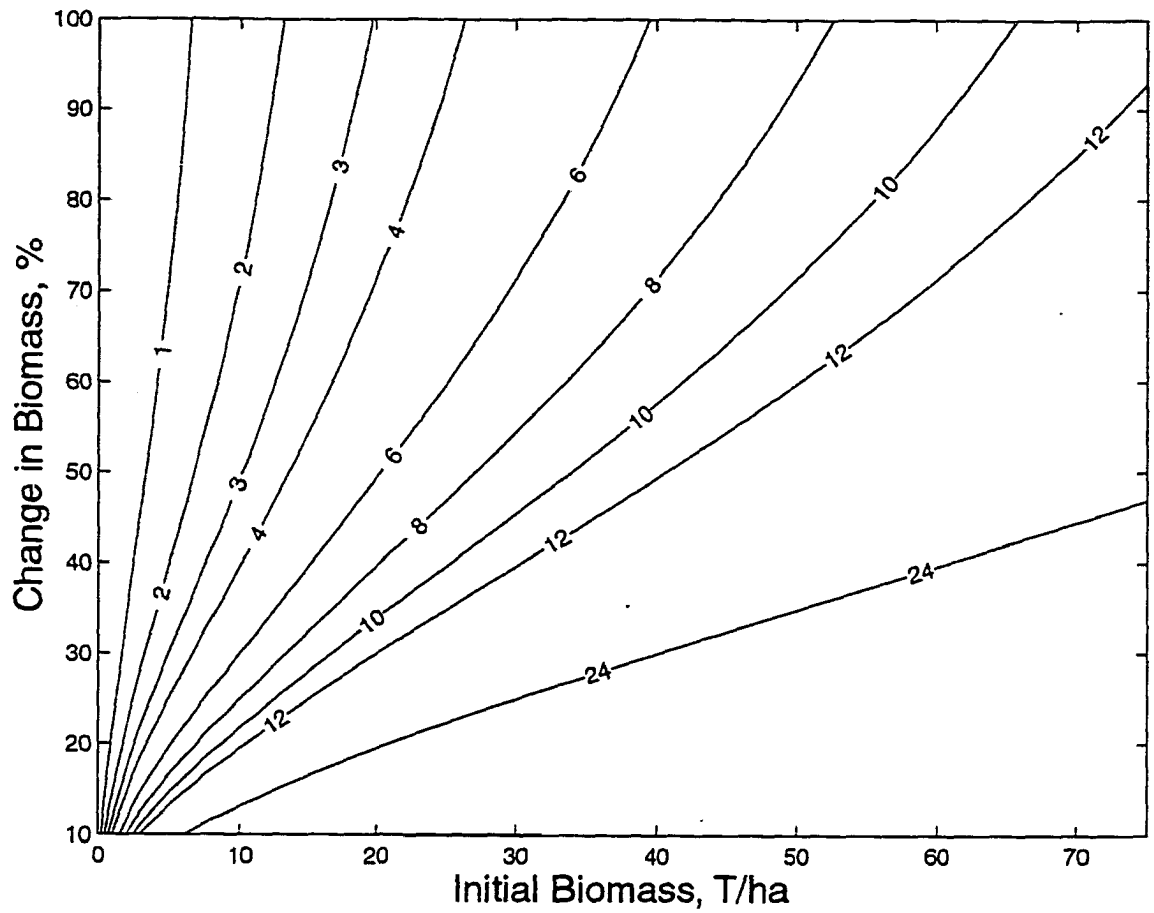


Figure 4.7. Number of contemporaneous scenes at each time period required to achieve a 50% coefficient of variation on biomass change estimates, as a function of initial biomass and percent change.

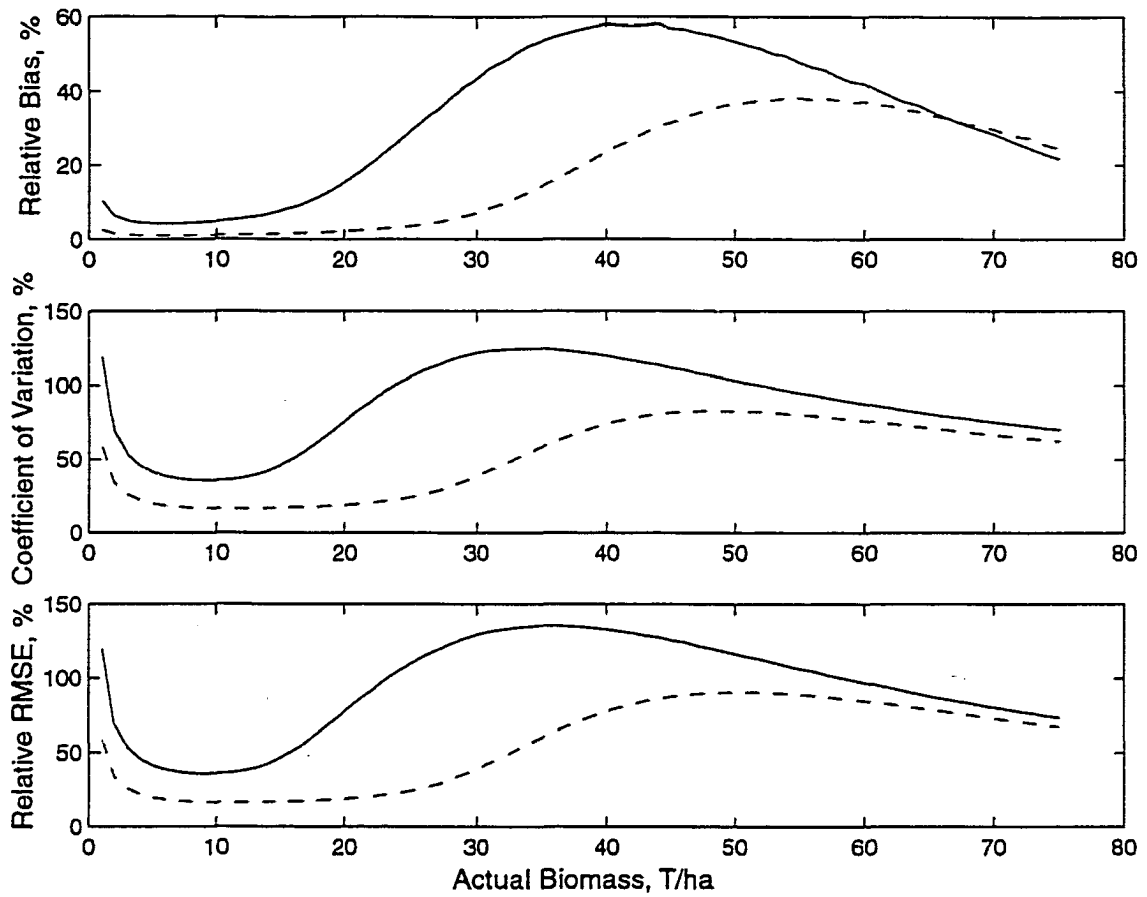


Figure 4.8. Differences in relative bias, coefficient of variation, and relative RMSE (expressed as percentages) for "observed" biomass from JERS due to normally distributed noise of 0.5 dB (dashed line) and 1.0 dB (solid line). The non-linear relationship between backscatter and biomass is readily apparent.

Appendix A: Description of Spectral Indices

EVI (Enhanced vegetation index by Huete and Justice 1999): While NDVI is sensitive to APAR, it saturates quickly during forest succession (Steininger 1996). EVI is more sensitive than NDVI to canopy structure and it saturates at higher LAI levels. To enhance sensitivity at higher density, the soil and atmospheric adjustment factors in the EVI equation will be optimized for tropical forests using an approach similar to Qi et al. (1994). The adjustment factors will be optimized for forest application using in-situ data from the proposed study sites. This optimized vegetation index is expected to be sensitive to NIR reflectance patterns that are controlled by canopy moisture and architecture and is more useful for mapping differences in forest canopies (Huete et al. 1997).

Successional Development Index (SDI): This index is based on mapping the spectral pattern of forest succession. The spectral angle approach to mapping land cover analyzes spectral responses in such a way as to be minimally affected by atmospheric or topographic variations (Sohn et al. 1999). When using a multi-spectral data set (n channels), the spectral signature of a certain surface type can be represented in n -dimensional feature space as multiple vectors (each vector representing one spectral channel). Spectral angle mapping uses the cosine of the angles between these multi-dimensional vectors. Sohn et al. (1999) used pre-defined reference spectra collected from sites of known successional stages to map, with very high accuracy, three stages of forest succession in the Yucatan Peninsula. Signatures for SDI will be derived from field data on stand structure and regrowth stands will be classified into areas with similar spectral patterns.

Successional Development Ratios (SDR): This index is the ratio of the reflectance of a regrowth stand to the reflectance of a mature forest. We expect the SDR values to approach unity as regrowth stands become spectrally similar to mature forest. We have chosen to calculate SDRs for NIR and MIR data based on results from the linear discriminant analyses in Nelson et al. (2000) and Boyd et al. (1996) that revealed these bands were more correlated with regeneration stage (see figure A.1). We have begun to investigate the relationship between the SDRs and regrowth stand age across a gradient of growing season degree years (GSDY). The SDR indices all increased with stand age and exhibited differences across the sites with a relatively short and long GSDY on similar soils (Latosolos) (see figure A.2). Differences in regrowth structure across these sites appeared to be more pronounced in the younger stands, indicating that differences in rates of regrowth may become less visible with age. In addition, we will explore this ratioing technique using modified EVI. Since EVI is more sensitive to structural properties than individual spectral bands, the ratioing of this index is expected to further enhance structural discrimination of forest succession.

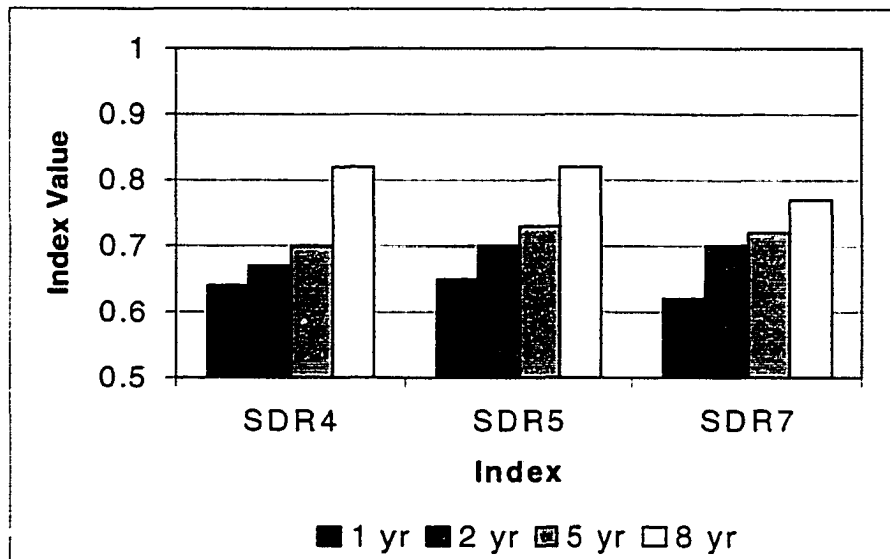


Figure A.1. Changes in stand development ratios with age. SDR4, SDR5, SDR7 ratios of bands 4,5 and 7, respectively for a series of secondary vegetation stands in Rondonia after 1,2,5, and 8 years. The SDR indices all increase with stand age, indicating that as the stands age their spectral properties become more similar to mature, undisturbed forest.

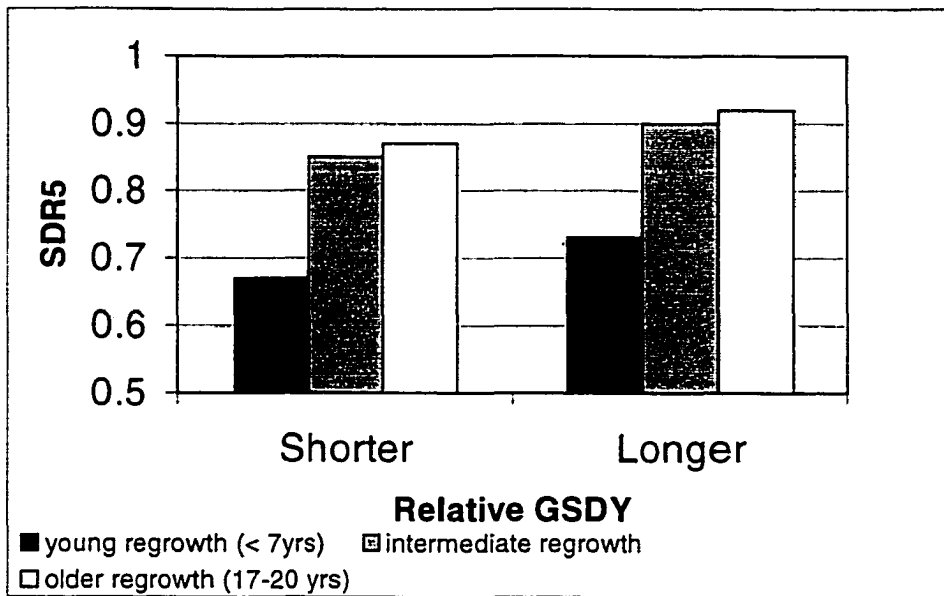


Figure A.2. Differences in average SDR5 values across ranges of stand ages for two sites with a relatively short (dry season with <5mm precipitation/day, in Amazonas) and long (dry season with >1.5 mm precipitation/day in Mato Grosso) GSDY on similar soils (Latosolos). The SDR5 values in this figure are the averages for at least 40 stands of regrowth in each age category. Differences in regrowth structure across these sites appear to be more pronounced in the younger stands, indicating that differences in rates of regrowth may become less visible with age.

Appendix B: Contingency tables from accuracy assessment.

Accuracy assessment: Alto Paraiso 1998

This spreadsheet estimate accuracy assessment based on different approaches. Changes on the contingency table will be reflected on different types of accuracies for each individual class*.

Classified Data	Reference Data				Row Total	Correct (%)	Commission (%)
	Forest	Deforestation	2o Growth	Water			
Forest	11	0	0	0	11	100	0
Deforestation	0	154	2	0	156	99	1
2o Growth	0	1	18	0	19	95	5
Water	0	0	0	0	0		
Column Total	11	155	20	0	186		
Omission (%)	0	1	10				

Definitions:

Omission: Refers to the samples of a certain class of the reference data that were not classified as such.

Commission: Refers to the samples of certain class that were wrongly classified

User's Accuracy: The probability that a pixel classified on the image actually represents that category in ground, also known as reliability. Error of commission.

Producer's Accuracy: The probability of a reference pixel being correctly classified. Error of omission.

		95% confidence Limits	
		Lower	Upper
User's Accuracy (forest)=	100 %	95	105
Producer's Accuracy (forest)=	100 %	95	105
User's Accuracy (Defores)=	99 %	97	101
Producer's Accuracy (Defores)=	99 %	98	101
User's Accuracy (2o Growth)=	95 %	82	108
Producer's Accuracy (2o Growth)=	90 %	73	107
Sum of major diagonal=	183		
Overall Accuracy=	98 %		

Tau Coefficient Analysis (Ma & Redmond, 1995):

Po=	0.98 (Percentage agreement)
Pc=	0.74
K=	0.94 (Kappa coefficient)
Pr=	0.25
Te=	0.98

Tau Coefficient Analysis (Ma & Redmond, 1995):

Interpretation:

1. Te is an adjustment of percentage of agreement (Po) by the number of groups and, as a measure of classification accuracy, it is independent of group size.

2. The Tau coefficient indicate that 98 % more pixels were classified correctly than would be expected by random assignment. This means that based on the data collected we were 98 % of the time.

Kappa Hat coefficient analysis:

Sum Xii=	183
Sum Xi+ * X+i=	24681
N=	186
KHat =	0.94

Comparison of the three accuracy measures:

Overall Accuracy:	98 %
Tau Accuracy:	98 %
KHAT Accuracy:	94 %
* Sheet developed by Arturo Sanchez	

Accuracy assessment: Chiang Mai 1996

This spreadsheet estimate accuracy assessment based on different approaches. Changes on the contingency table will be reflected on different types of accuracies for each individual class*.

Classified Data	Reference Data				Row Total	Correct (%)	Commission (%)
	Forest	Deforestation	2o Growth	Water			
Forest	16	2	0	0	18	89	11
Deforestation	2	20	0	0	22	91	9
2o Growth	0	0	0	0	0		
Water	0	0	0	0	0		
Column Total	18	22	0	0	40		
Omission (%)	11	9					

Definitions:

Omission: Refers to the samples of a certain class of the reference data that were not classified as such.

Commission: Refers to the samples of certain class that were wrongly classified

User's Accuracy: The probability that a pixel classified on the image actually represents that category in ground, also known as reliability. Error of commission.

Producer's Accuracy: The probability of a reference pixel being correctly classified. Error of omission.

		95% confidence Limits	
		Lower	Upper
User's Accuracy (forest)=	89 %	70	107
Producer's Accuracy (forest)=	89 %	70	107
User's Accuracy (Defores)=	91 %	76	106
Producer's Accuracy (Defores)=	91 %	76	106

Note: Six of the 1996 reference sites were omitted due to leaf off phenology.

Sum of major diagonal=	36
Overall Accuracy=	90 %

Tau Coefficient Analysis (Ma & Redmond, 1995):

Po=	0.90 (Percentage agreement)
Pc=	0.62
K=	0.73 (Kappa coefficient)
Pr=	0.25
Te=	0.87

Tau Coefficient Analysis (Ma & Redmond, 1995):

Interpretation:

1. Te is an adjustment of percentage of agreement (Po) by the number of groups and, as a measure of classification accuracy, it is independent of group size.

2. The Tau coefficient indicate that 87 % more pixels were classified correctly than would be expected by random assigment. This means that based on the data collected we were 87 % of the time.

Kappa Hat coefficient analysis:

Sum Xii=	36
Sum Xi+ * X+i=	808
N=	40
KHat =	0.80

Comparison of the three accuracy measures:

Overall Accuracy:	90 %
Tau Accuracy:	87 %
KHAT Accuracy:	80 %
* Sheet developed by Arturo Sanchez	

Accuracy assessment: Chiang Mai 1997

This spreadsheet estimate accuracy assessment based on different approaches. Changes on the contingency table will be reflected on different types of accuracies for each individual class*.

Classified Data	Reference Data				Row Total	Correct (%)	Commission (%)
	Forest	Deforestation	2o Growth	Water			
Forest	16	4	0	0	20	80	20
Deforestation	1	19	0	0	20	95	5
2o Growth	0	1	0	0	1	0	100
Water	0	0	0	0	0		
Column Total	17	24	0	0	41		
Omission (%)	6	21					

Definitions:

Omission: Refers to the samples of a certain class of the reference data that were not classified as such.

Commission: Refers to the samples of certain class that were wrongly classified

User's Accuracy: The probability that a pixel classified on the image actually represents that category in ground, also known as reliability. Error of commission.

Producer's Accuracy: The probability of a reference pixel being correctly classified. Error of omission.

		95% confidence Limits	
		Lower	Upper
User's Accuracy (forest)=	80 %	57	103
Producer's Accuracy (forest)=	94 %	79	109
User's Accuracy (Defores)=	95 %	83	107
Producer's Accuracy (Defores)=	79 %	58	100

Note: 13 forest and 2 cleared reference sites were omitted due to leaf off or clouds.

Sum of major diagonal=	35
Overall Accuracy=	85 %

Tau Coefficient Analysis (Ma & Redmond, 1995):

Po=	0.85 (Percentage agreement)
Pc=	0.67
K=	0.56 (Kappa coefficient)
Pr=	0.25
Te=	0.80

Tau Coefficient Analysis (Ma & Redmond, 1995):

Interpretation:

1. Te is an adjustment of percentage of agreement (Po) by the number of groups and, as a measure of classification accuracy, it is independent of group size.

2. The Tau coefficient indicate that 80 % more pixels were classified correctly than would be expected by random assignment. This means that based on the data collected we were 80 % of the time.

Kappa Hat coefficient analysis:

Sum Xii=	35
Sum Xi+ * X+i=	820
N=	41
KHat =	0.71

Comparison of the three accuracy measures:

Overall Accuracy:	85 %
Tau Accuracy:	80 %
KHAT Accuracy:	71 %

* Sheet developed by Arturo Sanchez

References

- Adams, J.B., Kapos, V., Smith, M.O., Filho, R.A., Gillespie, A.R., and Roberts, D.A., 1990, A new Landsat view of land use in Amazonia, *Int. Arch. Photogramm. Remote Sensing*, 28:177-185.
- Adams, J.B., Sabol, D.E., Kapos, V., Filho, Roberts, D.A., Smith, M.O., Gillespie, A.R. 1995. Classification of multispectral images based on fractions of end members: Application to land-cover change in the Brazilian Amazon. *Remote Sensing of Environment*. 52:137-154.
- Ahern, F., Janetos, A.C., and Langham, E., 1998, Global Observation of Forest Cover : one component of CEOS' Integrated Global Observing Strategy, *Proceedings of the 27th International Symposium on Remote Sensing of Environment, Tromso, Norway, June 8-12, 1998*.
- Alencar, A.A., Nepstad, D., Mendoza, E., Brown, I.F., and Lefebvre, P., 1997, Fires in Amazonia in 1994 and 1995: Four case studies along the arc of deforestation, *World Bank*, unpublished report.
- Alves, D., 2000, An analysis of the geographical patterns of deforestation in Brazilian Amazonia in the 1991-1996 period, In *Deforestation in the Amazon*, Ed. Wood, C.H., and Porro, R., **in press**.
- Alves, D.S., Filho, L.G.M., d'Alge, J.C.L., Mello, E.K., Moreira, J.C., de Medeiros, J.S. The amazonia information system.
- Alves, D.S., Pereira, J.L.G., De Souza, C.L., Soares, J.V., and Yamaguchi, F., 1999, Characterizing landscape changes in central Rondonia using Landsat TM imagery, *International Journal of Remote Sensing*, 20:2877-2882.
- Alves, D.S, Skole, D.L. 1996. Characterizing land cover dynamics using multi-temporal imagery. *International Journal of Remote Sensing*. 17:835-839.
- Alves, D.S., J.Viane Soares, S. Amaral, E.M.K. Mello, S.A.S. Almeida, O. Fernandes da Silva and A.M. Silveira, 1997, Biomass of primary and secondary vegetation in Rondônia, western Brazilian Amazon, *Global Change Biology* 3:451-461.
- Andriessse, J.P., Schelhaas, R.M. 1987. A monitoring study on nutrient cycles in soils used for shifting cultivation under various climatic condition in Tropical Asia. III. The

effects of land clearing though burying on fertility level. *Agriculture, Ecosystems, and Environment*. 19:311-332.

Asner G. P., B. H. Braswell, D. S. Schimel, C. A. Wessman. 1998. Ecological research needs from multiangle remote sensing data. *Remote Sensing of Environment*. 63:155-165.

Asrar, G., 1989, *Theory and applications of optical remote sensing*, John Wiley & Sons, New York, 734p.

Bazzaz, F.A., Pickett, S.T.A. 1980. Physiological ecology of tropical succession: A comparative review. *Ann. Rev. Ecol. Syst.* 11:287-310.

Boyd, D.S., Foody, G.M., Curran, P.J., Lucas, R.M., and Honzak, M., 1996, An assessment of radiance in Landsat TM middle and thermal infrared wavebands for the detection of tropical forest regeneration, *International Journal of Remote Sensing*, 17:249-261.

Bormann, F.H., and Likens, G.E., 1979, *Pattern and process in a forested ecosystem*. Springer-Verlag.

Bousquet, P., Peylin, P., Ciais, P., Le Quere, C., Friedlingstein, P., and Tans, P., 2000, Regional changes in carbon dioxide fluxes of land and oceans since 1980, *Science*, 290:1342-1346.

Brondizio, E.S., Moran, E.F., Mausel, P., Wu, Y. 1994. Land use change in the Amazon estuary: Patterns of Cabocolo settlement and landscape amangement. *Human Ecology*. 22:249-278.

Brondizio, E.S., Moran, E.F., Mausel, P., Wu, Y., 1996, Land cover in the Amazon estuary : linking Thematic Mapper with botanical and historical data, *Photogrammetric Engineering and Remote Sensing*, 62:921-929.

Brown, S., and Lugo, A.E., 1990, Tropical secondary forests, *Journal of Tropical Ecology*, 6:1-32.

Chapman, B., Freeman, A., and Siqueira, P., 1999, JERS-1 SAR Global Rain Forest Mapping (GRFM) Project – Data Quality for Multi-temporal Studies. *JERS-1 Science Program '99 PI Reports: Global Forest Monitoring and SAR Interferometry*. Earth Observation Research Center, National Space Development Agency of Japan, pp. 13-17.

Chomentowski, W.H., Salas, W.A., Skole, D.L. 1994. Landsat Pathfinder project advances deforestation mapping. *GIS World*. 7:34-38.

Ciais, P., and 9 others. 1995a. Partitioning of ocean and land uptake of CO₂ as inferred by $\delta^{13}\text{C}$ measurements from the NOAA Climate Monitoring and Diagnostic Laboratory Global Air Sampling Network. *Journal of Geophysical Research*. 100(D3):5051-5070.

- Ciais, P., Tans, P.P., Trolier, M., White, J.W.C., Francey, R.J. 1995b. A large northern hemisphere terrestrial CO₂ sink indicated by the ¹³C/¹²C ratio of atmospheric CO₂. *Science*. 269:1098-1102.
- Cochrane, M.A., and Souza, C.M., 1998, Linear mixture model classification of burned forests in the Eastern Amazon, *International Journal of Remote Sensing*, 19:3433-3440.
- Cohen, W.B., and Spies, T.A., 1992, Estimating structural attributes of Douglas-Fir/Western Hemlock forest stands from Landsat and SPOT imagery, *Remote Sensing of Environment*, 41:1-7.
- Collins, J.B., and Woodcock, C.E., 1996, An assessment of several linear change detection techniques for mapping forest mortality using multi-temporal Landsat TM data, *Remote Sensing of Environment*, 56:66-77
- Congalton, R.G., 1991, "A Review of Assessing Accuracy of Classifications of Remotely Sensed Data," *Remote Sensing of Environment*, Vol. 37 pp. 35-46.
- Crist, E.P., Laurin, R., and Cicone, R.A., 1986, Vegetation and soils information contained in transformed Thematic Mapper data, In *Proceedings, IGARSS '86 Symposium, Zurich, Switzerland, 8-11 September 1986*, (Paris, ESA).
- Cross, A.M., Settle, J.J., Drake, N.A., and Pavinen, R.T.M., 1991, Subpixel measurement of tropical forest cover using AVHRR data, *International Journal of Remote Sensing*, 12:1119-1129.
- Curran, P.J. and Kuplich, T.M., 1999, Temporal analysis of JERS-1 SAR images over regenerating forests in Brazilian Amazonia. JERS-1 Science Program '99 PI
- Denich, M., 1991, *Estudo da Importância de uma Vegetação Secundária Nova para o Incremento da Produtividade do Sistema de Produção na Amazônia Oriental Brasileira*. CPATU-EMBRAPA, Belém, Pará, Brazil, 284pp.
- Dobson, M.C., Ulaby, F.T., LeToan, T., Beaudoin, A., Kasischke, E.S., Christensen, N. 1992. Dependence of radar backscatter on conifer forest biomass. *IEEE Trans. Geosci. Remote Sensing*. 30:412-415.
- D'Souza, G., and Malingreau, J.P., 1994, The use of NOAA AVHRR for vegetation mapping and monitoring in the Amazon Basin, *Remote Sensing Reviews*, 10:5-34.
- Edwards, P.J., Grubb, P.J., 1977, Studies on mineral cycling in a montane rain forest in new guinea, I, The distribution of organic matter in the vegetation and soil, *Journal of Ecology*, 65:943-969.

- Ewel, J.J., 1983, Succession. in Galley, F.B. (ed) Tropical rain forest ecosystems, Elsevier Scientific Publishing, Amsterdam, Netherlands, 217-223.
- Ewel, J., Berish, C., Brown, B., Price, N., and Raich, J., 1981, Slash and burn impacts on a Costa Rican wet forest site, *Ecology*, 62:816-829.
- FAO. 1993. Forest resources assessment 1990 - Tropical countries. UN FAO. Rome.
- FAO. 1996. Forest resources assessment 1990 - Survey of tropical forest cover and study of changes processes. UN FAO. Rome
- Fearnside, P.M. 1990, The rate and extent of deforestation in Brazilian Amazonia. *Environmental Conservation*, 17:213-226.
- Fearnside, P.M., Guimaraes, W.M. 1996. Carbon uptake by secondary forests in Brazilian Amazon. *Forest Ecology and Management*. 80:35-46.
- Fearnside, P.M., 1996, Amazonian deforestation and global warming: Carbon stocks in vegetation replacing Brazil's Amazon forest, *Forest Ecology and Management*, 80:21-34.
- Fiorella, M., and Ripple, W.J., 1993, Determining the successional stage of temperate coniferous forests with Landsat satellite data, *Photogrammetric Engineering and Remote Sensing*, 59:239-246.
- Fittkau, E.J., Klinge, H. 1973. On biomass and trophic structure of the central amazonian rain forest ecosystem. *Biotropica*. 5:2-14.
- Foody, G.M., and Curran, P.J., 1994, Estimation of tropical forest extent and regenerative stage using remotely sensed data, *Journal of Biogeography*, 21:223-244.
- Foody G. M., Lucas, R. M., Curran, P. J., and M. Honzak, 1997a, Mapping tropical forest fractional cover from coarse spatial resolution remote sensing imagery, *Plant Ecology*, 131:143-154.
- Foody G. M., Lucas, R. M., Curran, P. J., and M. Honzak, 1997b, Non-linear mixture modeling without end-members using an artificial neural network, *International Journal of Remote Sensing*, 18:937-953.
- Foody, G.M., Palubinskas, G., Lucas, R.M., Curran, P.J., Honzak, M., 1996, Identifying terrestrial carbon sinks: Classification of successional stages in regenerating tropical forest from Landsat TM data, *Remote Sensing of Environment*, 55:205-216.
- Geol, N. S. 1988. Models of vegetation canopy reflectance and their use in estimation of biophysical parameters from reflectance data, *Remote Sensing Reviews*. 4:1-212.

- Goel, N. S., Thompson, N.L. 1984. Inversion of vegetation canopy reflectance models for estimating agronomic variables. IV. Total inversion of the SAIL model. *Remote Sensing of Environment*. 15: 237-253.
- Gopal, S., and Woodcock, C.E., 1994, Theory and methods for accuracy assessment of thematic maps using fuzzy sets, *Photogramm. Eng. Remote Sens.* 60(2):181-188.
- Goward, S.N., Markam, B., Dye, D., Dulany, W., and Yang, J., 1991, Normalized difference vegetation index measurements from the Advanced Very High Resolution Radiometer, *Remote Sensing of Environment*, 35:257-277.
- Grace, J., Lloyd, J., McIntyre, J., Miranda, A.C., Meir, P., and Miranda, H.S., 1997, Carbon dioxide flux over Amazon rainforest in Rondonia, *In Amazonian Deforestation and Climate*, Gash, Nobre, Robert and Victoria, eds, John Wiley & Sons, New York.
- Grover, K., Quegan, S., and da Costa Freitas, C., 1999, Quantitative estimation of tropical forest cover by SAR, *IEEE Trans. Geosci. & Remote Sensing*, 37:479-490.
- Guimarães, W.M., 1993, Liberação de carbono e mudanças nos estoques dos nutrientes contidos na biomassa aérea e no solo resultante de queimadas de florestas secundárias em áreas de pastagens abandonadas, em Altamira, Pará. M.Sc. dissertation, INPA/UFAM, Manaus, Amazonas, Brazil.
- Hall, F.G., Strebel, D.E., Nickerson, J.E., and Goetz, S.J., 1991, Radiometric rectification: Toward a common radiometric response among multirate, multisensor images, *Remote Sensing of Environment*, 35:11-27.
- Hashimoto, Y., Tsuchiya, K., and Iijima, T., 1997, Normalized back scattering radar cross section of tropical rain forest in Rondonia, Northern Brazil, *Adv. Space Res.*, 19(9):1425-1428.
- Helmer, E.H., Brown, S., and Cohen, W.B., 2000, Mapping motane tropical forest successional stage and land use with multi-date Landsat imagery, *International Journal of Remote Sensing*, 21:2163-2183.
- Hinton, P. 1978. Declining production among sedentary swidden cultivators: The case of the Pwo Karen. IN Kunstadter, P., Chapman, E.C., Sabhasri, S. eds. *Farmers in the Forest*. University Press of Hawaii.
- Hoekman, D.H. and Quinones, M.J., 2000, Land cover type and biomass classification using AIRSAR data for evaluation of monitoring scenarios in the Colombian Amazon, *IEEE Trans. Geosci. and Remote Sensing*, 38:685-696.
- Houghton, R.A., Boone, R.D., Fruci, J.R., Hobbie, J.E., Melillo, J.M., Palm, C.A., Peterson, B.J., Shaver, G.R., Woodwell, G.M., Moore, B., Skole, D., and Myers, N., 1987, The flux of carbon from terrestrial ecosystems to the atmosphere in 1980 due to changes in land use: geographic distribution of the global flux, *Tellus*, 39B: 122-139.

Houghton, R.A., Skole, D.L. 1990. Carbon. In *The Earth as transformed by human action*. Turner et al. eds. Cambridge University Press. New York.

Houghton, R.A., 1991, Biomass burning from the perspective of the global carbon cycle, In: Levine JS (ed) *Global Biomass burning*, The MIT Press, Cambridge, MA, USA.

Houghton, R.A., Skole, D.L., Nobre, C.A., Hackler, J.L., Lawrence, K.T., and Chomentowski, W.H., 2000, Annual fluxes of carbon from deforestation and regrowth in the Brazilian Amazon, *Nature*, 403:301-304.

Hudson, W.D. and Ramm, C.W., 1987, Correct formulation of the Kappa coefficient of agreement, *Photogrammetric Engineering & Remote Sensing*, 53:1459-1460.

Huete, A. R., Liu, H. Q., Batchily, K., and van Leeuwen, W. (1997), A comparison of vegetation indices over a global set of TM images for EOS-MODIS, *Remote Sens. Environ.*, 59:440-451.

Huete A. R. and C. Justice, 1999, MODIS Vegetation Index, ATBD. *MODIS Product #13*.

Huffman, G. J. and Adler, R. F. and Arkin, P. A. and Chang, A. and Ferraro, R. and Gruber, A. and Janowiak, 1997, The Global Precipitation Climatology Project (GPCP) Combined Precipitation Dataset, *Bulletin of American Meteorological Society*, Vol:78, No:1, pages:5-20.

Imhoff, M.L., 1995, Radar backscatter and biomass saturation: ramification for global biomass inventory. *IEEE Trans. Geosci. & Remote Sensing*. 33:511-518.

INSTITUTO NACIONAL DE PESQUISAS ESPACIAS (INPE), 2000, Monitoramento da floresta Amazonica Brasileira por satellite, INPE, Sao Jose des Campos. SP, Brazil.

IPCC. 1994. Radiative forcing of climate change and an evaluation of the IPCC IS92 emission scenarios. Cambridge University Press.

Jacquemoud, S., Baret, F., Andrieu, B., Danson, F.M., Jaggard, K. 1995 Extraction of vegetation biophysical parameters by inversion of the PROSPECT + SAIL models on sugar beet canopy reflectance data. Application to TM and AVIRIS sensors. *Remote Sensing of Environment*. 52:163-172.

Janeczek, D.J., 1999, Detection and measurement of Amazon tropical forest logging using remote sensing data, MA Thesis, Department of Geography, Michigan State University.

Janetos, A.C. and F. Ahern. (eds) 1997. CEOS Pilot Project: Global Observations of Forest Cover (GOFC), Ottawa, Ontario, Canada, July 7-10.

- Johnson, R.D. and Kasischke, E.S., 1998, Change vector analysis: a technique for the multispectral monitoring of land cover and condition, *International Journal of Remote Sensing*, 19:411-426.
- Johnson, C.M., Zarin, D.J., Johnson, A.H. 2000. Post-disturbance aboveground biomass accumulation in global secondary forests: climate, soil texture, and forest type effects. *Ecology* 81:1395-1401.
- Jupp, D. L. B., and Walker, J. (1997), Detecting structural and growth changes in woodlands and forests: The challenge for remote sensing and the role of geometric-optical modelling. In *The Use of Remote Sensing in the Modelling of Forest Productivity* (H. L. Gholz, K. Nakane, and H. Shimoda, REFERENCES Eds.), Kluwer Academic Publishers, The etherlands, pp. 75–108.
- Kasischke, E.S., Melack, J.M., Dobson, M.C., 1997, The use of imaging radars for ecological applications - A review, *Remote Sensing of Environment*, 59:141-156.
- Kauffman, J.B., Cummings, D.L., Ward, D.E., Babbitt, R. 1995, Fire in the Brazilian Amazon: 1. Biomass, nutrient pools, and losses in slashed primary forests. *Oecologia*. 104:397-408.
- Keeling, R.F., Piper, S.C., Heimann, M. 1996. Global and hemispheric CO₂ sinks deduced from changes in atmospheric O₂ concentration. *Nature*. 381:218-221.
- Keeling, R.F., Shertz, S.R. 1992. Seasonal and interannual variations in atmospheric oxygen and implications for the global carbon cycle. *Nature*. 358:723-727.
- Khorrán, S., "Accuracy Assessment of Remote Sensing-Derived Change Detection", *ASPRS Monograph Series*, Bethesda, Maryland, 1999.
- Kidwell, K.B., 1991, *NOAA Polar Orbiter Data User's Guide*, Washington, DC: National Oceanic and Atmospheric Administration.
- Kimes, D.S., Nelson, R.F., Skole, D.L., Salas, W.A. 1999. Mapping secondary tropical forest and forest age from Spot HRV data. *Remote Sensing of Environment*, 20: 3625-3640.
- Kimes, D.S., 1991, Radiative transfers in homogeneous and heterogeneous vegetation canopies. In *Photon-Vegetation Interaction: Applications in optical remote sensing and plant ecology*, Ed Myneni, R.B., and Ross, J., New York, Springer, pp 339-388.
- Kimes, D.S., Nelson, R.F., Skole, D.L., Salas, W.A. 1998. Accuracies in Mapping Secondary Tropical Forest Age from Sequential Satellite Imagery. *Remote Sensing of Environment*. 65:112-120.

- Kunstadter, P. 1978. Subsistence agriculture economics of the Lua' and Karen hill farmers, Mae Sariang District, Northwest Thailand. IN Kunstadter, P., Chapman, E.C., Sabhasri, S. eds. *Farmers in th Forest*. University Press of Hawaii.
- Knyazikhin, Y., Martonchik, J. V., Myneni, R. B., Diner, D. J., Running, S. W. 1998. Synergistic algorithm for estimating vegetation canopy leaf area index and fraction of absorbed photosynthetically active radiation from MODIS and MISR data. *Journal of Geophysical Research*. **103**:32,257-32,276.
- Laurance, W. F., Laurance, S.G., Ferreira, L.V., Rankin-de Morona, J.M., Gascon, C., and Lovejoy, T.E., 1997, Biomass collapse in Amazonian Forest Fragments, *Science*, **278**:1117-1118.
- Leckie, D.G., 1990, Synergism of synthetic aperture radar and visible/infrared data for forest type discrimination, *Photogramm. Eng. And Remote Sensing*, 56(9):1237-1246.
- Leckie, D.G. and Ranson, K.J., 1998, Forestry applications using imaging radar, In Principles and applications of imaging radar, Henderson and Lewis (eds), John Wiley & Sons, New York.
- Legates, D.R. and C. J. Willmott. 1990. Mean Seasonal and Spatial Variability in Gauge-Corrected, Global Precipitation. *Intl. J. of Climatolgy* 10: 111-127
- Le Toan, T., Beaudoin, A., Riom, J., and Guyon, D., 1992, Relating forest biomass to SAR data, *IEEE Transactions on Geoscience and Remote Sensing*, 30:403-411.
- Li, Y., Mausel, P., Wu, Y., Moran, E., and Brondizion, E., 1994, Discrimination between advanced secondary succession and mature moist forest near Altimira, Brazil using Landsat TM data, *Proceedings of the American Society for Photogrammetry and Remote Sensing*, p. 350-364.
- Li, X., Strahler, A.H. 1985. Geometric-optical modeling of a coniferous forest canopy. *IEEE Transactions on Geoscience and Remote Sensing*. **23**:207-221.
- Li, X., and A. H. Strahler, 1992, Geometrical-optical bidirectional reflectance modelling of the discrete-crown vegetation canopy: Effect of crown shape and mutual shadowing. *IEEE Transact. Geosci. Remote Sens.* GE-30:276-292.
- Lucas, R.M., Honzak, M., Foody, G.M., Curran, P.J., Corves, C. 1993, Characterizing tropical secondary forests using multi-temporal Landsat sensor imagery, *International Journal of Remote Sensing.*, 14:3061-3067.
- Lucas, R.M., Curran, P.J., Honzak, M., Foody, G.M., do Amaral, I., and Amaral, S., 1996, Disturbance and recovery of tropical forests: balancing the carbon account, in *Amazonian Deforestation and Climate*, edited by J.H.C. Gash, C.A. Nobre, J.M. Roberts, and R.L. Victoria, Chichester, John Wiley, pp. 383-398.

- Lucas, R.M., Honzák, M.L., Do Amaral, I., Curran, P.J., Foody, G.M., and Amaral, S., 1998, *Avaliação da composição florística, biomassa e estrutura de florestas tropicais em regeneração: a contribuição do sensoriamento remoto*. Pages 61-82 in C. Gascon and P. Moutinho, editors. *Floresta Amazônica: Dinâmica, Regeneração e Manejo*. INPA, Manaus, Brazil.
- Lucas, R.M., Honzák, M.L., Curran, P.J., Foody, G.M., Milne, R., Brown, T., and Amaral, S., 2000a, Mapping the regional extent of tropical forest regeneration stages in the Brazilian Legal Amazon using NOAA AVHRR data, *International Journal of Remote Sensing*, 21:2855-2881.
- Lucas, R.M., Honzák, M.L., Do Amaral, I., Curran, P.J., Foody, G.M., and Nelson, B., 2000b, Tropical forest regeneration on abandoned clearances in Central Amazonia, *International Journal of Remote Sensing*, submitted.
- Lucas, R.M., Honzák, M.L., Curran, P.J., Foody, G.M., and Nguete, D.T., 2000c, Characterizing tropical forest regeneration in Cameroon using NOAA AVHRR data, *International Journal of Remote Sensing*, 21:2831-2854.
- Luckman, A., Baker, J., Kuplich, T.M., Yanasse, C.C.F., Frery, A.C., 1997a, A study of the relationship between radar backscatter and regenerating tropical forest biomass for spaceborne SAR instruments, *Remote Sensing of Environment*, 60:1-13.
- Luckman, A., Baker, J., Honzak, M., and Lucas, R., 1998, Tropical forest biomass density estimation using JERS-1 SAR: Season variation, confidence limits, and application to images mosaics, *Remote Sensing of Environment*, 63:126-139.
- Luckman, A., Baker, J., and Wegmuller, 2000, Repeat-Pass interferometric coherence measurements of disturbed tropical forest from JERS and ERS satellites, *Remote Sensing of Environment*, 73:350-360.
- Luckman, A., Frery, A.C., Yanasse, C.C.F., and Groom, G.B., 1997b, Texture in airborne SAR imagery of tropical forest and its relationship to forest regeneration stage, *International Journal of Remote Sensing*, 18(6): 1333-1349.
- Ma, Z and Redmond, R.L., 1995, Tau coefficients for accuracy assessment of classification of remote sensing data, *Photogrammetric Engineering & Remote Sensing*, 61:435-439.
- Malingreau, J.P., 1990, The contributions of remote sensing to the global monitoring of fire in the tropical and subtropical ecosystems, In: Goldammer, J.G. (ed), *Fires in tropical biota, Ecol. Studies* 82, Springer, Berlin, pp. 337-370.
- Malingreau, J.P., Tucker, C.J., 1988, Large-scale deforestation in the southeastern Amazon basin of Brazil, *Ambio*, 17:49-55.

- Malingreau, J.P., Tucker, C.J., and Laporte, N., 1989, AVHRR for monitoring global tropical deforestation, *International Journal of Remote Sensing*, 10:855-867.
- Mausel, P., Wu, Y., Li, Y., Moran, E.F., Brondizio, E.S., 1993, Spectral identification of successional stages following deforestation in the Amazon. *Geocarto International*. 4:61-71.
- Moraes, J.F.L., Seyler, F., Cerri, C.C., and Volkoff, B., 1998, Land cover mapping and carbon pools estimates in Rondonia, Brazil, *Int. J. Remote Sensing*, 19(5): 921-934.
- Moran, E.F., Brondizio, E.S., Tucker, J., Silva-Forsberg, M.C., Falesi, I.C., and McCracken, S., 2000, Strategies for Amazonian forest restoration: Evidence for afforestation in five regions of the Brazilian Amazon, In *Amazonia at the crossroads: the challenge of sustainable development*, Ed. Hall, A., Institute of Latin American Studies, London, p.129-149.
- Myneni, R. B., Ross, J., Asrar, G. 1989. A review on the theory of photon transport in leaf canopies. *Agric. For. Meteorol.* **45**: 1-153.
- Myneni, R. B., Asrar, G. 1993. Radiative transfer in three-dimensional atmosphere-vegetation media. *J. Quant. Spectrosc. Radiat. Transfer.* **49**:585-598
- Myneni, R. B., Nemani, R.R., Running, S.W. 1997. Algorithm for the estimation of global land cover, LAI and FPAR based on radiative transfer models. *IEEE Transactions on Geoscience and Remote Sensing.* **35**: 1380-1393.
- Moran, E.F., Brondizio, R., and Mausel, P., 1994a, Integrating Amazonian vegetation land use and satellite data, *Bioscience*, 44:329-338.
- Moran, E.F., Brondizio, R., and Mausel, P., 1994b, Secondary succession, *National Geographic Society's Research and Exploration*, 10:458-476.
- Nelson, R.F., Kimes, D.S., Salas, W.A., and Routhier, M., 2000, Secondary forest age and tropical forest biomass estimation using Thematic Mapper imagery, *Bioscience*, 50, 419-431.
- Nepstad, D.C., Verissimo, A., Alencar, A., Nobre, C., Lima, E., Lefebvre, P., Schlesinger, P., Potter, C., Moutinho, P., Mendoza, E., Cochrane, M., and Brooks, V., 1999, Large-scale impoverishment of Amazonian forests by logging and fire, *Nature*, 398:505-508.
- Nepstad, D.C., Uhl, C., Serrao, E.A.S., 1991, Recuperation of a degraded amazonian landscape: Forest recovery and agricultural restoration, *Ambio*, 20:248-255.

- Oliver, C.D. 1981. Forest development in North America following major disturbances. *Forest Ecology and Management*. 3:153-168.
- Palubinskas, G., Lucas, R.M., Foody, G.M., and Curran, P.J., 1995, An evaluation of fuzzy and texture-based classification approaches for mapping regenerating tropical forest classes from Landsat-TM data, *International Journal of Remote Sensing*, 16:747-759.
- Pinty, B. and Verstraete, M.M., 1992, GEMI: a non-linear index to monitor global vegetation from satellites, *Vegetatio*, 101:15-20.
- Privette, J.L., Emery, W.J., Schimel, D.S. 1996. Inversion of a vegetation reflectance model with NOAA AVHRR data. *Remote Sensing of Environment*. 58:187-200.
- Quay, P.D., Tilbrook, B., Wong, C.S. 1992. Oceanic uptake of fossil fuel CO₂: Carbon-13 evidence. *Science*. 256:74-79.
- Qi, J., Cabot, F., Moran, M.S., Dedieu, G. 1995. Biophysical parameter retrievals using multidirectional measurements. *Remote Sensing of Environment*. 54:71-83.
- RADAMBRASIL, Ministerio das Minas e Energia, Departamento Nacional de Producao Mineral (DNPM), Projecto RADAMBRASIL: 1973-1983, *Levantamento de Recursos Naturais*, Vols. 1-23, DNPM, Rio de Janeiro.
- Ranson, K.J. and Sun, G., 1994, Mapping biomass of a northern forest using multifrequency SAR data, *IEEE Trans. Geosci. and Remote Sensing* 32:388-396.
- Rayner, P.J., Enting, I.G., Francey, R.J., and Langenfelds, R., 1999, Reconstructing the recent carbon cycle from atmospheric CO₂, $\delta^{13}\text{C}$, O₂/N₂ observations, *Tellus*, 51B: 231-232.
- Rignot, E. and Kwok, R., 1993, Characterization of spatial statistics of distributed targets in SAR, *Int. J. Remote Sensing*, 14(2):345-363.
- Rignot, E.J., Salas, W.A., Skole, D.L., 1997, Mapping deforestation and secondary growth in Rondonia, Brazil, using imaging radar and Thematic Mapper data, *Remote Sensing of Environment*, 59:167-179.
- Rignot, E.J., Zimmermann, R., van Zyl, J.J., 1995, Spaceborne application of P Band imaging radars for measuring biomass, *IEEE Trans. Geosci. and Remote Sensing*, 33:1162-1169.
- Rosenqvist, A., Shimada, M., Chapman, B., Freeman, T., De Grandi, F., Saatchi, S., and Rauste, Y., 2000, The Global Rain Forest Mapping project – a review, *International Journal of Remote Sensing*, 21, 1375-1387.

- Running, S.W., C.O. Justice, V. Salomonson, D. Hall, J. Barker, Y.J. Kaufman, A.H. Strahler, A.R. Huete, J.P.Muller, V. Vanderbilt, Z.M. Wan, P. Teillet, and D. Carnegie. 1994. Terrestrial remote sensing science and algorithms planned for EOS/MODIS. *International Journal of Remote Sensing*. **15**:3587-3620.
- Saatchi, S.S., Soares, J.V., Alves, D.S. 1997. Mapping deforestation and land use in Amazon rainforest using SIR-C imagery. *Remote Sensing of Environment*, 59:191-202.
- Sabhasri, S. 1978. Effects of forest fallow cultivation on forest production and soil. In *Farmers in the Forest*, Eds Kunstadter, P., Chapman, E.C., Sabhasri, S., University Press of Hawaii, pp.160-174.
- Sader, S.A., 1987, Forest biomass, canopy structure, and species composition relationships with multipolarization L-band synthetic aperture radar data, *Photogrammetric Engineering and Remote Sensing*, 53:193-202.
- Sader, S.A., Wade, R.B., Lawrence, W.T., and Joyce, A.T., 1989, Tropical forest biomass and successional age class relationships to a vegetation index derived from Landsat TM data, *Remote Sensing of Environment*, 28:143-156.
- Sader, S.A., 1995, Spatial characteristics of forest clearing and vegetation regrowth as detected by Landsat Thematic Mapper imagery, *Photogrammetric Engineering and Remote Sensing*, 61:1145-1151.
- Salas, W., Boles, S., Froking, S., Li, C., and X. Xiao. 2001. Analysis of land-use change in the Pearl River Delta of Southern China with Thematic Mapper data. Submitted to *GEOCARTO*.
- Salas, W.A., Ducey, M.J., Rignot, E., and D. Skole, 2000, Assessment of JERS-1 SAR for Monitoring Secondary Vegetation in Amazonia: Spatial, Temporal, and Radiometric Considerations for Operational Monitoring, *International Journal of Remote Sensing*, *Accepted*.
- Salas, W.A., Skole, D., Chomentowski, W., Townshend, J., Bell, V., Justice, C., and C.J. Tucker. 1998. NASA's Landsat Pathfinder Humid Tropical Forest Project. *ECO BP'98 International Symposium on Resource and Environmental Monitoring*, ISPRS, Budapest, September, 1998.
- Saldarriaga, J.G., West, D.C., Tharp, M.L., Uhl, C., 1988, Long-term chronosequence of forest succession in the upper Rio Negro of Colombia and Venezuela, *Journal of Ecology*, 76:938-958.
- Salinon, C.I. and I.F. Brown. 2000. Secondary forests in western Amazonia: significant sinks for carbon released from deforestation? *Interciência*. **In press**.

Sant'Anna, S.J., Yanasse, C. F., Filho, P.H., Kuplich, T.M., Dutra, L.V., Frery, A.C., and P.P. Santos, 1995, Secondary forest age mapping in Amazonia using multi-temporal Landsat TM imagery, *IGARSS'95*, pp 323-325.

Sanchez, A. 1996. Can stratified sampling be used to estimate tropical deforestation. Chapter 2 in Ph. D. Thesis. Univeristy of New Hampshire.

Sanchez, G.A., Skole, D.L., Chomentowski, W.H., 1997, Sampling global deforestation databases : the role of persistence, *Mitigation and adaptation strategies for global climate change*, 2:177-189.

Sarmiento, J. L., 1993, Atmospheric CO₂ stalled, *Nature*, 365:697-698.

Scarth P. and S. Phinn, 2000, Determining forest structure attributes using an inverted geometric-optical model in mixed eucalypt forests, southeast Queensland, Australia, *Remote Sens. Environ.*, 71:141-157.

Setzer, A.W., and Pereira, M.C., 1991, Amazon biomass burning in 1987 and an estimate of their tropospheric emission, *Ambio*, 20(1):19-22.

Shimada, M., 1998, User's guide to NASDA's SAR products, NASDA document # HE-930014, revision 1, February 16, 1998.

Shukla, J.C.N., Nobre, C., and Sellers, P., 1990, Amazon deforestation and climate change, *Science*, 247:1322-1325.

Singh, A., 1987, Spectral separability of tropical forest cover classes, *International Journal of Remote Sensing*, 8:971-979.

Siegenthaler, U., Sarmiento, J.L. 1993. Atmospheric carbon dioxide and the ocean. *Nature*. 365:119-125.

Skole, D.L. 1992. Measurement of deofrestation in the Brazilian Amazon using remote sensing. Ph. D. Thesis. University of New Hamshire.

Skole, D.S., 1994, Data on global land cover change: acquisition, assessment, and analysis, In *Changes in land use and land cover: A global perspective*, Ed Meyer, W.B. and Turner, B.L., Cambridge University Press.

Skole, D.S., Chomentowski, W.H., Salas, W.A., Nobre, A.D., 1994, Physical and human dimensions of deforestation in Amazonia, *BioScience*, 44:314-322.

Skole, D.S., Justice, C.O. 1995. A land cover change monitoring change program: A federal agency initiative. Report to Science Policy Associates.

Skole, D.L., Salas, W.A. and Silapathong, C., 1998, Interannual Variation in the Terrestrial Carbon Cycle: Significance of Asian Tropical Forest Conversion to

Imbalances in the Global Carbon Budget, *In Asian Change in the Context of Global Climate Change*, Ed. James Galloway, Cambridge University Press.

Skole, D.S., Tucker, C.J., 1993, Tropical deforestation and habitat fragmentation in the Amazon: Satellite data from 1978 to 1988, *Science*, 260:1905-1910.

Spanner, M.A., Pierce, L.L., Peterson, D.L., and Running, S.W., 1990, Remote sensing of temperate coniferous forest leaf area index: the influence of canopy closure, understory vegetation and background reflectance, *International Journal of Remote Sensing*, 11:95-111.

Sohn, Y., Moran, E., and Gurri, F., 1999, Deforestation in North-Central Yucatan (1985-1995): Mapping secondary succession of forest and agricultural land use in Sotuta using the cosine of the angle concept, *Photogrammetric Engineering and Remote Sensing*, 65:947-958.

Sorrensen, C.L., 2000, Linking smallholder land use and fire activity: examining biomass burning in the Brazilian Lower Amazon, *Forest Ecology and Management* 128:11-25.

Steininger, M.K., 2000, Secondary forest structure and biomass following short and extended land-use in central and southern Amazonia, *Journal of Tropical Ecology*, **In press**.

Steininger, M.K., 1996, Tropical secondary forest growth in the Amazon: age, area and change estimation with Thematic Mapper data, *International Journal of Remote Sensing*, 17:9-17.

Stone, T.A., Schlsinger, P., Houghton, R.A., and Woodwell, G.M., 1994, A map of the vegetation of South America based on satellite imagery, *Photogrammetric Engineering and Remote Sensing*, 60:541-551.

Strahler, A. 1997. Vegetation canopy reflectance modeling-recent developments and remote sensing perspectives. *Remote Sensing Reviews*. 15:179-194.

Strahler, A.H. and D. L. B. Jupp, 1990, Modelling bidirectional reflectance of forests and woodlands using Boolean models and geometric optics, *Remote Sens. Environ.*, 34:153-178.

Swain, P.H., and Davis, S.M., 1978, *Remote Sensing: The Quantitative Approach*, New York: McGraw Hill.

Tans, P.P., Fung, I.Y., and Takahashi, T., 1990, Observational constraints on the global atmospheric CO₂ budget, *Science*, 247:1431-1438.

Teillet P. M. , Staenz K. , Williams D., 1997, Effects of Spectral, Spatial, and Radiometric Characteristics on Remote Sensing Vegetation Indices for Forested Regions; *Remote Sens. Environ.*, 61:139-149

Tian, H., Melillo, J.M., Kicklighter, D.W., McGuire, A.D., Helfrich, J.V.K. III, Moore, B. III, and Vorosmarty, C.J., 1998, Effect of interannual climate variability on carbon storage in Amazonian ecosystems, *Nature*, 396:664-667.

Townshend, J.G.R., Justice, C.O. 1988. Selecting the spatial resolution of satellite sensors required for global monitoring of land transformations. *International Journal of Remote Sensing*. 9:187-236.

Townshend, J.R.G., Bell, V., Desch, A., Havlicek, C., Justice, C.O., Lawrence, W.E., Skole, D., Chomentowski, W., Salas, W.A., 1995, *The NASA Landsat Pathfinder Humid Tropical Deforestation Project. Land Satellite Information in the Next Decade* (Tyson's Corner, Virginia: American Society of Photogrammetry and Remote Sensing), pp. IV76-IV87.

Townshend, J.G.R., Justice, C.O., 1988, Selecting the spatial resolution of satellite sensors required for global monitoring of land transformations, *International Journal of Remote Sensing*, 9:187-236.

Trevet, J.W., 1986, *Imaging radar for resource surveys*, Chapman and Hall, New York, 313p.

Tucker, C.J., 1979, Red and photographic infrared linear combinations for monitoring vegetation, *Remote Sensing of Environment*, 5:492-501.

Tucker, C.J., Holben, B.N., Elgin, J.H., and McMurtrey, E., 1981, Remote sensing of total dry matter accumulation in winter wheat, *Remote Sensing of Environment*, 11:171-190.

Tucker, C.J., Holben, B.N., Goff, T.E., 1984, Intensive forest clearing in Rondonia, Brazil as detected by satellite remote sensing, *Remote Sensing of Environment*, 15:255-261.

Tucker, C.J, Townshend, J.G.R., 2000, Strategies for mapping tropical deforestation using satellite data, *International Journal of Remote Sensing*, 21:1461-1471.

Tucker, J.M., E.S. Brondizio, F. de Castro and E. Moran., 2000, Biomass estimation at the tree, stand, and landscape level: the use of allometric equations to estimate aboveground biomass in Amazonian secondary forests, *Global Change Biology*, **In review**.

Uhl, C., 1987, Factors controlling succession following slash-and-burn agriculture in Amazonia, *Journal of Ecology*, 75:377-407.

- Uhl, C., Buschbacher, R., Serrao, E.A.S., 1988, Abandoned pastures in eastern Amazonia. I. Patterns of plant succession, *Journal of Ecology*, 76:663-681.
- Uhl, C., Jordan, C.F., 1984, Succession and nutrient dynamics following forest cutting and burning in Amazonia, *Ecology*, 65:1476-1490.
- Uhl, C., and Vieira, I.C.G., 1989, Ecological impacts of selective logging in the Brazilian Amazon: a case study from the Paragominas region in the State of Para, *Biotropica*, 21:98-106.
- Uhl, C., and Kauffman, J.B., 1990, Deforestation, fire susceptibility and potential tree responses to fire in the Eastern Amazon, *Ecology*, 71:437-449.
- Verbyla, D.L and Boles, S.H., 2000, Bias in land cover change estimates due to misregistration, *International Journal of Remote Sensing*, 21:3553-3560.
- Vieira, P.R., 1996, Desenvolvimento de classificadores de máxima verossimilhança pontuais e para imagens de abertura sintética, INPE, São José dos Campos. SP, Brazil.
- Walker, R., Salas, W., Urquhart, G., Keller, M., Skole, D., and Pedlowski, M., 2000, Secondary vegetation: Ecological, social, and remote sensing issues. *Bioscience, in review*.
- Whitmore, T.C., 1990, *An introduction to tropical rain forests*, Clarendon Press, Oxford.
- Wickware, G.M. and P.J. Howarth, 1981, Change detection in the Peace-Athabasca Delta using digital Landsat data, *Remote Sensing of Environment*, Vol. 11, pp. 9-25.
- Yanasse, C.C.F., Sant'Anna, S.J.S., Frery, A.C., Renno, C.D., Soares, J.V., Luckman, A.J., 1997, Exploratory study of the relationship between tropical forest regeneration stages and SIR-C L and C data, *Remote Sensing of Environment*. 59:180-190.
- Zarin, D.J., Ducey, M.J., Tucker, J.M., and Salas, W.A., 2001, Potential biomass accumulation in Amazonian regrowth forests, *in press Ecological Applications*.